Royal Netherlands Academy of Arts and Sciences
P.O. Box 19121, 1000 GC Amsterdam, the Netherlands

Proceedings of the International Colloquium,
Amsterdam, 18–20 June 1990

ISBN 0-444-85735-4

Koninklijke Nederlandse Akademie van Wetenschappen
Verhandelingen, Afd. Natuurkunde, Eerste Reeks, deel 35

Particle Acceleration near Accreting Compact Objects

Edited by J. van Paradijs, M. van der Klis and A. Achterberg
Center for High Energy Astrophysics UVA / RUU / NIKHEF-H

North-Holland, Amsterdam / Oxford / New York / Tokyo, 1991

Contents

Preface

A variety of observations obtained during recent years suggest that acceleration of particles to very high energies and the production of relativistic beamed flows occur, and may actually be rather common, in X-ray binaries and their evolutionary descendants. These observations include the non-thermal radio emission of low-mass X-ray binaries and its relation to their X-ray properties, the presence of jets and extended double radio emission around X-ray binaries, and the reported detections of these systems at very-high photon energies. It is not clear whether there is a direct relation between these different observations.

Under the auspicies of the Royal Netherlands Academy of Sciences a meeting was held in Amsterdam from June 18 to 22, 1990, in which 45 active researchers, theorists as well as observers, and graduate students participated, to discuss these results. In these proceedings we have collected the written versions of the invited reviews which were received by us by mid-February 1991.

The meeting was made possible by the support of the Royal Netherlands Academy of Sciences. We like to thank here Mrs. C.E. Zwager and Mrs. Y. Smits of the Academy, for their help in organizing this meeting, which contributed in no small way to its success.

Amsterdam / Utrecht, February 21, 1991
J. van Paradijs, M. van der Klis, A. Achterberg

R. D. Blandford

Hydromagnetic Outflow from Accretion Disks

ABSTRACT
Accretion disks are believed to be present with decreasing conviction in cataclysmic variables, X-ray binaries, protostars and active galactic nuclei. Collimated jets or bipolar outflows have been reported in examples of all four types of source. Magnetic extraction of disk angular momentum provides a generic method of launching and collimating these jets. A model for broad emission lines in quasars and Seyfert galaxies involving a disk- driven hydromagnetic outflow is outlined. This explanation may be appropriate to other classes of accretion disks.

INTRODUCTION

The interplay between gravitation, rotation and magnetic field, long studied in the classical theory of star formation, is notoriously subtle *e.g.*Parker (16). The initial concern that centrifugal force and magnetic pressure w ould prevent gravitational collapse has been replaced by the twin realisations that hydromagnetic torque provides a convenient means of extracting angular momentum and that magnetic flux can readily escape through buoyancy and ambipolar diffusion. Magnetic torques can be observed at work in the solar wind and have presumably slowed the sun's rotation over its lifetime just as appears to be the case for other F and G stars. Magnetic torques are also widely believed to establish the period distribution in cataclysmic variable stars longward of the period gap. The case for the dynamical importance of magnetic fields in stellar systems has been amply made.

Magnetic fields may also have a crucial role in the dynamics of two common astronomical structures, accretion disks and jets. Indeed, disks and jets (or bipolar outflows) are increasingly found in association, in active galactic nuclei (AGN), X-ray binaries, cataclysmic variables and protostars. It is reasonable to hypothesise that a magnetic field constitutes the mechanical link between these two types of flow.

In the standard theory of accretion disks, it is supposed that there exists a local viscosity responsible for angular momentum transport in the disk. This allows matter to sink slowly towards the central object, while its liberated angular momentum is removed to progressively larger radii. The viscous agent is generally supposed to be either turbulence or small scale magnetic field. It is my contention that, under many circumstances, much of the angular momentum is instead removed by surface magnetic stress and carried by a pair of jets.

These jets are probably launched centrifugally. To see how this might operate,

consider an electrically conducting accretion disk threaded by magnetic field which is "frozen in" to moving gas. Plasma on the surface of the disk will also be constrained to move with the field line at the angular velocity of the disk, rather like a bead on a wire. Now if the field line leaves the disk vertically, the plasma will be bound stably and will simply undergo vertical epicyclic oscillation. However if the field direction is radially outward, then centrifugal force will dominate and the gas will be flung out. It turns out that for intermediate angles, the gas is unstable when the angle between the field and the disk vertical exceeds 30° (3). A modest radial variation of field strength with disk radius ensures that this condition will be satisfied.

Independent of these considerations, jets, most notably those associated with powerful radio sources and SS433, must be collimated by some form of external stress and observational arguments suggest that, in most instances, this is neither gas pressure nor radiation pressure. This leaves magnetic field. The simplest means of magnetic collimation operates when the jet carries a current so that a toroidal field is wrapped around it. There is magnetic tension associated with the field lines which, in association with the magnetic pressure, exerts a "hoop stress" on the jet. Although this magnetic field must itself be confined, presumably by thermal gas, the necessary pressure can be much smaller than the stress exerted on the jet walls. Loops of magnetic field can concentrate the stress onto a slender jet core. The origin of the toroidal magnetic field responsible for jet collimation is generally supposed to be gas orbiting a central compact object. A jet may therefore be a disk's way of shedding angular momentum.

I should relate my talk to the topic of this conference, particle acceleration in accreting compact objects. In a strict sense, the formation of jets by accretion disks is particle acceleration. However, our main concern here is with relativistic particles. I shall not discuss the direct acceleration of jets to flow speeds comparable with that of light as is observed to occur in compact extragalactic radio sources and SS433. This involves consideration of the central black hole, when present, and, necessarily, general relativity. However, relativistic electrons (and protons) can be accelerated by non-relativistic flows especially when the speeds are supersonic (*cf.*Achterberg's contribution). This is observed to occur in interplanetary shock waves and expanding supernova remnants. If real jets are formed in the manner outlined above, then they are unlikely to be as steady and axisymmetric as numerical and analytical simulations. Instead, they will be subject to a variety of instabilities and intermittency associated with activity in the disk which will create fast streams and internal shocks. It is hard to imagine that relativistic particle acceleration can be avoided under these circumstances, although it is not possible to quantify the fraction of the jet power that is likely to be dissipated in this manner.

I recently summarised the subject of hydromagnetic outflows from disks in a widely available conference proceedings Meyer *et al.*(1). Several articles in this book and the procedings edited by Belvedere (2) also cover this territory. I refer the reader to these references for general discussion. In this article, I shall therefore confine my attention to describing some work in progress on a model for the formation of AGN broad emission lines in a hydromagnetic outflow from an accretion disk.

BROAD EMISSION LINES FROM ACTIVE GALACTIC NUCLEI

One of the primary characteristics of quasars and Seyfert galaxies is broad emission lines. For a long while, these have been supposed to be formed by the photionisation of dense gas clouds by the central UV continuum source. Observations of

the relative strengths of the lines have helped define the likely physical conditions in these clouds. Measurement of the line velocity profiles and, to a limited extent, their temporal variation, has stimulated a variety of kinematic proposals concerning the disposition of these clouds in phase space. However, some significant difficulties remain. Motivated by these problems, Robert Emmering, Isaac Shlossman and I are currently studying if these lines may be formed in a magnetically driven wind from a disk and I would like to report on our progress.

The permitted lines that are observed in most quasars and Seyfert 1 galaxies have velocity widths (HWZI) $\sim 10,000$km s^{-1} (15). The range of ionisation states observed is consistent with photoionisation by an extended UV and soft X-ray spectrum and the lines are sufficiently similar in profile that they are commonly characterised by a single ionisation parameter $n_{ion}/n_e \sim 10^{-2}$, where n_{ion} is the number density of (hydrogen) ionising photons and n_e is the electron density. The electron density is estimated from various spectral indicators, for example the presence of CIII]λ1909 and the absence of broad [OIII]λ5007to lie in the range 10^8cm$^{-3} \lesssim n_e \lesssim 10^{10}$cm^{-3} (Recent studies suggest that some denser gas may also contribute (18).) If the continuum radiation originates from a central source, the clouds must then be concentrated at a distance of $R \sim L_{UV\,46}^{1/2}$pc. Combining this distance estimate with the velocity width allows a virial mass of the central black hole to be estimated and values $\sim 10^{10}$M$_\odot$ are typically derived for quasars.

There are four problems with this standard interpretation.

(i) Emission lines are commonly observed to be cusped. The sharpness of the cusp is unclear, but it may often have a velocity width as small as ~ 300km s^{-1}. The maximum velocity can be as large as 30,000km s^{-1} but is typically ~ 10000km s^{-1}. If these velocities are representative of the local virial speed, then the gravitational potential must be dominated by the central black hole. A factor ~ 30 in characteristic velocity then corresponds to a dynamic range $\sim 10^3$ in radius and a range $\sim 10^6$ in ionizing photon flux. This is inconsistent with the inferred approximate constancy of the ionization parameter and the limited range of allowed electron density.

(ii) The inferred black hole masses are surprisingly large, significantly larger than the upper limit central masses inferred in nearby galaxies. As more than $\sim$ one per cent of galaxies must once have been quasars, the nearest such mass should be $\sim$20Mpc away and it has not yet been identified (9).

(iii) Estimates of the size of Seyfert 1 broad line regions due to "reverberation mapping" in which the time delay between an observed variation in the strength of the continuum flux and the response of the emission lines is measured. In the best documented cases, these are inferred to be a factor $3-5$ smaller than sizes inferred from the ionization parameter (17).

(iv) The inferred pressures in the densest broad line clouds ($\sim$ 0.03dyne cm^{-2}), are too large to be confined by an inter-cloud medium, without invoking some extraneous heating mechanism. (The original suggestion that the intercloud medium is Compton-heated by a hard X-ray continuum, (10), fails because most AGN lack this hard component and their Compton temperatures are too low.)

There are some additional observational clues.

(i) The velocity profiles of the emission lines are not symmetric (22). Typically their peaks are blue-shifted by $\sim 500-1000$km s^{-1} with respect to the forbidden lines. Blue asymmetries in the line profile are also common.

(ii) The relationship between Seyfert 1 and Seyfert 2 galaxies has recently been clarified by polarisation observations (1). Seyfert 2 galaxies which do not exhibit

broad wings in total intensity may do so in polarised light. This has been taken to imply that all Seyfert galaxies are essentially similar, but that the broad line region cannot be seen directly when viewed from an equatorial direction in Seyfert 2 galaxies. It can, however, be seen in light that is Thomson scattered by free electrons at high latitude.

(iii) It seems increasingly likely that broad absorption line quasars are normal emission line quasars viewed from special directions through a dense outflowing wind (21).

These factors motivated us to propose that the emission lines are formed by clouds of photoionised gas that are flung out from the surface of an accretion disk by magnetic stresses. (Although the gas in the disk may be originally neutral, it will almost certainly have sufficient ionisation for it to be tied to the magnetic field lines.) Let us consider our problems in turn.

The characteristic cusp profile can be reproduced if the outflow originates from several octaves of disk radius. The line profile associated with the outflow from a single ring of disk has a "twin peak" profile with a width that is a measure of the amplitude of the Keplerian velocity on the ring. Typically, the gas is accelerated to a velocity having both circular and poloidal components whose magnitude is several times the orbital speed in the disk. However what is observed is the projection of this velocity along the line of sight which is somewhat smaller. Only one hemisphere will be seen, and as there is net motion towards the observer, the centre of the profile will be blue-shifted. The total line profile is reproduced by the superposition of twin peaks from a range of radii, the net shape being a determined by the variation of emissivity with radius. We have computed total line profiles for a variety of emissivity prescriptions for an outflowing hydromagnetic wind. We find that the observed profiles can roughly be reproduced if the volume emissivity scales as the product of the magnetic pressure and the mean density in the outflow as we might expect. (At a fixed emission line gas temperature of $\sim 10^4$K, the emissivity per unit mass might scale as the recombination rate per unit mass, proportional to the pressure. The emissivity per unit volume is then formed by multiplying by the cloud density.)

However, this leaves the problem of explaining the large velocity range. To alleviate this problem, we propose that the broad wings may not be due to high bulk velocity of the emitting gas, but may instead be caused by electron scattering. To be more specific, we note that the outer parts of accretion disks are believed to be largely molecular and dusty (19). They can therefore re-radiate incident UV as infra red emission and most of the IR spectrum in normal quasars is thought to be produced in this manner. Now gas can only remain molecular as long as it can cool and this, in turn, requires that the dust remain cool enough ($T \lesssim 1500$K) not to sublime. By equating the radiation incident upon a grain to it emission, we find that the minimum radius for cool gas is ~ 0.1pc, where the Keplerian velocity is ~ 3000km s^{-1} for a powerful quasar.

The minimum velocity in the disk is unlikely to be less than the central velocity dispersion of a galaxy (~ 300km s^{-1}). (Indeed, it is an interesting observational project to see if observed line profiles are more cuspy than this.) In order to produce the full range of observed velocity width in the lines we propose that the lines are actually broadened by electron scattering. Roughly half the line photons emitted by outflowing clouds will illuminate the disk. Now, if the sun is any guide, it is quite likely that there be a hot corona above the surface of the accretion disk. If the coronal temperature is $T \sim 10^6$K, and the corona is optically thick to Thomson scattering, then the back-scattered radiation will be Doppler-shifted by the hot electrons to produce the observed broad wings (20). More detailed simulations verify that this does occur. (It might be thought that

electron scattering will broaden the line profile. However, it turns out that the electron scattering redistribution function itself has a sharp gradient discontinuity at zero velocity shift and this preserves the cusp in the emission line profile.) By reducing the range of emission radius, we find that the range of ionisation parameter is also reduced.

Invoking electron scattering also alleviates our second problem above because the characteristic Keplerian velocity at the radius of the emission line clouds is reduced, thereby lowering the inferred central mass to $\sim 3 \times 10^8 M_\odot$ for a typical quasar.

We suspect that the third problem has a different solution. The cloud and gas density will be quite large close to the disk and this will render a large number of lines of sight partially opaque to the ionising UV radiation. The clouds will therefore be located closer to the central continuum source at a given photon density. An unrelated possibility, mentioned above, is that there may be a population of denser, optically thick clouds which would also be located closer to the continuum source.

The magnetic field is directly responsible for solving the final problem as it can confine clouds in the perpendicular direction. We envisage that cool clouds will be flung off the disk and, when they are exposed to the ionising flux, they will be heated to a higher pressure which will cause them to expand into the magnetic field until they achieve pressure balance. The clouds are free to expand along the direction of the magnetic field. However, this expansion will only be at the internal sound speed (as opposed to external fast mode speed for the transverse expansion). As the clouds move at high (sonic) Mach number, they will typically leave the emission region before they expand very much.

There is a second consequence of invoking magnetic pressure confinement and this involves the postulated electron scattering corona. One reason why electron scattering has not often been invoked in the past to broaden the emission line profiles is that gas at the required temperature of $\sim 2 \times 10^6$K is thermally unstable. Either it will heat to the Compton temperature $\sim 10^7$K or cool to 10^4K like the emision line clouds. However, the instability criterion must be modified if the confinement is by magnetic as opposed to thermal gas pressure. It turns out that gas at $\sim 10^6$K can be rendered thermally stable if magnetically confined.

What happens to the emission line gas after it leaves the disk? There is a substantial mass flux involved. Some of it may be decelerated by interaction with the ambient gas in the nucleus and may form the narrow line-emitting gas. It can also fall back onto the disk and be recycled several times.

Naturally, there are several predictions that follow from this interpretation. The most direct follow from our velocity field which is a superposition of axisymmetric rings that rotate, expand radially and translate vertically with respect to the disk. The line cores should be formed at greater distances than the gas at $\sim 1000 - 3000 \mathrm{km\ s^{-1}}$. This can be probed by comparing in detail the line profiles for different ions with different critical densities for collisional ionisation and by using "reverberation mapping". We also expect that the vertical velocity, measured by the blueshift, will be systematically larger for AGN observed at large angles to the disk. This effect may be detectable by comparing the velocity profiles of the different classes of Seyfert galaxy.

If electron scattering is responsible for the broad wings, then we expect that they should be linearly polarised and may show up in polarised light. As we have noted broad lines in polarised flux are observed from Seyfert 2 galaxies. However, we expect that the wings of Seyfert 1 galaxies should also be linearly polarised, although to a weaker degree on account of the different viewing angle. (Note that our explanation of the polarised wings seen in Seyfert 2 galaxies is subtly different

from the standard explanation because the scattering electrons are located in a disk and seen along lines of sight where the optical depth is reduced. This is in contrast to invoking an otherwise very high density of free electrons.)

The Relationship to Jets

If this is the correct interpretation of the kinematics of emission line clouds, we must consider the connection between this outflow and that more directly observed in the form of extragalactic radio jets. Most AGN are radio quiet (though not silent). Nevertheless, observations of Seyfert galaxies suggest that they create weak, bipolar ouflows which produce biconical regions in which the narrow emission lines are often concentrated. (These lines may be excited directly by the outflow or may be photoionised by the central UV continuum which escapes preferentially along the directions evacuated by the outflow.)

Similarly, the majority of radio galaxies are relatively weak in emission lines and central bolometric luminosity. They are divided into two classes on the basis of their radio luminosities (4). Powerful radio galaxies appear to produce relativistic jets, which are responsible for beamed emission and apparent superluminal expansion when observed along their symmetry directions. The jets associated with lower power sources appear to move with speeds much less than that of light and are may not even be supersonic with respect to their internal sound speeds.

These observations can be interpreted in the following manner. Suppose that essentially all AGN contain accretion disks and associated bipolar outflows. Now the power liberated by the outer parts of the accretion disk is proportional to the mass accretion rate and is a relatively small fraction of the power that can be liberated when (and if) this gas reaches the innermost parts of the disk near the black hole. There is an additional source of power, the spin energy of the central black hole. If the central black hole is active, a powerful relativistic jet core will be produced and this will be collimated by the more slowly moving and essentially invisible outflow from the outer disk. If the central black hole is inactive, there will only be a weak and slow jet. The strength of the emission lines will be largely a reflection of the strength of the UV continuum produced by the inner disk and the relative importance of the broad components will be a measure of the orientation of our line of sight. On this interpretation, powerful jets will not be characterised by a single outflow speed, but will instead be cocooned in a slower moving sheath of denser gas.

The Galactic Centre

Although not "active" in the usual meaning of the word, our Galactic Centre may be the best environment in which to observe magnetically driven dynamical evolution of an accretion disk. Morris (12) has summarised observations on length scales of $\sim 10 - 100$pc of long, linear features variously called arcs filaments and threads, some of which exhibit linear polarisation consistent with synchrotron emission. Some of these features appear to pass straight through the plane of the Galactic disk. They have been widely interpreted as magnetic field bundles perhaps being illuminated by twisting in a fashion similar to that believed to occur in coronal loops and prominences. On a smaller scale ($\sim 1 - 10$pc), exists a molecular torus (6) in orbit about a central mass of a few million solar masses, possibly, though not necessarily, a black hole. 100μ polarisation observations (7) suggest that the magnetic field direction lies mainly in the disk rather than perpendicular to it. Furthermore, Zeeman splitting observations of the parallel component of the

magnetic field, (*e.g.*Killeen, Lo and Crutcher 1990, preprint) indicate a strength $\sim$1mG. slightly larger than the inferred equipartition magnetic field strengths. The simplest interpretation of these observations is that an open, poloidal field is convected inward by the disk gas and sheared by the differential rotation to become predominantly toroidal there. However, it may also be consistent with a model in which the disk magnetic field is more poloidal with a strength limited by the influence of ambipolar diffusion (Königl, 1990, preprint). Future observations should settle the matter.

Application to other Disk Systems

Broad emission lines have also been seen from other disk systems, notably protoplanetary disks (14), cataclysmic variables (13), SS433 (5) and the black hole candidate A 0620+00 (8). These may also originate, not in the accretion disk itself, but, instead, from a hydromagnetic bipolar outflow. This will increase the observed line widths. More detailed modelling is neccessary to determine of the salient features of the line profiles can be reproduced in this manner.

ACKNOWLEDGEMENTS

I am indebted to Bram Achterberg, Michiel van der Klis and Jan van Paradijs for the invitation to attend this meeting and travel support. I thank Robert Emmering and Isaac Shlossman for collaboration on some of the research described above. I also acknowledge financial support under NASA GRANT NAGW1301.

REFERENCES

(1) Antonnucci, R. J. J. and Miller, J. S., 1985. In: Astrophys. J., 297, 621.
(2) Belvedere, G. (ed.), 1989. *Accretion Disks and Magnetic Fields in Astrophysics* (Dordrecht: Kluwer).
(3) Blandford,R. D. and Payne, D. G., 1982. In: Mon. Not. R. astr. Soc., 199, 883.
(4) Bridle, A. H. and Perley, R. A., 1984. In: Ann. Rev. Astron. Astrophys., 22, 319.
(5) Filippenko, A. V., Romani, R. W., Sargent, W. L. W. and Blandford, R. D., 1988. In: Astronom. J., 96, 242.
(6) Genzel, R., (1989): In: *The Center of the Galaxy*, ed. by M. Morris (Dordrecht: Kluwer) p.393
(7) Hildebrand, R. *et al.*, 1990. In: Astrophys. J.. (in press)
(8) Johnston, H., Kulkarni, S. and Oke, J. B., 1989. In: Astrophys. J., 345, 492.
(9) Kormendy, J., 1988. In: Astrophys. J., 325, 128.
(10) Krolik, J., McKee, C. F. and Tarter, C. B., 1981. In: Astrophys. J., 249, 422.
(11) Meyer, P., Duschl, W., Frank, J. and Meyer-Hofmeister, E. (ed.), 1989. *Theory of Accretion Disks* (Dordrecht: Kluwer).
(12) Morris, M., 1990.: In: *Galactic and Intergalactic Magnetic Fields* ed. by R. Beck, P. Kronberg and R. Wielbinski (Dordrecht: Kluwer)(in press)
(13) Mauche, C. W. and Raymond, J. C., 1987. In: Astrophys. J., 323, 690.

(14) Mundt, R., (1985): In: *Protostars and Planets*, ed. by D. C. Black and M. S. Matthews (Tucson: University of Arizona Press) p.
(15) Osterbrock, D. E., 1989. *Astrophysics of Gaseous Nebulae and Active Galactic Nuclei* (Mill Valley: University Science Books).
(16) Parker, E. N., 1979. *Cosmical Magnetic Fields* (Oxford: Clarendon Press).
(17) Peterson, B. M., 1988. In: Publ. Astr. Soc. Pacific, 100, 18.
(18) Rees, M. J., Netzer, H. and Ferland, G. J., 1989. In: Astrophys. J., 347, 640.
(19) Sanders, D. B., Phinney, E. S., Neugebauer, G., Soifer, B. T. and Matthews, K., 1989. In: Astrophys. J., 347, 29.
(20) Shields, G. A. and McKee, C. F., 1981. In: Astrophys. J. Lett., 246, L57.
(21) Weymann, R. J., Turnshek, D. A. and Christiansen, W. A., (1985): In: *Astrophysics of Active Galaxies and Quasi-Stellar Objects*, ed. by J.Miller (Mill Valley: University Science Books) p.333
(22) Wilkes, B. J., 1986. In: Mon. Not. R. astr. Soc., 218, 331.

R. D. Blandford
Theoretical Astrophysics
130-33 Caltech
Pasadena
California 91125
U. S. A.

A.C. Fabian

Pairs in Compact Objects – Clues to Particle Acceleration

ABSTRACT

Electron-positron pairs are created by photon-photon collisions in compact objects such as Active Galactic Nuclei and Galactic Black Hole sources. The production of the pairs and their radiation change the emergent spectrum to make it steeper than the primary spectrum emitted by the accelerated electrons. Recent evidence for a reflected component – radiation scattered back by the accretion disc – causes emitted the spectrum to be further changed and to resemble the observed spectrum. Although this allows us to understand the observed radiation better, it masks the operation of the electron accelerator.

INTRODUCTION

The spectrum and variability of Active Galactic Nuclei (AGN) and Galactic Black Hole sources are the best handles we have on the electron population in these objects, and thus of the processes which accelerate the electrons. Understanding these processes should eventually give us a much clearer picture of the operation of the central engine.

The most rapid variability observed so far is in the X-ray band (*e.g.* Tennant [13]; Kunieda [9]), which suggests that it is in this band that we see deepest into AGN and similar sources. Simultaneous optical and X-ray observations of the rapidly X-ray varying nucleus of the nearby Seyfert Galaxy NGC4051 by Done (3) show less than 1 per cent variations in the optical band while the X-ray flux changed by a factor of two. This means that the region emitting the optical flux must be at least 10 times larger than the X-ray emission region, since the varying X-ray flux must correspond to a varying electron population in the region. This would produce a detectable, variable, Compton-scattered flux in the optical if there were a significant energy density of infrared and optical photons in the X-ray emission region. For these reasons, the discussion in most of this paper is concentrated on the X-ray emission in AGN and on what it implies for the radiation and particle acceleration processes.

The X-ray spectra of AGN (and of Galactic Black Hole candidates) are hard. There is a turnover in the spectrum at 100 – 2000 keV, giving what is called the 'MeV turnover' in AGN. This has suggested to many of us that the central engine is responding to the electron rest mass; the turnover is not a coincidence of parameters but something basic which is common to all the objects. There are many detailed ways in which this can occur, but in general we can predict that electron-positron pairs are common. The reasons for this are dis-

cussed in the next Section, together with some of the 'simple' attempts made to explain the overall X-ray spectrum using pair models.

Another, more complicated, way in which pairs might be involved is through what has been termed 'pair loading'. This is outlined in the following part. It involves considerable feedback on the acceleration process. The problem of so-called 'dead' electrons is also outlined. It concerns what happens to electrons that have cooled. They cannot just accumulate in the source or, through Compton scattering, they produce observable effects on the spectrum.

Many of the models for the spectrum of the X-ray emission regions in AGN produced so far are not able to account simply for the apparently standard power-law continuum observed over the 1 – 100 keV band (*e.g.* Turner [14]). The energy index of the spectrum $\alpha \sim 0.7$. Pair models for example generally predict a spectral index of 0.9 and so were appearing to be ruled out. Recent work however on the observed X-ray spectrum indicate that it consists of both 'direct' and 'reflected' components (Pounds [11]; Matsuoka [10]). The direct component does have a spectrum of about 0.9, so reviving the pair models (Zdziarski [15]). This is discussed in the final Section, with further comments on the particle acceleration process.

PAIRS AND THE COMPACTNESS PARAMETER

The general picture that is building up for the central engine of AGN is of a single massive compact object, a black hole, powered by accretion (or possibly by extraction of spin energy in some objects). The accretion flow is probably in the form of an accretion disc with a quasi-blackbody spectrum. The temperature of the disc material is then a few hundred thousand degrees.

The observational evidence for this picture is principally the strong variable X-ray component, which carries several tens per cent of the total power in many objects. (The work of Terlevich and others has shown that extreme stellar processes – multiple supernovae in dense gas – may simulate many of the properties seen in the optical and UV spectra of AGN.) The X-ray spectra are hard, as mentioned before, and strong variability, with a factor of 2 change in an X-ray luminosity of $\sim 10^{42}\,\mathrm{erg\,s^{-1}}$ being observed on a timescale of 300s (Matsuoka [10]) or even $\lesssim 50\,\mathrm{s}$ (Kunieda [9]). There is also a 'soft excess' observed in the spectrum below 1 keV which is identified with the accretion disc (Arnaud [1]; Turner [14]).

Most AGN that have been well-studied in the X-ray band appear to have a 2 – 10 keV spectral index of about 0.7. Their spectra also appear to turnover at about an MeV (although the data here are sparse and not very reliable). This raises the questions of why 0.7 and why an MeV? What we need to know is whether these are fundamental questions or simply the result of hard radiation being produced in a compact region.

One way in which this has been tackled is to search for mechanisms that give the observed spectrum in a robust manner from some simple input parameters. If successful, then the spectral shape of an AGN is not particularly informative about the fundamental workings of the central engine. The essential ingredients of most such models are soft photons and relativistic electrons. The soft photons may be from the accretion disc, which has a temperature close to the blackbody value, $kT_b = (L/R^2\sigma_{SB})$ where R is the size of the emission region. The relativistic electrons are due to some acceleration process. Since the protons in an accretion flow may attain energies up to m_pc^2, then it does not seem unreasonable that electrons are accelerated to high Lorentz factors, γ_{max}. Inverse Compton scattering of the soft photons by the electrons then leads to a hard spectrum extending to gamma-ray energies.

Superficially, this does not seem to account for a 0.7 index power law or an MeV turnover. As the electrons lose energy, they do create a steep elec-

tron spectrum which makes the photon index 0.5, but not 0.7. However, if the source is compact, then the gamma-rays can collide with the X-rays to produce electron-positron pairs. These then radiate so that the hardest radiation is degraded through a cascade of pairs and reprocessed into softer radiation. The threshold for the process is about an MeV, so a deficit of higher energy gamma-rays is expected and the MeV turnover can form.

The compactness of the region is defined in terms of the ability to make pairs. Basically, pairs are produced if the probability of photon-photon collisions is high. This is measured by the optical depth,

$$\tau_{\gamma\gamma} = n_\gamma \sigma_{\gamma\gamma} R,$$

where the X-ray photon density $n_\gamma > L/R^2 c m_e c^2$ and the cross-section $\sigma_{\gamma\gamma} \sim 0.2\sigma_T$. σ_T is the Thomson cross-section. Consequently, significant reprocessing of the power in the source occurs when the (dimensionless) compactness parameter,

$$\ell = \frac{L}{R} \frac{\sigma_T}{m_e c^3} \gtrsim 5.$$

This limit is exceeded by many AGN (Fig. 1).

The 'secondary' radiation from the pairs steepens the emergent X-ray spectrum at the expense of the gamma ray spectrum. Although it acts in the right sense to agree with the observations, detailed studies (Lightman [8]; Done [2]) have shown that pair production does not simultaneously give $\alpha \sim 0.7$ and an MeV turnover. Generally, if $\alpha \sim 0.7$ then there are too many gamma-rays, and if there is an MeV turnover, then $\alpha \gtrsim 0.9$. There is only a very narrow part of the parameter space ($\ell \sim 30$ and $\gamma_{max} \sim 200$) where some agreement is found with both the X-ray and gamma-ray spectra. Instead, the input electron spectrum may have the 'right' shape to produce the observed photon spectrum. All of these solutions appear to put the onus on the acceleration process for understanding the spectrum. I say appear, since there is another solution, to which I return later.

Another way in which the MeV turnover can be explained by pairs is to rely on 'pair loading' (Done [4]; see also Cavaliere [5]; Svensson [12]). This means that the pairs apply feedback to the acceleration process to cause the MeV turnover. To see how this might happen, consider that the acceleration process works on all the particles on the region. Then, if the available power is limited, as is likely, the production of pairs causes more particles to be accelerated and so the mean particle energy to drop, until a balance is reached. This tends to occur when the photon spectrum turns over around an MeV. It does not however appear to explain the spectral index in any simple manner.

A further problem that is generally ignored in discussions of compact hard sources is the 'dead electron' problem. This is the accumulation of cooled electrons (or pairs) which have lost their energy to radiation. If the Thomson depth in such pairs exceeds unity, which is easily attained, then electron scattering of hard radiation by the dead electrons produces features of characteristic shape – which are not observed. For example, a Thomson depth of τ_T in dead electrons will cause a break at an energy of $\tau^{-2} m_e c^2$, or at less than 20keV if $\tau > 5$. The standard way of overcoming this problem is to argue that there are few electrons in the source and that they are rapidly re-accelerated when on losing their energy. This does not help in a compact hard source since this just creates more electrons (and positrons) from photon-photon collisions. Nor does pair loading provide much improvement. The only solutions that we can devise (Done [4]), apart from that discussed in the next Section, are to argue that the cooled electrons are strongly clumped in the source, so that the covering fraction is low, to

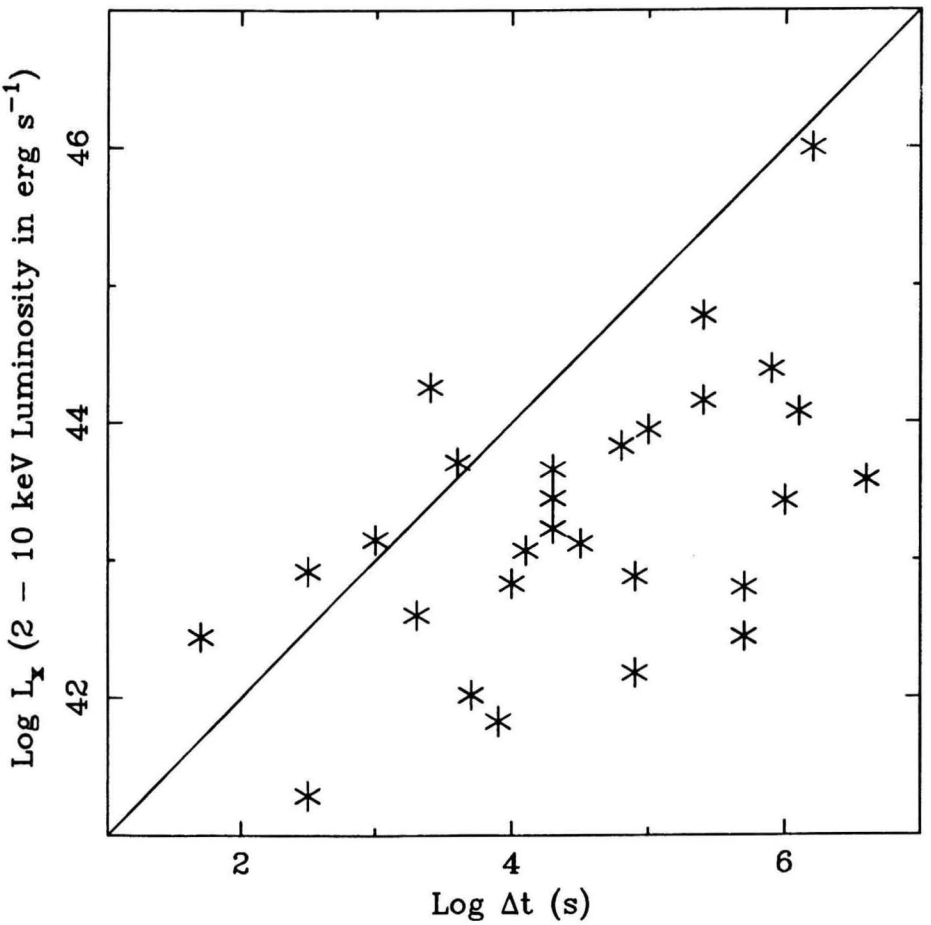

Figure 1. X-ray luminosity plotted against 2-folding variability timescale from Done (2). The diagonal line corresponds to $\ell = 5$ and is based only on the 2 – 10 keV luminosity. If, as is likely, the spectra extend to an MeV, then the line moves down by about a factor of 5 in luminosity. Pairs are then expected in most of the sources.

make the accelerator move rapidly or to appeal to rapid variations. In the last two possibilities, the source may just switch off once it has filled with electrons.

THE REFLECTED COMPONENT

The soft excess emission in AGN, if quasi-thermal, suggests that there is an optically-thick, cool ($T \sim 10^5$ K) accretion disc present in the central engine. The hard X-rays incident onto such material will be photo-absorbed and electrons scattered, creating a reflection spectrum. At low energies (less than about 5 keV) few X-rays will be scattered back into our line of sight because the photoelectric absorption cross-sections of disc matter are so high. Only above about 10 keV is there a substantial albedo of about 30 per cent. It drops again above about 100 keV since the Compton effect significantly reduces the energy of back-scattered photons. For photons between 7.1 and about 9 keV there is a strong chance of absorption by iron ions, which results in the emission of a fluorescent

photon at 6.4 keV. The net reflected spectrum is then one of rising flux below 10 keV, with a strong iron line at 6.4 keV, bending over to follow the incident spectrum between about 30 and 100 keV and falling off at higher energies.

The observer sees a combination of the direct spectrum and the reflected spectrum. This predicted spectrum (Guilbert [6]; Lightman [7]) has now been confirmed by observations with the GINGA satellite (Pounds [11]; Matsuoka [10]), which show the iron line and the beginning of the relection hump above 10 keV. The interesting point here about the multi-component spectrum is that although the observed energy index is about 0.7, the addition of the flat reflection spectrum to the direct spectrum means that the direct spectrum must be steeper than the observed one. The required spectral index is now $\alpha = 0.9$, not 0.7, and so the pair models are revived (Zdziarski [15]). Indeed, the pair models discussed above saturate at an energy index of 0.9 to 1 in the case of very compact sources. The steepening effects of the pair cascade and of Thomson down-scattering by the cooled pairs (before they annihilate) is masked by the flat reflection hump.

SUMMARY

At the present time it looks as if electron-positron pairs are important in AGN. The simple pair models in which an accelerator injects relativistic electrons into the emission region, which also contains soft photons, perhaps from an accretion disc, appear to give good spectral agreement with the observations, provided that there is a also a reflected component. It means that the primary spectrum produced by the accelerated electrons is almost totally hidden by the radiation of pairs created in photon-photon collisions and by the reflected continuum. This is both good news and bad news; good because we may at last be understanding the origin of the continuum, bad because it tells us very little about the accelerator itself.

The accelerator must take electrons to Lorentz factors of 10^3 or higher very quickly. Much faster than the cooling time which is presumably much less than the observed variability time (at least $\ell\gamma$ times less), and so less than 50s in the case of NGC 6814. The effects of dead electrons are perhaps minimized if they are pairs and annihilate. Whether there is any feedback such as pair loading is not yet clear.

Perhaps we shall learn more about the operation of the central engine, rather than about radiation from a compact region, when the Gamma-Ray Observatory is operational and when we begin to understand the rapid variability common to the sources.

REFERENCES

1. Arnaud, K.A. *et al.* 1985. *Mon. Not. R. astr. Soc.*, bf 217, 105.
2. Done, C. & Fabian, A.C., 1989. *Mon. Not. R. astr. Soc.*, **240**, 81.
3. Done, C., Ward, M.J., Fabian, A.C., Kunieda, H., Tsuruta, S., Lawrence, A., Smith, M.G. & Wamsteker, W., 1990. *Mon. Not. R. astr. Soc.*, **243**, 713.
4. Done, C., Ghisellini, G. & Fabian, A.C., 1990. *Mon. Not. R. astr. Soc.*, **245**, 1.
5. Cavaliere, A., 1982. In 'Plasma Astrophysics', SP-161, p97, ESA.
6. Guilbert, P.W. & Rees, M.J., 1988. *Mon. Not. R. astr. Soc.*, **233**, 475.
7. Lightman, A.P., & White, T.R., 1988. *Astrophys. J.*, **335**, 57.
8. Lightman, A.P., & Zdziarski, A. A., 1987. *Astrophys. J.*, **319**, 643.
9. Kunieda, H., Turner, T.J., Awaki, H., Kojama, K., Mushotzky, R. & Tsusaka, Y., 1990. *Nature*, **345**, 786.
10. Matsuoka, M., Yamauchi, M., Piro, L. & Murakami, T., 1990. *Astrophys. J.*, **361** 440.
11. Pounds, K.A. *et al.* 1990. *Nature*, **344**, 132.
12. Svensson, R., 1987. *Mon. Not. R. astr. Soc.*, **227**, 403.

13. Tennant, A.F., Mushotzky, R.F., Boldt, E.A. & Swank, J.H., 1981. *Astrophys. J.*, **251**, 15.
14. Turner, T.J. & Pounds, K.A., 1988. *Mon. Not. R. astr. Soc.*, **232**, 463.
15. Zdziarski, A., Ghisellini, G., George, I.M., Svensson, R., Fabian, A.C. & Done, C., 1990. *Astrophys. J.*, **363**, L1.

Institute of Astronomy, Madingley Road, Cambridge CB3 0HA, U.K.

G. Hasinger

X-ray Diagnostics of Accretion Disks

1 Introduction

Within this article the very wide field of accretion phenomena observed in X-rays is restricted to bright low-mass X-ray binaries (LMXB), where recent observational evidence leads to a global picture that for the first time sheds light on the innermost regions of an accretion disk. LMXB are actually very similar to cataclysmic variables, one just has to replace the central white dwarf by a neutron star. Given a small enough neutron star magnetosphere the disk then reaches to much smaller radii and therefore much higher temperatures. Consequently, radiation pressure can become important in the inner part of accretion disks around neutron stars.

Table 1 from the recent review by van der Klis (1989b) shows the known LMXB sorted according to apparent X-ray brightness and marked as "Z-sources" and "Atoll-Sources" according to the classification scheme by Hasinger and van der Klis (1989). The class of LMXB we are concerned here – the Z-sources – belong to the brightest X-ray objects in the sky. They are characterized by Z-shaped X-ray colour-colour diagrams and comparatively narrow peaks of quasi-periodic oscillations (QPO) at frequencies between 5 and 50 Hz in their power spectra.

In the recent years it turned out that in the handful Z-sources nature has provided us with a magnificent laboratory to study the innermost regions of accretion disks – not at least at X-ray wavelengths.

Table 1. The brightest low-mass X-ray binaries (adapted from van der Klis, 1989b)

Source Name	I_x [μJy]	P_{orb} [hr]	Type A/Z	Phenome-nology
Sco X-1 (1617-155)	12400	19.2	Z	QPO
GX 5-1 (1758-259)	1200	—	Z	QPO
GX 349+2 (1702-363)	780	—	Z	QPO
GX 17+2 (1813-140)	680	19.8?	Z	QPO, (bu)
GX 9+1 (1758-205)	650	—	A	—
GX 340+0 (1642-455)	490	—	Z	QPO
GX 3+1 (1744-265)	430	—	A	(QPO),(Bu)
Cyg X-2 (2142+380)	430	235.	Z	QPO,(bu)
GX 13+1 (1811-171)	340	—	A	—
GX 9+9 (1728-169)	290	4.2	A	Mo
4U 1820-30 (NGC 6624)	260	0.2	A	(QPO),(Bu),Mo
4U 1705-44	260	—	A	Bu
4U 1636-53	220	3.8	A	Bu
Ser X-1 (1837+049)	200	—	-	Bu
GCX-1 (1742-294)	170	—	A	Bu?
4U 1728-33	170	—	A	Bu
GX 339-4 (1659-487)	160	14.8?	-	QPO,BH?
4U 1735-44	160	4.6	A	Bu

2 X-ray Spectrophotometry

The technique we utilize here is rather simple and similar to the UBV spectroscopy in optical astronomy. The raw X-ray spectrum is divided into three rather broad energy bands - typically 1-3 keV, 3-6 keV and 6-15 keV. From the ratio between the middle and the soft X-ray band a so-called *soft colour* is derived, the ratio between the hard and the middle X-ray band gives the *hard colour.*

Figure 1 shows X-ray data from Cyg X-2 measured over four days with the Japanese satellite *Ginga* during a multifrequency campaign in 1988 (from Hasinger et al., 1990, hereafter HA90). The lowest panel shows the X-ray intensity as a function of time, the middle one gives the hard colour. The uppermost panel shows the times of simultaneous observations in other wavebands (see below). Both X-ray intensity and X-ray colour vary quite erratically on a variety of

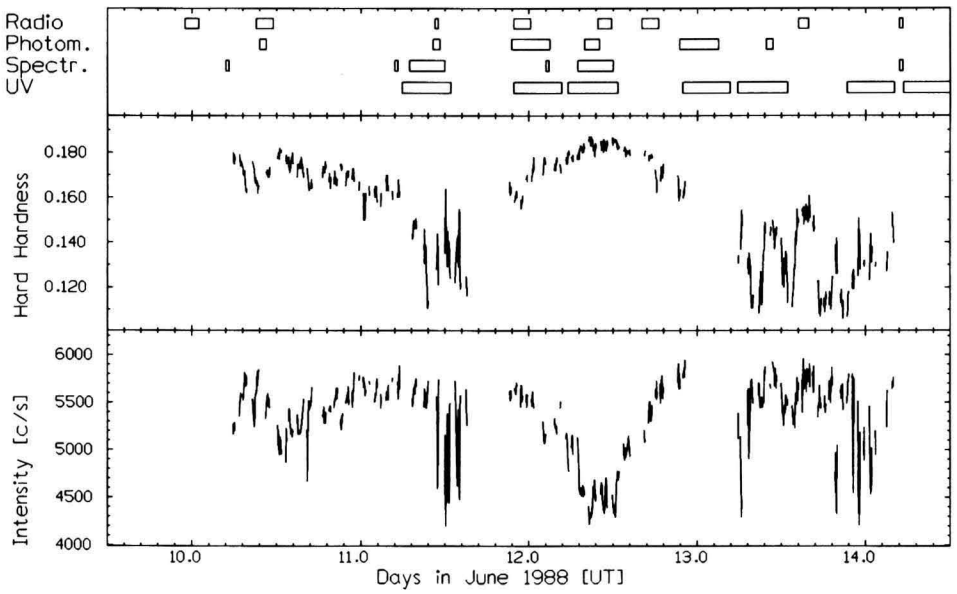

Fig. 1. X-ray lightcurve (lower panel) and hard colour (middle panel) of Cyg X-2 as a function of time for the 4-day Ginga observation in June 1988. The upper panel shows the time interval of observations in other wavebands. Taken from Hasinger et al., 1990

different timescales. However, the source has been observed in different modes of activity. Phases of slowly variing intensity and hardness are interrupted by periods of rapidly variing colour or intensity.

3 The "Z-Diagram"

The chaotic nature of the temporal variability changes into very well structured and characteristic patterns when one plots the same data into a colour-intensity diagram (similar to the Hertzsprung-Russel diagram of optical astronomy) or into a colour-colour diagram. These two diagrams are given in Figs. 1 and 2. Now three well separated "spectral branches" are visible which form an elongated "Z-shape" in the colour-colour diagram which gave these sources their name.

The three branches are called "horizontal branch" (HB; upper left) where the hard colour stays almost constant while the intensity varies, "normal branch" (NB; middle) where both soft and hard colour change in a correlated fashion while the X-ray intensity stays almost constant, and "flaring branch" (FB; bottom) which again is characterized by a correlated variation of soft and hard colour, however along a different track. (The dramatic intensity decrease along the flaring branch is peculiar to Cyg X-2, in most other Z-sources a similarly dramatic intensity increase has been observed, thus the term "flaring".)

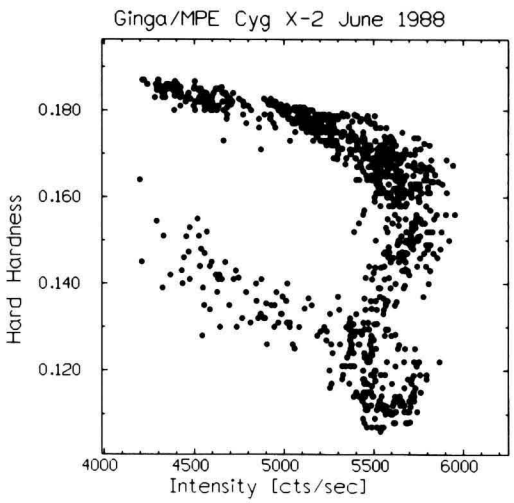

Fig. 2. Colour-intensity diagram from the data in Fig. 1 (HA90)

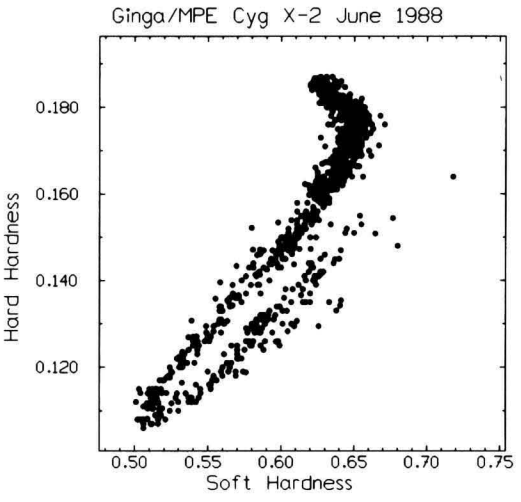

Fig. 3. Colour-colour diagram for the same data (HA90).

The same technique has been applied to a large body of data from the European X-ray satellite EXOSAT (Hasinger and van der Klis, 1989, hereafter HK89) and a total of 6 bright LMXB have been identified as Z-sources. Figure 4 shows their colour-colour diagrams which display a similar complete Z-pattern or at least fragments of it.

The existence of these characteristic, well confined tracks of spectral and intensity evolution calls for a simple explanation. One interpretation assumes that the observed changes are governed by the variation of a single parameter, which most likely is the mass-accretion rate $\dot{M}$ fed through the disk onto the central engine (Priedhorsky et al., 1986). If this is the case, then there are only two choices how $\dot{M}$ can vary along the "Z": either in the "positive" sense (from the upper left to the lower right) or in the opposite direction. In order to solve this question simultaneous observations in other wavebands had to be performed.

4 Observations in Other Wavebands

Simultaneously with the X-ray measurements two multifrequency campaigns with observations of Cyg X-2 in the UV, optical, and radio range have been performed (see figure 1). The IUE observations (Vrtilek et al., 1990), the optical spectroscopy from La Palma (van Paradijs et al., 1990) and the VLA radio measurements (Hjellming et al., 1990) will be published together with the Ginga X-ray data (HA90) soon. Luckily enough the source collaborated: it displayed all three spectral states during the simultaneous observations and

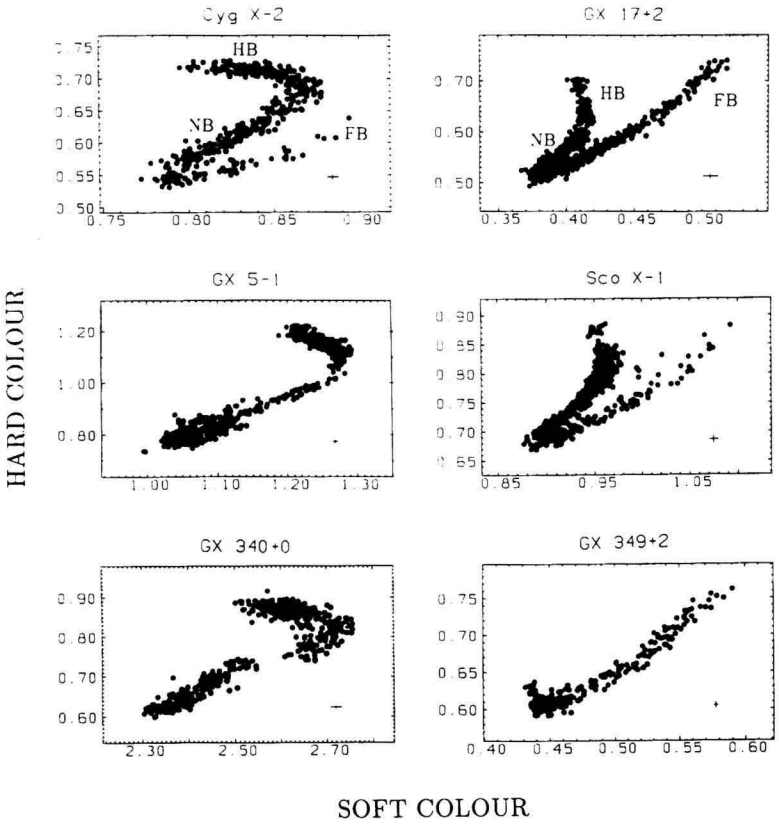

Fig. 4. Colour-colour diagram of EXOSAT data from 6 Z-sources (HK89)

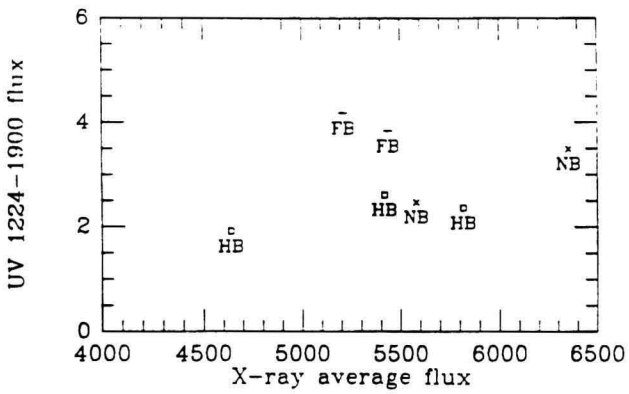

Fig. 5. UV continuum flux as (IUE) versus X-ray flux (Ginga). The X-ray spectral state is indicated for each measurement. The UV flux increases continuously from horizontal to normal branch. Taken from Vrtilek et al., 1990

in all wavebands clear correlations with the source position in the Z-diagram were found.

The UV continuum and line flux increase steadily by a factor of about 2 as the source moves from the horizontal branch to the flaring branch (Vrtilek et al., 1990, see fig. 5). The same is true for the equivalent width of the He II λ4686 and λ4640 Bowen emission lines as well as the Hβ and Hγ absorption lines (van Paradijs et al., 1990). A similar behaviour was found already in the seventies for Sco X-1, where the optical flux increases by about one magnitude from the top to the bottom of the normal branch normal and further up the flaring branch (Canizares et al., 1975). Since the optical and UV flux of the X-ray irradiated disk is dominated by reprocessed radiation, one can conclude that the X-ray (or EUV) illumination of the disk increases from HB to FB – and thus the mass accretion rate has to increase in the same way (Vrtilek et al., 1990, HA90)

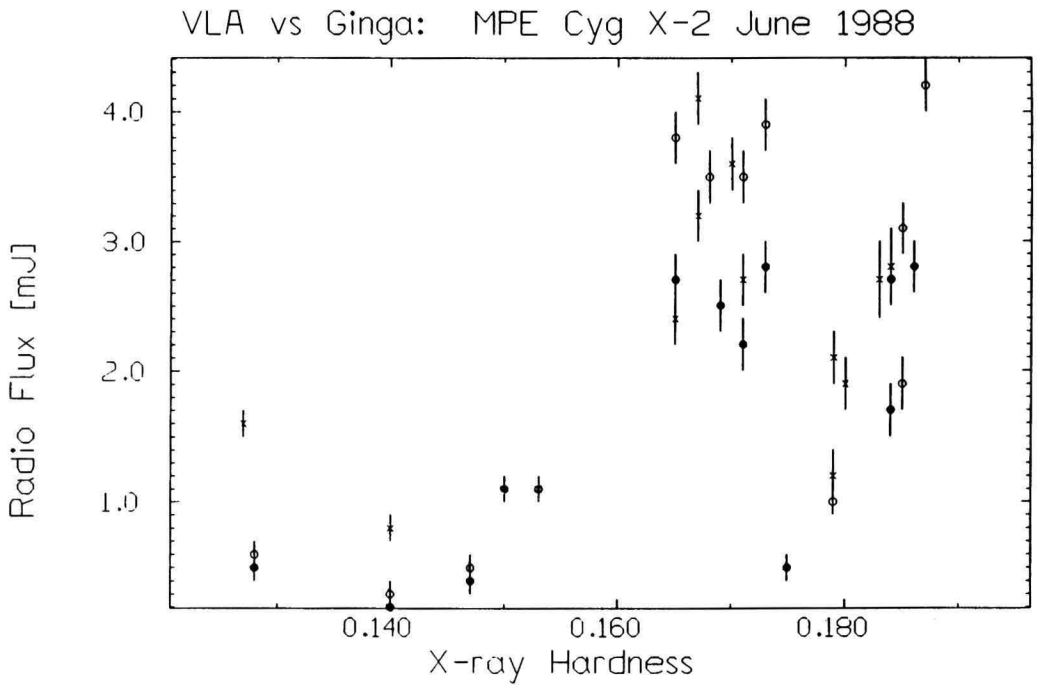

Fig. 6. Radio flux density (VLA) versus X-ray hardness (Ginga). Hardness is the same 'hard hardness' as in fig. 1-3, thus the source is on the horizontal branch for a hardness larger than 0.16. The radio flux density is high and strongly variable on the horizontal branch and low and quiescent on the normal and flaring branch.

The radio flux behaves in a completely different manner: as Figure 6 shows, the radio flux is loud and highly variable on the horizontal branch, and quiet and quiescent on the normal and flaring branch (Hjellming et al., 1990). This is similar as observed before in the radio/X-ray correlation in GX 17+2 (Penninx et al., 1988).

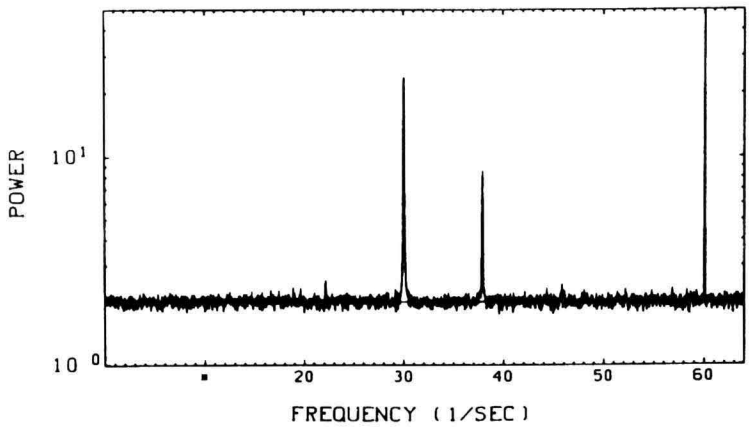

Fig. 6. Power spectrum of the Crab Nebula and its pulsar as observed with EXOSAT. The fundamental pulsar frequency (30 Hz) and its first harmonic (60 Hz) are visible as sharp spikes. A third peak is seen at a frequency of 38Hz, it is the aliased signal of the second harmonic (90 Hz).

5 Quasi-Periodic Oscillations and Noise

The last pieces to solve the puzzle of the Z-sources comes from a systematic analysis of their X-ray flickering in the sub-second range. As diagnostic tool the segmented Fourier analysis technique (see van der Klis, 1989a) is utilized: the observation is divided into small continuous stretches of data (typically 8-32 seconds), the power spectra of which are averaged to enhance the statistical significance of the signal. If this method is applied to the 33ms- pulsar in the Crab Nebula a series of sharp spikes at the fundamental pulsar frequency and its harmonics is observed (see figure 6) on top of a constant (white noise) signal which is due to the counting statistics of the data.

In a search for possible millisecond pulsars in low-mass X-ray binaries van der Klis et al. (1985) analysed data of the bright galactic bulge source GX 5-1. However, instead of several sharp spikes they found a single broad peak in the power spectra, signalling that not a strictly periodic, but a *quasi periodic oscillation* (QPO) is present in the data. Additionally a component called 'red noise' or 'low-frequency noise' (LFN), i.e. excess power which rises continuously towards the lowest frequencies, is visible in the power spectra (see figure 7).

Moreover, as the X-ray source intensity varies, the centroid frequency of the QPO peak is not stable but varies as a function of time, roughly in the frequency range 20-45 Hz – the two quantities go hand in hand.

It turns out, that the presence of QPO peaks in the power spectra is a class property of all Z-sources (see HK89). However, the rapid, intensity-dependent QPO are mainly visible in the horizontal branch. As soon as the source 'turns the corner' into the normal branch the power spectra change dramatically. Figure 8 shows a comparison of two power spectra of Cyg X-2, taken in the horizontal and normal branch, respectively. Compared to figures 6 and 7 the

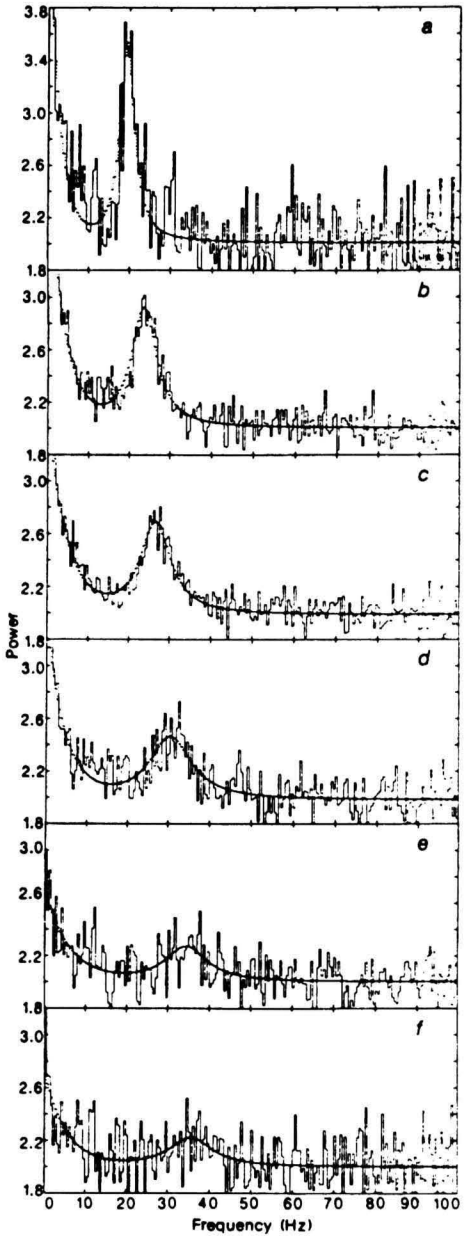

Fig. 7. Six different power spectra of the bright galactic bulge source GX 5-1 in the same representation as figure 6. The X- ray source intensity rises from approximately 2200 cts/s to 3800 cts/sec in the EXOSAT detector from top to bottom (from van der Klis et al., 1985).

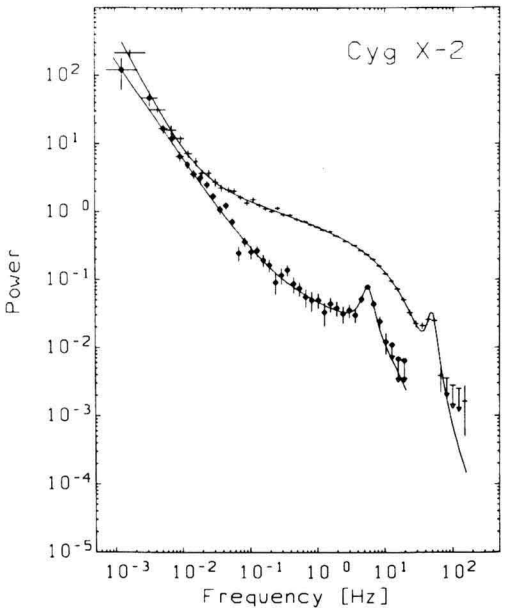

Fig. 8. Two power spectra of the Z-source Cyg X-2 taken in the horizontal (upper) and normal (lower) branch. The power spectra are displayed on a logarithmic scale, with the white noise level due to counting statistics removed. Note that the power spectra are not shifted with respect to each other (from Hasinger, 1987a).

power spectra here are displayed on a logarithmic scale and the white noise due to counting statistics has been subtracted. One sees, that the strong and characteristically shaped low-frequency noise component, dominating in the horizontal branch at frequencies 0.05 - 50 Hz, is almost completely gone in the normal branch. The same is true for the fast (50 Hz) QPO peak. Roughly in the middle of the normal branch another, slower QPO peak occurs, its centroid remains rather stable at frequencies 5-7 Hz throughout the lower part of the normal branch.

These dramatic changes of the different power spectral components are further highlighted in figure 9 where all Cyg X-2 power spectra from the EXOSAT and Ginga X-ray observations have been systematically analysed to trace the source behaviour throughout the whole Z-diagram. Particularly interesting seems the variation of the LFN, which first increases on the horizontal branch and the abruptly dies out close to the HB/NB-corner. This transition has become one of the most important ingredients in the interpretation discussed below. The changes in the HBO (horizontal-branch oscillation) and NBO (normal-branch oscillation) power are anticorrelated, while the former continuously decreases from HB to NB, the latter increases abruptly along the normal branch and is most prominent in the middle of the NB. There are actually NB power spectra which show both HBO and NBO peaks simultaneously (HA90).

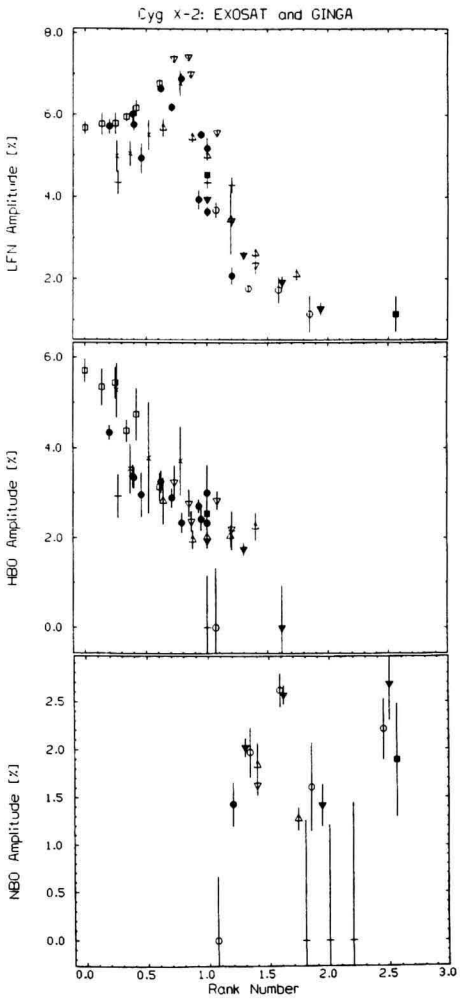

Fig. 9. Variation of the main power spectral components of Cyg X-2. The figures display the rms. variability in the red noise (upper), in the horizontal-branch QPO (middle) and in the normal- branch QPO (lower panel) as a function of position along the Z- diagram. The abscissa (called 'rank number') gives an arbitrary coordinate that increases monotonically from the left of the HB (0.0) over the HB/NB-transition (1.0) and the NB/FB-transition (2.0) to the upper right of the flaring branch (3.0), following the change in mass-accretion rate. Data from the EXOSAT and Ginga X-ray satellites have been merged (Hasinger, et al. 1990, in prep.

The same analysis applied to other Z-sources reveals almost carbon-copy results. Figure 10 shows a selection of power spectra from the same set of sources the colour-colour diagrams of which are given in figure 4 (HK89). Where available, power spectra have been accumulated separately for each branch. The sense and magnitude of variation in the different power spectral components is very similar to Cyg X-2.

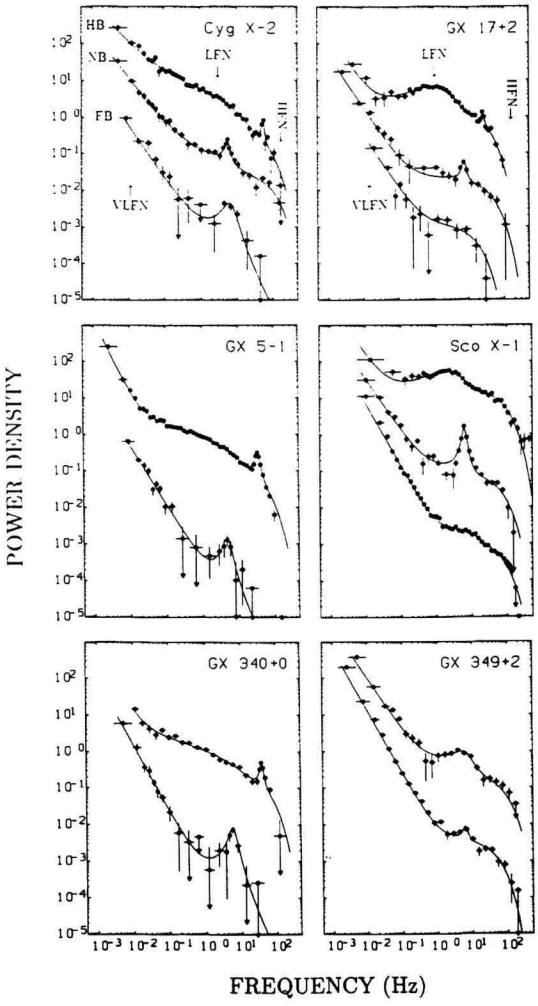

Fig. 10. Power spectra of six Z-sources in the different spectral branches, corresponding to figure 4. Power spectra are given on logarithmic scales with white noise background subtracted. For clarity power spectra from different branches (from top to bottom: HB, NB, FB) are shifted by two decades with respect to each other (from HK89).

6 The Big Picture: a Jumping Accretion Disk ?

Figure 11 summarises the complex variation of some of the observable quantities as a function of mass accretion rate along the Z-diagram: $\dot{M}$ increases monotonically from HB to FB by about a factor of 2 (panel 1). The UV and blue optical light and the emission lines follow hand in hand (panel 2). This is also true for the X-ray flux on the horizontal branch, however, at the HB/NB

transition it starts to deviate from this one-to-one correspondence (panel 3). The latter three quantities all show marked transitions close to the corner between horizontal and flaring branch: horizontal-branch QPO and normal branch QPO change importance in the upper normal branch, where they can coexist simultaneously (panel 4). The LFN, which is strong on the HB, dies out at the same transition (panel 5; see also Figure 9), and finally, strong nonthermal radio flares occur only on the horizontal branch.

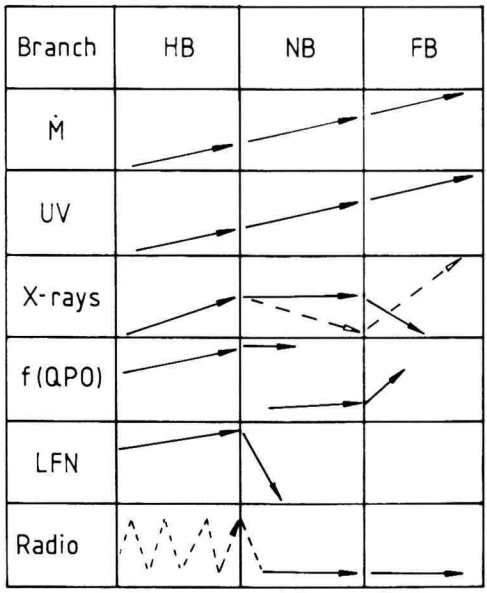

Fig. 11. Schematic display of the variation of important observables and the mass-accretion rate as a function of source position along the Z-profile (see text) (from HA90).

We have now collected the ingredients neccessary to to interpret the complex spectral, power spectral and multifrequency behaviour of Z-sources. Most important is the knowledge that the observed variations are most likely driven by a simple change of mass accretion rate. The second most important feature - at least in my judgement - is the dramatic phase transition when the source moves from the horizontal to the normal branch. X-ray spectrum, and intensity, noise and QPO as well as the radio flux all change dramatically and almost simultaneously there. These phenomena suggest a scenario (Hasinger 1988, HA90), which is sketched in Figure 12, and which is similar to the 'unified QPO model' by Lamb (1989, 1990) in some important features.

At low accretion rates (HB) the source starts out in a configuration with a geometrically thin inner disk which is cutting into a small magnetosphere as shown in figure 12a. This is the geometry required for the 'accretion modulated beat frequency model' for the horizontal-branch QPO (Alpar and Shaham, 1985; Lamb et al., 1985). Turbulence at the magnetospheric boundary

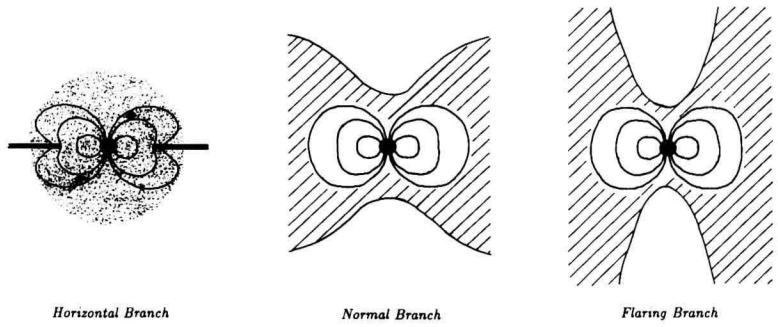

Fig. 12. Schematic display of the accretion geometry in the adopted scenario for the (a) horizontal, (b) normal, and (c) flaring branch (from HA90).

produces clumps, causing an instationary accretion which is responsible for the LFN. Interaction between the clumps in Keplerian motion and between the rotating neutron star magnetic field cause quasi-periodic intensity enhancements leading to HBO. The turbulent magnetospheric boundary may also be the site of electron acceleration which we observe through the HB radio flares.

When a critical value of mass accretion rate is exceeded, but still well below the neutron star Eddington limit, the inner disk is suddenly flaring up to form a thick torus (see Fig. 12b), engulfing the whole magnetosphere (Hasinger, 1988; HK 1989). All the dramatic changes observed at this transition can be explained by this postulated instability. The additional cool disk material in the line of sight causes the softening of the observed spectrum by Compton degradation (Hasinger, 1987b; Lamb, 1990). The interface between the disk torus and the magnetosphere is probably much less turbulent than in the horizontal branch and matter can accrete smoothly onto the neutron star. Therefore LFN and HB QPO are reduced in strength (although the existence of weak HB QPO in the upper normal branch indicates that some inhomogeneities are still present). The flux of energetic electrons producing the HB radio flares may be quenched in two ways: first, the reduced turbulence at the magnetospheric boundary may be less efficient in accelerating particles, and second, the thick inner disk torus will trap the electrons.

Down the normal branch the mass accretion rate is increasing even further and approaches the Eddington limit. At this moment the effective gravity is reduced by the strong radiation pressure, enough to slow down the dynamic timescales so that sound waves (Hasinger 1987a, Alpar et al., 1990) or other resonances in the flow (Lamb 1989, 1990) will become important and possibly form the 6 Hz normal-branch QPO.

Finally, on the flaring branch the mass accretion rate has increased above the Eddington limit and matter will be ejected, probably through the narrow funnel formed by the thick inner disk torus (see Fig. 12c). The funnel might

also effectively beam the X-ray radiation, so that the line-of sight inclination becomes important for a distant observer. This may explain the different intensity behaviour on the flaring branch between e.g. Sco X-1 and Cyg X-2 (Hasinger et al., 1989)

References

Alpar, M.A., Shaham, J.: 1985, *Nature* **316**, 239
Alpar, M.A., Hasinger, G., Shaham, J., Yancopoulos, S., 1990 (in prep.)
Canizares C.R. et al.: 1975 *Ap. J.* **197**, 457
Hasinger, G.: 1987 a, *Astron. Astrophys.* **186**, 153.
Hasinger, G.: 1987 b, *IAU Symp.* **125**, 333.
Hasinger, G.: 1988 Proc. Symp. *"Physics of Neutron Stars and Black Holes"*, Tokyo: Universal Academy Press, p. 97
Hasinger, G., Priedhorsky, W.C., Middleditch, J.: 1989, *Ap. J.* **337**, 843.
Hasinger, G., van der Klis, M.: 1989, *Astron. Astrophys.* **225**, 79
Hasinger, G., van der Klis, M., Ebisawa, K., Dotani, T., Mitsuda, K.: 1990 *Astron. Astrophys.* (in press)
Hjellming, R.M., Han, X.H., Cordova, F.A., Hasinger, G.: 1990 *Astron. Astrophys.* (in press)
Lamb, F.K., Shibazaki, N., Alpar, M.A., Shaham, J.: 1985 *Nature* **317**, 681
Lamb, F.K.: 1989, Proc. 23rd ESLAB Symposium, ESA SP-296, Part 1., p. 215
Lamb, F.K.: 1990, *Ap. J.* (in press)
Penninx, W., Lewin, W.H.G., Zijlstra, A.A., Mitsuda, K., van Paradijs, J., van der Klis, M.: 1988 *Nature* **336**, 146
Priedhorsky, W., Hasinger, G., Lewin, W.H.G., Middleditch, J., Parmar, A., Stella, L., White, N.: 1986, *Ap. J. Lett.* **306**, L91.
Shakura, N.I., Sunyaev, R.A.: 1973 *Astron. Astrophys.* **24**, 337
Van der Klis, M., Jansen, F., van Paradijs, J., Lewin, W.H.G., van den Heuvel, E.P.J., Trümper, J.E., and Sztajno, M.: 1985 *Nature* **316**, 225.
Van der Klis, M.: 1989a, Proc. NATO ASI *"Timing Neutron Stars"*, Çeşme, Turkey. Dordrecht: Reidel p.27
Van der Klis, M.: 1989b, *Ann. Rev. Astron. Astrophys.* **27**, 517
Van Paradijs, J., Allington-Smith, J., Callanan, P., Charles, P.A., Hassal, B.J.M., Machin, G., Mason, K.O., Naylor, T., Smale, A.P.: 1990 *Astron. Astrophys.* (in press)
Vrtilek, S.D., Raymond, J.C., Garcia, M.R., Verbunt, F., Hasinger, G., Kürster, M.: 1990 *Astron. Astrophys.* (in press)

This article was processed by the author using the TEX Macropackage from Springer-Verlag.

Max-Planck-Institut für extraterrestrische Physik, 8046 Garching, FRG

F. K. Lamb and P. Ghosh

Interaction of Accretion Disks with Magnetospheres

ABSTRACT. Disk-magnetosphere interaction strongly affects the observable properties of magnetic compact stars accreting from disks. This article reviews some of the physical processes that are thought to be important in low-mass binary systems containing weakly magnetic neutron stars. We summarize recent work on the interaction of the inner disk with the stellar magnetic field in such systems and on a unified model of their X-ray spectral states and quasi-periodic intensity oscillations. Finally, magnetospheric mechanisms are described that may accelerate particles to GeV or even TeV energies.

1. INTRODUCTION

Interaction of the inner part of the accretion disk with the magnetic field of the star plays an important role in determining the observable properties of compact stars accreting from disks. This article reviews some of the physical processes that are thought to be important in low-mass X-ray binaries (LMXBs) containing weakly magnetic accreting neutron stars. These processes include electrodynamic interaction of the disk plasma with the stellar magnetic field, termination of the Keplerian disk flow by magnetic stresses, creation of a compact central corona surrounding the magnetosphere, Comptonization of radiation produced near the neutron star, and acceleration of charged particles to high energies.

In §2 we summarize recent work on the interaction of the inner disk with the stellar magnetic field in binary systems containing weakly magnetic neutron stars. We describe various processes by which the accretion disk interacts with the stellar magnetic field, the generation of toroidal magnetic fields in the magnetosphere, and termination of the Keplerian disk flow by the interaction.

In §3 we describe recent work on a unified model of the X-ray spectral states and quasi-periodic intensity oscillations (QPOs) of LMXBs. In this model, interaction of the disk with the small magnetosphere produces a hot central corona around the magnetosphere. When the luminosity approaches the Eddington critical luminosity, a cooler, more extensive corona forms above the inner part of the disk, and the neutron star begins to accrete matter from this corona as well as from the disk itself. Interaction of the photons from the neutron star with the inflow from the corona shapes the X-ray spectrum and can produce quasi-periodic intensity oscillations.

Finally, in §4 we describe several mechanisms that may accelerate particles to GeV or even TeV energies within the magnetosphere. These mechanisms include

acceleration by electric fields produced by interruption of field-aligned currents within the magnetosphere, formation of double layers, and release of stored magnetic energy via reconnection. Interaction of the resulting energetic charged particles with accreting matter may produce GeV or even TeV γ-radiation.

2. DISK-MAGNETOSPHERE INTERACTION

The interaction between the plasma in the accretion disk and the stellar magnetic field involves a variety of physical processes. We first describe current models of the inner part of geometrically-thin accretion disks and then discuss some of the physical processes by which the plasma in the inner part of the disk may interact with the stellar magnetic field. Next, we describe how these processes have been incorporated into a quasi-steady accretion flow model. Finally, we summarize the results of recent work on disk accretion by weakly magnetic neutron stars.

2.1 The Inner Part of Accretion Disks

The standard α-model of geometrically-thin, optically-thick accretion disks (62,63) divides naturally into three distinct parts: an "outer" part, where gas pressure exceeds radiation pressure and free-free absorption is more important than scattering; a "middle" part, where gas pressure exceeds radiation pressure but electron scattering is the dominant source of opacity; and an "inner" part, where electron scattering is the dominant opacity source and radiation pressure exceeds the gas pressure.

The structure and stability of the outer and middle parts of the α-disk are comparatively well understood. Cooling is efficient in these parts, and the disk is therefore quite thin ($h/r \sim 10^{-2}$–10^{-3}). The structure of the inner, radiation-pressure-dominated (RPD) part of the α-disk is much less clear. In particular, models of the RPD region that are optically thick in the vertical direction are thermally and viscously unstable if the shear stress is, as originally assumed, proportional to the *total* pressure (57,43,56,64,54). Because these models are unstable, alternative models of the inner part of the disk have been explored.

One of the first alternative models to be studied is the so-called β-model proposed by Cunningham (10), which assumes that the shear stress in the RPD region is proportional to the gas pressure alone. This model is both thermally and viscously stable. However, whether the shear stress can be proportional to the gas pressure in the RPD region remains uncertain, although it has been argued (72) that the shear stress produced by small-scale magnetic fields in the disk is proportional to the gas pressure, rather than the total pressure. Models in which the shear stress is proportional to the product of various fractional powers of the gas pressure and the total pressure have also been investigated (74,75).

An alternative approach has been to construct models of the inner disk that are *optically thin* in the vertical direction, in contrast to the models just described. Optically-thin models are much hotter than their optically-thick counterparts. As a result, gas pressure dominates radiation pressure. Also, the ions are typically much hotter than the electrons. Examples of such "two-temperature" disk models include the model proposed by Shapiro, Lightman, and Eardley (65), in which the electrons are cooled by Comptonization of an external source of soft photons, and so-called "Comptonized bremsstrahlung

Table 2.1 Models of the Inner Region of Accretion Disks

Disk Model	Thermal Modes	Viscous Modes
1T Opt thick GPD, shear stress $\propto P_{\rm tot}$	Stable	Stable
1T Opt thick RPD, shear stress $\propto P_{\rm tot}$	Unstable	Unstable
1T Opt thick RPD, shear stress $\propto P_{\rm gas}$	Stable	Stable
2T Opt thin GPD, Compt soft photons	Stable?[a]	Stable
2T Opt thin GPD, Compt brems	Stable?[a]	Stable

[a]The stability properties of these models are not yet certain (42,56,84,85).

models" (84,85), in which the dominant cooling mechanism is emission of bremsstrahlung which at high accretion rates is Comptonized by the electrons in the disk. In these models, the α prescription for the shear stress has generally been retained. In recent years, the effects of electron-positron pairs on such hot disk models have also been considered (41,30–32,76,84,85,6,7). Some essential features of the disk models described in this section are summarized in Table 2.1.

2.2 Physical Processes

Consider now the physical processes that create a couple between the disk flow and the neutron star. Near the inner edge of the Keplerian flow, the interface between the disk plasma and the magnetospheric plasma is Kelvin-Helmholtz unstable, as shown by Ghosh and Lamb (14–16; hereafter referred to as GL). Penetration of the Keplerian flow by the stellar magnetic field is assured if unstable modes grow to an amplitude comparable to the semi-thickness h of the disk. Modes with wavelengths λ greater than h can achieve such an amplitude while still in the linear regime. Since the growth times of the Kelvin-Helmholtz modes in the linear regime can be estimated analytically, using the MHD dispersion relation appropriate to the disk-magnetosphere interface, GL concentrated on long-wavelength modes. They found that near the inner edge of the disk, the growth time for long-wavelength Kelvin-Helmholtz modes is $\sim 10^{-5}$ times the radial drift time. Thus, there appears to be plenty of time for these modes to grow to sufficiently large amplitude to greatly disturb the disk surface and allow the magnetospheric magnetic field to mix with the disk plasma before the plasma drifts significantly inward. This mixing couples the stellar magnetic field and the disk.

The disk and the star are also coupled by turbulent diffusion of the stellar magnetic field into the disk (GL). This process is important in the region where the kinetic energy density of convective or turbulent motions in the disk exceeds the energy density of the stellar magnetic field just outside the disk. In this region one expects the stellar magnetic field to be entrained by the convective motions and carried into the disk. In order to make an estimate of the efficiency of this process, GL adopted a mixing length approach, assuming a diffusion coefficient $\sim 0.1\, u_t \ell_t$, where u_t is the turbulent velocity and ℓ_t is the length scale of the largest eddies. They found that the stellar magnetic field would

diffuse through the disk in a fraction $\sim 10^{-3}$ of the radial drift time. Thus, there appears to be ample time for the magnetic field to diffuse into the disk. Once inside the disk, magnetic field lines that were formerly above the disk can reconnect to magnetic field lines that were formerly below the disk, creating an additional couple between the disk and the neutron star just outside the inner edge.

A third process that couples the disk and the star is reconnection of the stellar magnetic field to magnetic fields in the disk (GL). The shear flow in the disk amplifies and reconnects any seed field in the stream of plasma that feeds it, creating closed loops of magnetic flux within the disk. These flux loops are continually distorted by convection and turbulence within the disk, and subdivided by reconnection (see [72] and references therein). Even if there were no magnetic field threading the disk plasma initially, turbulent diffusion of the magnetospheric magnetic field into the disk would create such a field. Once there are magnetic flux loops within the disk, either because magnetic fields were present initially or because the stellar magnetic field earlier diffused into the disk, it is be energetically favorable for the stellar magnetic field to reconnect to the magnetic fields in the disk. GL estimated that the time scale for this to occur near the inner edge of the disk is $\sim 10^{-3}$ times the radial drift time. In the usual reconnection picture, almost all of the magnetic flux is conserved, but the topology is completely changed. As a result, field lines that initially formed closed loops in the disk now connect to the star, producing a couple between the disk and the star.

In summary, even if the Keplerian disk plasma is not initially coupled to the stellar magnetic field, a significant couple will develop in a time short compared to the radial drift time.

The difference in the angular velocities of the star and the disk generates enormous electromotive forces that can drive large electrical currents within the magnetosphere if there is even a small density of charged particles there. Due to the plentiful supply of accreting plasma, the magnetosphere is expected to be almost exactly electrically neutral, and hence the electrical currents driven by the electromotive forces are conduction currents. The resulting $\mathbf{j} \times \mathbf{B}$ forces act on the matter in the star, the magnetosphere, and the disk to reduce their relative motion. The character of this electrodynamic interaction depends on the distribution of electrical resistance along the current paths.

GL examined this question and found that the electrical conductivity along field lines in the magnetosphere is high whereas the cross-field conductivity is likely to be much lower. They therefore concluded that cross-field currents are more likely to flow in the disk and the star than in the magnetosphere. As a result, they arrived at a system of field-aligned currents similar to the polar-cap ionospheric current system that is thought to couple the rotation of Jupiter's ionosphere to its magnetospheric sheath (27,28).

The velocity and magnetic fields in the picture proposed by GL are shown in the top panel of Figure 2.1. The azimuthal motion of the disk plasma relative to the star twists the stellar magnetic field, generating a toroidal component. The resulting magnetic stress acts to synchronize the orbital motion of the disk plasma and the rotation of the star. In an analogous manner, the radial inward motion of the plasma pinches the stellar magnetic field inward, partially screening the stellar magnetic field from the disk.

An equivalent circuit with lumped circuit elements is shown in the bottom panel of Figure 2.1. The rotation of the neutron star and the orbital motion of the disk plasma through the magnetic field generate the electromotive forces

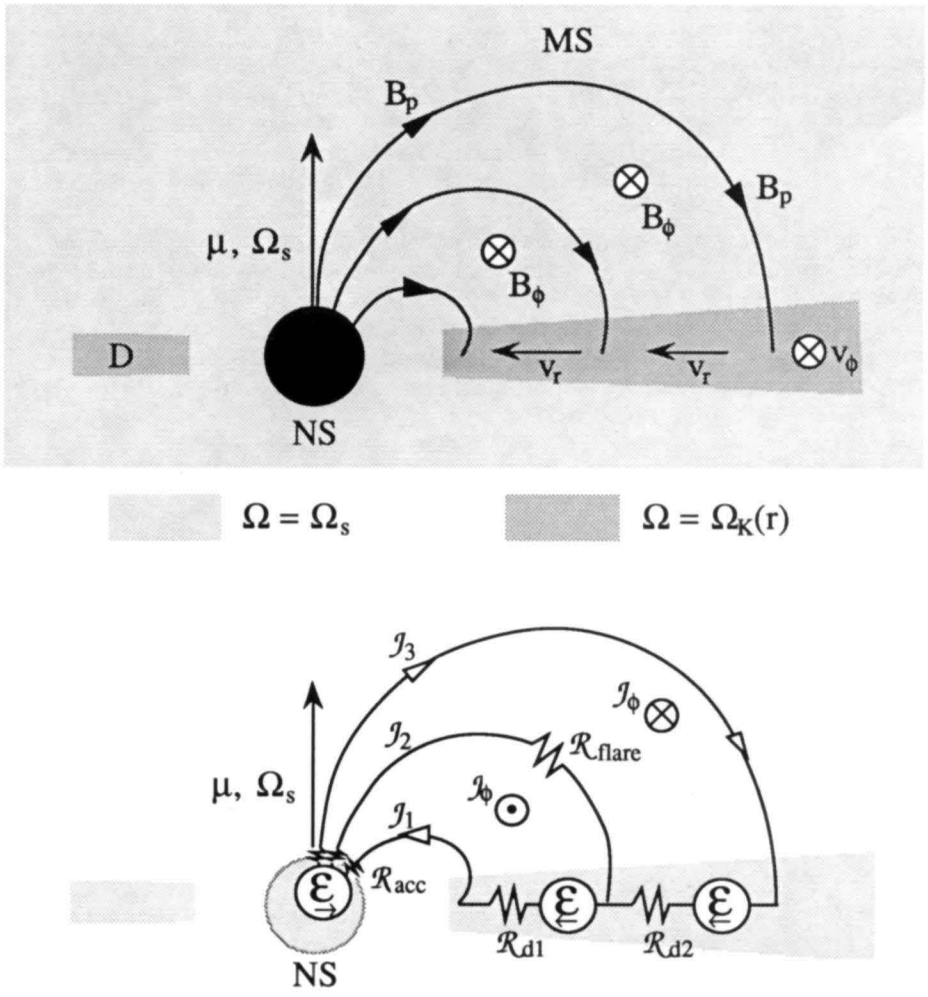

Fig. 2.1.—*Top*: Side view of a magnetic neutron star NS interacting with an acccretion disk D. Plasma in the lightly-shaded region corotates with the star, whereas plasma in the the heavily-shaded region circles the star in Keplerian orbits. *Bottom*: An equivalent circuit, showing the electromotive forces $\mathcal{E}$ produced by the rotation of the neutron star and the orbital motion of the disk plasma through the magnetic field, the resulting poloidal currents $\mathcal{J}_1$, $\mathcal{J}_2$, and $\mathcal{J}_3$, the corresponding azimuthal currents $\mathcal{J}_\phi$, and the circuit resistances $\mathcal{R}_{acc}$ in the accretion funnel and $\mathcal{R}_{d1}$ and $\mathcal{R}_{d2}$ in the disk. A steep rise in the resistance within the magnetosphere ($\mathcal{R}_{flare}$) will create a large potential drop. The resulting strong electric field can accelerate charged particles along the magnetic field.

labelled $\mathcal{E}$. These forces drive field-aligned currents within the highly-conducting magnetosphere, here represented by the poloidal currents $\mathcal{J}_1$, $\mathcal{J}_2$, and $\mathcal{J}_3$, and the azimuthal currents $\mathcal{J}_\phi$. The circuit is closed by cross-field currents flowing in the disk and the star. The flow of these currents through the resistances $\mathcal{R}_{\rm acc}$ in the accretion funnel and $\mathcal{R}_{\rm acc}$ and $\mathcal{R}_{\rm acc}$ in the disk produce potential drops that oppose the electromotive forces produced by the motion of the star and the disk plasma. Also important but not explicitly shown are the inductances of the current loops.

As the differential rotation of the disk plasma and star proceeds, the magnetic field linking them is increasingly twisted. The growing twist implies an ever increasing magnetic free energy and electrical current density within the magnetosphere. As GL emphasized, this increase in magnetic energy cannot continue indefinitely. Instead, the twisted and pinched magnetic field will relax. GL stressed relaxation via reconnection in the magnetosphere and via turbulent diffusion and reconnection in the disk.

Another possibility is that the high current density that develops in the magnetosphere due to the twisting of the field and pinch effects may drive the Bunemann or other microinstabilities. These instabilities are expected to develop when the electron-ion relative velocity exceeds the local sound speed (see [68]). They can greatly increasing the resistivity in a small region of the magnetosphere, interrupting the current and dissipating the magnetic energy.

Whatever the particular processes involved in a given system, the currents within the magnetosphere and the magnetic fields that they generate will be limited by instability. Depending on whether or not the dominant instability is self-adjusting, the free energy of the twisted magnetic field may be released fairly steadily, in freqent microflares, or in less frequent but much larger flares.

2.3 Steady Flow Models

GL emphasized that the magnetic free energy would almost surely be released in an episodic way. However, they also called attention to the difficulty of treating the release of this energy in any detailed way. They therefore suggested that, as a first step in understanding the large-scale behavior of disk-accreting neutron stars, it might be useful to attempt to describe the *time-averaged* properties of the magnetic field and the flow using a time-independent, non-ideal MHD model.

In order to proceed with this program, GL introduced an *effective* conductivity tensor $\sigma_{\rm eff}$ for the disk plasma, to describe the time-averaged effects of dissipative processes such as current-driven instabilities and reconnection. For simplicity, they assumed that $\sigma_{\rm eff}$ is isotropic and were then able to show that the value of $\sigma_{\rm eff}$ is determined by the assumption of a steady flow. They argued that magnetic field reconnection and other magnetic field dissipation processes are to some extent self-adjusting and therefore might maintain the time-averaged effective conductivity at this value. Using this approach, GL were able to develop a quantitative model of steady disk accretion by an aligned rotator by solving the 2D, non-ideal MHD equations in and near the disk plane and in the inner magnetosphere. GL emphasized that while time-independent solutions of the MHD equations may be useful for calculating average velocities, magnetic pitches, and the time-averaged accretion torque, time-dependent phenomena, such as flares, could also have observational consequences.

GL showed that the region where the stellar magnetic field threads the disk constitutes a *transition region* between undisturbed disk flow far from the star

and the flow inside the magnetosphere. The interaction between the *azimuthal* motion of the disk plasma in the transition region and the stellar magnetic field generates radial currents that tend to twist the field, as described above, creating an azimuthal field component. The interaction between the *radial* motion of the plasma in the transition region and the magnetic field generates azimuthal currents which tend to confine the poloidal field, creating a radial field component.

GL also showed that their 2D MHD model exhibits boundary layer behavior at the radius given implicitly by the angular momentum conservation condition

$$\frac{B_p B_\phi}{4\pi} 4\pi\varpi^2 \Delta\varpi \approx \dot{M}\varpi v_K \,, \tag{2.1}$$

that is, the velocity and magnetic fields in the model change on a length scale $\Delta\varpi \ll \varpi$ near the radius ϖ_0 given implicitly by equation (2.1). Thus, the transition region divides naturally into two zones: a broad outer zone, where the motion is Keplerian, and a narrrow inner zone, where the angular velocity falls sharply from the local Keplerian value to the stellar angular velocity at the radius ϖ_{co}. GL defined the radius ϖ_0 of the boundary between these two zones as the radius where $\partial\Omega/\partial\varpi = 0$. Thus, at $\varpi = \varpi_0$, the shear stress vanishes.

In the *inner transition zone*, between ϖ_{co} and ϖ_0, the interaction of the azimuthal flow with the magnetic field significantly reduces the angular velocity of the inflowing plasma from its Keplerian value just outside ϖ_0 to the corotational value at ϖ_{co}. In addition, azimuthal currents flowing in the disk plane and in the accreting plasma above and below the disk screen the poloidal component of the stellar magnetic field on the radial length scale

$$\Delta\varpi \approx \frac{c^2}{4\pi\sigma_{\rm eff} v_{\varpi 0}} \,, \tag{2.2}$$

where $v_{\varpi 0}$ is the radial velocity of plasma in the boundary layer. These screening currents reduce the poloidal field by a factor $\sim$5 between ϖ_{co} and ϖ_0.

In the *outer transition zone*, outside ϖ_0, the disk structure is similar to that of an undisturbed disk, except that angular momentum is removed from or fed into the disk by the stellar magnetic field, which is twisted by its interaction with the disk plasma. In addition, the total energy dissipation rate is augmented by resistive dissipation of the electrical currents flowing in the disk. GL found that the couple between the outer transition zone and the star is a substantial fraction of the total couple. Since the couple falls off gradually, the definition of the outer boundary of the outer transition zone is purely conventional.

The plasma in the disk is confined in the vertical direction by the pressure of the magnetospheric field rather than gravity inside a radius ϖ_p, which is somewhat larger than ϖ_0. Aly and Kuipers (2; see also ref. 29) have suggested that inside ϖ_p, plasma orbiting in the disk plane will break up into isolated clumps or blobs, which will then spiral inward due to their interaction with the stellar magnetic field. We emphasize that the time-averaged structure of this flow is necessarily similar to the structure in the same region of the quasi-steady GL model, and that the innermost radius at which the orbital motion of the blobs is Keplerian is, when calculated correctly, the same as the innermost radius of the Keplerian flow in the GL model.

2.4 The Inner Edge of the Disk

The radius ϖ_0 at which the Keplerian flow ends is an excellent diagnostic of conditions in the inner part of the disk, since it depends on the radial and vertical structure of this part, and directly affects several observable properties of accreting neutron stars, as well as their evolution (17).

The original work by GL concentrated on the strongly magnetic neutron stars that appear as accretion-powered pulsars. GL showed that the Keplerian flow in these systems is terminated by the stellar magnetic field in the middle part of the α disks. Subsequently, several developments have focused attention on disk accretion by weakly magnetic neutron stars. One was the discovery of weak-field millisecond pulsars and the proposal that they have been spun-up to millisecond periods by accretion from a disk while in a LMXB (see [5,71] and references therein). Another development was the discovery of high-frequency QPOs in the luminous LMXBs and the suggestion that these are caused by the interaction of a weak neutron star magnetic field with inhomogeneities in the inner part of the accretion disk (see §3).

In luminous LMXBs containing weakly magnetic neutron stars, the Keplerian disk flow is terminated by the stellar magnetic field in the inner part of the disk rather than in the middle part (83). However, the approach used by GL to determine the interaction of the stellar magnetic field with the middle disk is easily generalized to models of the inner disk (17). Whenever the Keplerian disk flow is terminated well within a given region of the disk, the innermost radius ϖ_0 of the Keplerian flow scales as particular fractional powers of the key accretion variables $\dot{M}$, μ, and M, that is

$$\varpi_0 \propto \dot{M}^a \mu^b M^c . \tag{2.3}$$

The values of the exponents a, b, and c depend on the particular model of the inner disk and boundary layer being considered. The values of these exponents are listed in Table 2.2 for the geometrically-thin α-disk models listed in Table 2.1

For Keplerian flows that end in the middle part of the disk, Table 2.2 lists the exact values of the exponents rather than the slightly different approximate values quoted in GL, to emphasize that the physical arguments used to derive the expression for ϖ_0 given in GL are fundamentally different from the physical arguments used to derive the expression for the radius of the magnetosphere in spherical accretion (40). Although these two expressions scale in almost the same way, the similarity of the scalings does *not* indicate that the basic physical processes are similar (35). This is a point on which there is considerable confusion in the literature.

Table 2.2 shows that when the Keplerian flow ends in the inner part of the disk, the scaling of ϖ_0 with the key accretion variables is generally quite different from the scaling when the Keplerian flow ends in the middle part of the disk. Moreover, different models of the inner disk produce quite different scalings of ϖ_0 with the key accretion variables. These scalings can be explored observationally in several ways (17). In particular, it may be possible to determine the scalings of the Keplerian frequency at ϖ_0 in different systems.

As one example, studies of the variation of the angular acceleration of accretion-powered pulsars with X-ray intensity can provide information on the scaling of the Keplerian frequency, and hence ϖ_0, with $\dot{M}$ (17). As another example, accurate measurements of the frequencies of the horizontal-branch

Table 2.2 Scaling of the Innermost Radius of the Disk

	$\varpi_0 \propto \dot{M}^a \mu^b M^c$		
Disk Model	Value of a	Value of b	Value of c
1T Opt thick GPD	−0.25	0.58	−0.21
1T Opt thick RPD*	−0.15	0.51	−0.13
2T Opt thin GPD Compt soft photon	−1.70	0.80	0.73
2T Opt thin GPD Compt brems	−0.48	0.57	0.05

*Scalings are the same for both prescriptions of the viscous shear stress listed in Table 2.1 (17), since the radius of the inner edge of the disk does not depend on the viscous shear stress (GL).

of QPOs—which are thought to reflect the difference between the stellar spin frequency and the Keplerian orbital frequency at ϖ_0 (see [38] and references therein)—may provide data on the variation of ϖ_0 with $\dot{M}$. Finally, studies of the so-called "spin-up line" for recycled pulsars in the P-$\dot{P}$ diagram—which is thought to reflect the Keplerian orbital frequency at ϖ_0 when the star is accreting at the Eddington critical rate $\dot{M}_E$ (see [77] and references therein)—may provide information on the scaling of ϖ_0 with μ. The details of these calculations and their implications are described elsewhere (17).

3. X-RAY SPECTRA AND QPOs

The unexpected discovery of quasi-periodic intensity oscillations (QPOs) in several LMXBs (80,44,23,52) has provided a wealth of information about these systems. By now, QPOs have now been detected in most of the luminous LMXBs.

Further clarity was achieved when it was realized that the spectral and temporal properties of the luminous LMXBs are closely correlated (55,79,19–22,33,24,26). In fact, recent studies (20–22,24,61,25,26) have shown that many of the most luminous LMXBs have three distinct spectral states, called the horizontal, normal, and flaring branches.

In the present section we described recent efforts to develop a unified model of the luminous LMXBs that can account for their X-ray spectral states and QPOs in a physically consistent way, emphasizing the physics of the accretion flow and the origin of the normal branch intensity oscillations. More detailed accounts of the model, including other aspects, may be found elsewhere (34–38,45,53,11–13,46,47).

3.1 Overview of the Unified Model

The unified model assumes that the X-ray source is a neutron star with a relatively weak ($B \sim 10^8$–10^9 G) magnetic field accreting matter from a disk fed by the companion star. The disk is disrupted by the magnetic field of the neutron star at ~15–20 km. The energy to power the X-ray emission comes

from release of the gravitational potential energy of the accreting matter as it approaches the neutron star. Most of the photons emitted by the source are produced in the inner disk and in a small central corona surrounding the neutron star magnetosphere.

When the luminosity is moderate, the optical depth of the inner disk corona and radial inflow is low and has only a small effect on the spectral and temporal properties of the emerging radiation. However, when the luminosity is within ~10% of the Eddington critical luminosity L_E, the outward force of the escaping radiation slows the radial inflow, the scattering optical depth of the inflow becomes ~5–15, and the inflow substantially alters the X-ray spectrum.

The ~20–50 Hz quasi-periodic oscillations observed primarily in the horizontal branch spectral state are assumed to be luminosity oscillations caused by interaction of the neutron star magnetosphere with the inner accretion disk (the magnetospheric beat-frequency modulated-accretion model; see [1,66]). The ~5–10 Hz quasi-periodic intensity oscillations observed in the normal branch spectral state are attributed to optical depth oscillations caused by interaction of escaping radiation with the radial inflow from the corona above the inner disk when the luminosity rises to within ~10% of L_E, as discussed below. The ~10–20 Hz quasi-periodic intensity oscillations observed in the flaring branch spectral state are attributed to photohydrodynamic modes that are excited by the oscillations in the radial flow and grow when the luminosity equals or exceeds the Eddington luminosity.

According to this model, the X-ray spectrum of LMXBs is formed in three physically distinct regions: (1) relatively cool ($T_e \sim 1$ keV), dense plasma near the neutron star, where comptonization is partially or fully saturated; (2) hotter ($T_e \sim$ 10–30 keV), less dense plasma in the inner disk and central corona, where comptonization is unsaturated; and, when the luminosity approaches and exceeds L_E, (3) a relatively cool ($T_e \sim 1$ keV) inner disk corona and radial flow, which partially degrades the radiation produced near the star. The sequence of horizontal, normal, and flaring branch spectral states observed in the Z-class sources is produced by the changing contributions of all three regions, as the mass accretion rate increases (34,36–38,46,47).

3.2 Accretion Flow

The inner disk probably consists of dense clumps of cooler plasma in Keplerian orbit, surrounded by a hot-proton plasma, as shown schematically in Figure 3.1. Protons in the hot plasma are heated by viscous energy dissipation and interaction with the magnetosphere and neutron star, and cooled by collisions with electrons. The resulting proton temperature in the hot plasma is ~100 MeV. The electrons in this plasma are heated by collisions with the protons and cooled by interaction with the ~1 keV radiation coming from the neutron star and magnetosphere. As a result, the electron temperature is ~10–20 keV.

The neutron star magnetosphere is filled with inflowing plasma, which is slowed by the outward force of radiation coming from near the star. Because of the high plasma density, the X-ray photosphere is some distance above the neutron star surface. Radiation produced in this region has a thermal spectrum with a characteristic temperature comparable to the effective temperature (~1 keV). High-harmonic cyclotron emission in the outer magnetosphere produces a substantial flux of soft photons.

The accretion flow pattern depends on the luminosity. At moderate luminosities (~0.5–0.9 L_E), the outward momentum of the radiation escaping from the

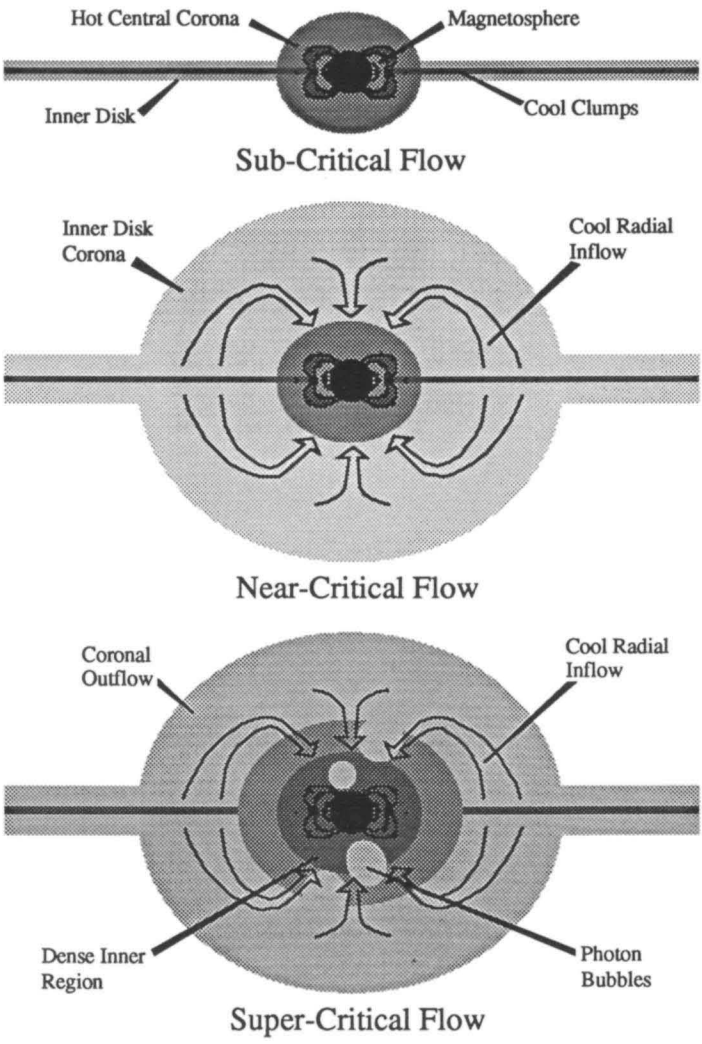

Fig. 3.1.—Schematic side views of the accretion flows discussed in the text. At moderate luminosities (top), the inner accretion disk consists of clumps of cooler plasma in Keplerian orbit, surrounded by a hot-proton plasma. Radiation forces cause the disk to thicken around the small neutron star magnetosphere, creating a compact central corona. At higher luminosities (middle), the inner disk expands vertically, forming a cool inner disk corona surrounding the hot central corona. The neutron star then accretes plasma from the inner disk corona as well as the disk (arrows). At luminosities above the Eddington limit, the radial flow near the central corona becomes unstable to growth of photohydrodynamic modes, which segregate the accreting plasma and outflowing radiation (bottom), allowing accretion to continue. After Lamb (36–38).

inner disk and neutron star causes the inner disk to thicken, forming a hot *central corona* around the small (radius ~15–20 km) magnetosphere of the neutron star, as shown schematically in the top panel of Figure 3.1. The electron scattering optical depth of the central corona is probably ~5. The radiation that emerges from the inner disk and central corona has a spectrum that is produced largely by unsaturated comptonization and therefore has a cutoff energy ~10–20 keV (36–38).

At luminosities $\gtrsim 0.9\,L_E$, the pressure of radiation escaping from the inner disk drives some plasma into a more extensive *inner disk corona* surrounding the central corona, as shown in the middle panel of Figure 3.1. Radiation drag causes plasma in the inner disk corona near the neutron star to lose its angular and vertical momentum and to fall approximately radially toward the star (11,12,37,38).

The size of the radiation drag and the structure of the radial flow depend on the mass flux $\dot{M}_d$ through the disk and the mass flux $\dot{M}_r$ in the radial flow. These are conveniently specified by the dimensionless parameters $\mu_d \equiv \dot{M}_d/\dot{M}_E$ and $\mu_r \equiv \dot{M}_r/\dot{M}_E$, where $\dot{M}_E$ is the mass flux that produces an accretion luminosity L_E. The total mass flux is then specified by the dimensionless parameter $\epsilon \equiv 1 - \mu_d - \mu_r$. Since $L_\infty/L_E \approx 1 - \epsilon$, the parameter ϵ is also a measure of the relative importance of the radiation force acting on the flow. Only two of the three parameters μ_r, μ_d, and ϵ are independent. When there is an adequate supply of matter, one expects $L_\infty \approx L_E$, and hence $\epsilon \ll 1$.

Inside the radius $r_{\rm radial} \approx 2\pi(1-\epsilon)^2 r_2$, where $r_2 \equiv GM/\epsilon c^2$, radiation drag removes the vertical and angular momentum of plasma orbiting in the inner disk corona in less than one Kepler period (11–13, 37,38). However, angular momentum conservation limits the radial mass flux to $\mu_r \leq \phi_s/c^2$, where ϕ_s is the gravitational potential at the neutron star surface (11,12,37,38). Thus, at most ~30% of the total mass flux onto the neutron star may come from the inner disk corona. If the inner disk corona is sufficiently dense, the actual radial mass flux should be near this maximum. Since the maximum is proportional to the luminosity, the radial mass flux may be approximately constant for luminosities near L_E.

Plasma in the inner disk corona that has lost angular momentum accelerates inward until its radial velocity reaches the value $\epsilon c/2$ at which the comoving luminosity equals L_E and the acceleration vanishes (45). Inside the inner critical radius $r_1 \equiv (\mu_r/\epsilon)R$ the flow becomes optically thick, radiation trapping is small but significant, and the flow velocity decreases linearly with radius (45) until gas pressure gradients become important (11–13). The time t_f required for gas captured from the inner disk corona to reach the neutron star is dominated by the inflow time from the outer part of the radial flow.

When the luminosity is $\gtrsim L_E$, nonaxisymmetric photohydrodynamic modes (69,70,18,81) develop in the slow radial flow near the neutron star magnetosphere (37,38,11). These modes may be metastable (69,70), requiring a finite-amplitude perturbation of the flow in order to grow. The normal branch oscillation of the radial flow provides such a perturbation, exciting photohydrodynamic modes of the same frequency (37,38,11). Growth of these modes segregates the accreting plasma and outflowing radiation as shown in the bottom panel of Figure 3.1, allowing the neutron star to continue to accrete even when its luminosity exceeds L_E. The optical depth oscillation produced by the dominant photohydrodynamic mode creates the X-ray intensity oscillation seen on the lower flaring branch (37,38,11).

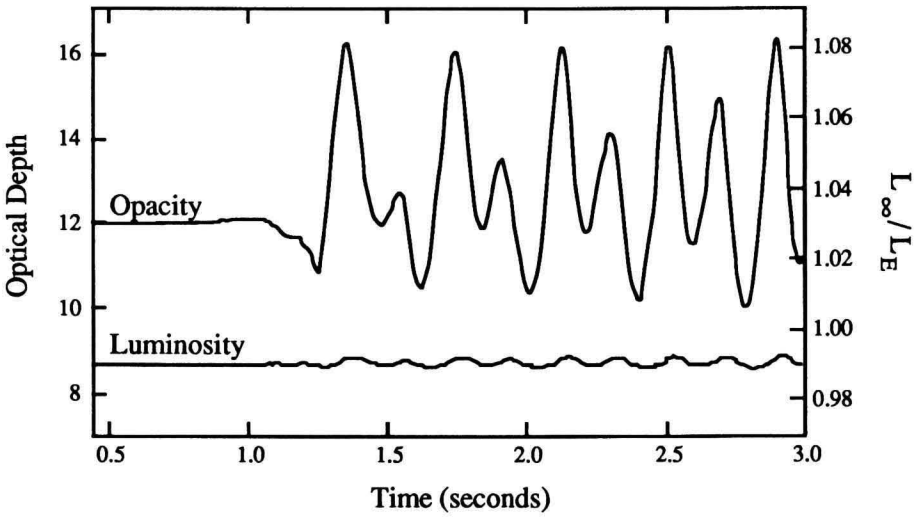

Fig. 3.2.—Variation of the electron scattering optical depth (left scale) and total luminosity (right scale) from a simulation of radial inflow from an inner disk corona. Note the stability of the flow before it was disturbed at 1.0 s, and the quasi-periodic oscillation that developed afterwards. The optical depth varies by ~30% whereas the luminosity varies by less than 1%. From ref. (11).

3.3 Normal Branch Oscillations

The accretion flow just described, which was originally developed to explain the X-ray spectral evolution on the normal branch, also provides a natural explanation of the NBOs (34–38,11–13). The reason is that the radial flow is very sensitive to perturbations in the mass flux and luminosity, when the luminosity is within ~10% of L_E. This sensitivity, and the unavoidable time lag between changes in the inward mass flux from the corona and the resulting luminosity changes, causes the radial flow to become overstable for luminosities sufficiently close to L_E.

This overstability has been demonstrated by an extensive study of the radial inflow of plasma from the inner disk corona, using a one-dimensional, time-dependent radiation hydrocode (11–13). In this study, steady, near-critical radial flows were first constructed. The stability of these flows was then investigated by disturbing the luminosity of the central corona or the inward mass flux from the outer boundary of the radial flow. The response of steady flows to perturbations of the luminosity or the mass flux was found to be very similar. When the luminosity is within ~10% of L_E and the fraction of the total mass flux in the radial flow is sufficiently high, both types of perturbations cause the radial flow to develop quasi-periodic oscillations.

Figure 3.2 shows results from an early simulation in which regular oscillations developed. For this particular run, $\mu_r = 0.05$ and $\epsilon = 0.01$. Similar results were obtained for ϵ values as large as 0.10. The inflow time t_f from the outer edge was ~0.3 s and the simulation was followed for ~10 inflow times.

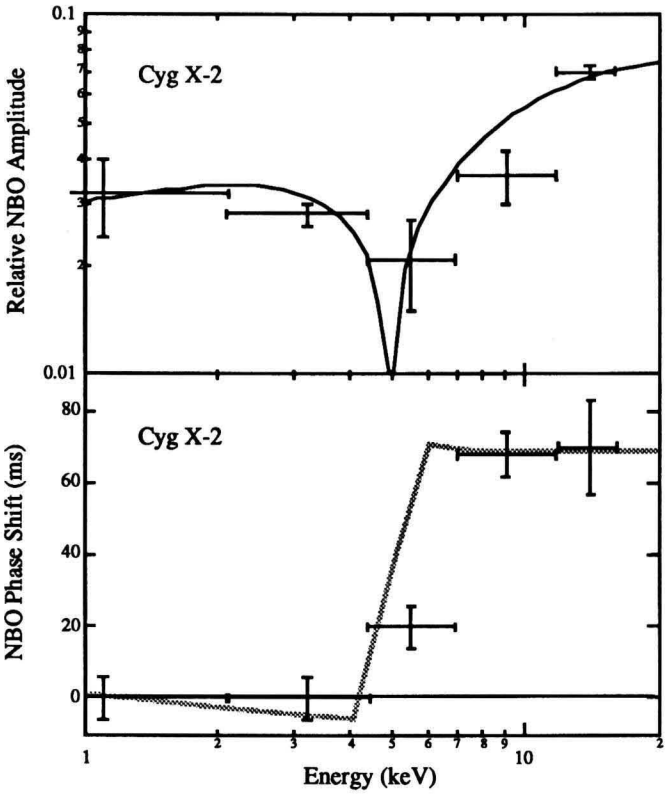

Fig. 3.3.—Observed (51) and calculated (47) Cyg X-2 normal branch oscillation amplitude (top) and phase (bottom), as a function of X-ray energy. The amplitude calculation assumes an optical depth of 10, an optical depth oscillation of 2, and an electron temperature of 0.8 keV.

The simulations that exhibited regular oscillations all had oscillation frequencies $f_{osc} \sim$ 5–10 Hz. These frequencies are comparable to the observed frequencies of NBOs at their onset near the middle of the normal branch. The scattering optical depths of the inflows that exhibited regular oscillations were all $\sim$10.

The relative amplitude $\Delta L/L$ of the luminosity oscillations tends to be much smaller than the relative amplitude $\Delta\tau_{es}/\tau_{es}$ of the oscillations in the scattering optical depth. This is to be expected, since the luminosity cannot vary by an amount greater than $\sim\epsilon L$ without disrupting the flow, whereas variations in the luminosity of this magnitude produce large variations in the density and optical depth of the flow. Thus, these simulations support the earlier suggestion (34,36–38) that NBOs are primarily oscillations in optical depth rather than luminosity.

Numerical calculations of the effect of optical depth oscillations on the X-ray spectrum (47) show that such oscillations cause the spectrum to rotate about a pivot energy E_p that depends on the spectrum, but is in the range 2–7 keV for observed spectra. The quasi-periodic oscillations in the optical depth of the radial flow therefore cause the X-ray spectrum to rock quasi-periodically about the energy E_p, in effect moving the source a small distance up and down the normal branch. A byproduct of this motion is that the X-ray intensity oscillates quasi-periodically in most energy bands.

These predictions agree quantitatively with the properties of the NBO in Cyg X-2, as shown in Figure 3.3. The amplitude minimum at $\sim$5 keV indicates that the electron temperature in the radial flow is $\sim$0.8 keV. The $\sim$150°. phase *lag* of the NBOs above E_s relative to the NBOs below E_s reported by Mitsuda (48,49) and Mitsuda and Dotani (51) is, in this model, actually a $\sim$210° phase *lead*, composed of the 180° phase lead produced by the rocking of the spectrum, plus an additional $\sim$20° phase lead (equivalent to $\sim$10 ms) due to the time required for photons to downscatter to energies less than E_s. These predictions also agree quantitatively with observations of GX 5−1, which has a normal branch pivot energy $\sim$2 keV (Hasinger, personal communication) and a minimum in the NBO amplitude at about the same energy (50).

4. PARTICLE ACCELERATION

The outer magnetosphere of an accreting neutron star, where the magnetic field of the star interacts strongly with a relatively dense plasma flow, is a natural site for acceleration of charged particles by a variety of mechanisms. Moreover, the presence of a strong magnetic field and accreting plasma may allow the energy of accelerated particles to be converted efficiently into γ-rays. Processes that may produce a substantial luminosity of MeV γ-rays are of special current interest, since the *Gamma-Ray Observatory* is scheduled for launch in the near future. In addition, there have been numerous reports of occasional detection of much higher-energy radiation from accretion-powered neutron stars, including radiation at TeV and even PeV energies.

In this section we summarize the basic features of the TeV radiation reported from neutron stars and indicate some of the constraints on models of TeV emission imposed by these reports. We then suggest that magnetospheric flares may be an important source of high-energy photons.

4.1 Observational Requirements

Detection of occasional TeV and even PeV radiation has been reported from about a dozen accretion-powered neutron stars, including Her X-1, and from about half a dozen rotation-powered neutron stars, including the Crab pulsar (8,82). In many cases, the reported detections have not yet been confirmed. The duty cycles of the emission appear to be quite small ($\lesssim 10^{-2}$). Moreover, there are indications that the radiation reported at PeV energies does not have the signature of γ-rays (9). Nevertheless, there are enough confirmed reports of TeV radiation from neutron stars that it seems worthwhile to consider what processes might produce such energetic radiation. Models of TeV γ-radiation from rotation-powered pulsars have been reviewed extensively by Ruderman (58,59). Here we restrict our discussion to models of TeV γ-ray emission from accretion-powered neutron stars.

The main arguments for interpreting the reported TeV radiation from neutron stars as γ-rays have been summarized by Ruderman (59). In order for the radiation to preserve an intensity oscillation with a period close to the neutron star spin period ($\sim$seconds) even after flight times much greater than 10^4 years, as claimed, and to arrive from the direction of the neutron star, the radiation must be neutral, almost massless relative to its energy, and able to penetrate at least $10^{-2}\,\mathrm{g\,cm^{-2}}$ of interstellar matter without degradation. Among known

particles, only photons and neutrinos meet these requirments, but TeV neutrinos would not cause the reported air showers.

Any mechanism for producing the presumed TeV γ-radiation from accreting neutron stars must meet the following basic observational requirements:

- It must be capable of producing γ-rays with energies of 10^{12} eV or higher.
- It must be capable of producing a γ-ray luminosity at least $\sim 10^{-2}$ times the X-ray luminosity of accretion-powered pulsars.
- It should account for the episodic character of the emission, which sometimes lasts $\sim 10^3$ s, and be compatible with the low observed duty cycles of the radiation ($\sim 10^{-2}$ to $\sim 10^{-7}$).
- It should explain the periodicity of the γ-ray emission in accretion-powered pulsars, which is reportedly close to but not exactly equal to the X-ray period, with typical differences of about 1 part in 10^3.
- If the radiation is beamed, it should be beamed in the disk plane, at least in Her X-1 and Vela X-1, since the TeV radiation reported from Her X-1 varies in phase with the 35-day cycle while the TeV radiation reported from Vela X-1 appears to be eclipsed by the neutron star's companion.

The above observational requirements impose strong constraints on models of the emission.

4.2 Theoretical Constraints

In order to produce TeV γ-rays, it is likely that charged particles must be accelerated to even higher energies. Several theoretical considerations are relevant to such models:

- Near accreting neutron stars, acceleration of electrons to energies as high as 10^{12}–10^{13} eV may sometimes, though not always, be prevented by the drag force produced by inverse Compton scattering of X-rays coming from the star. For this reason, most workers have focused on acceleration of protons.
- Proton acceleration cannot occur too far from the star, since the total luminosity available at the radius $R_{\rm acc}$ at which particle acceleration occurs is unlikely to exceed $(R/R_{\rm acc})\,L_x$, where L_x is the X-ray luminosity.
- The acceleration process must be consistent with the known environments of neutron stars. For example, observations indicate that the plasma particle density at 10^8–10^9 cm from the neutron star in Her X-1 is $\gtrsim 10^{12}\,{\rm cm}^{-3}$ (3,4).
- If protons are accelerated by an electric field, the acceleration must be parallel to the magnetic field, since the proton gyroradius is typically small compared to the acceleration length. Electric fields that exceed the magnetic field ($E > B$), allowing protons to move across magnetic field lines, are likely only in regions that are small compared to the acceleration length.
- Protons that have been accelerated to $\sim 10^{13}$ eV can convert their energy fairly efficiently to TeV γ-rays, if they traverse a plasma target of appropriate thickness. According to Stenger (73), the optimal column density for the target is $\sim 50\,{\rm g\,cm}^{-2}$. For such a target, each proton will produce about five γ-rays, each having an energy $\sim 3\%$ of the initial proton energy (see [67]). Since the absorption length for such γ-rays is $\sim 75\,{\rm g\,cm}^{-2}$, few are absorbed in the target.
- Production of TeV γ-radiation must occur sufficiently far from the neutron star that the magnetic field strength is less than 10^6 G; otherwise such

energetic γ-rays will be converted to electron-positron pairs after traveling only a short distance.

One process that may meet these requirements is electrodynamic acceleration of protons in the outer magnetosphere, above and below the inner edge of an accretion disk.

4.3 Magnetospheric Acceleration

The interaction of the disk with the stellar magnetic field described in §.2 suggests several scenarios for accelerating charged particles in the outer magnetosphere. Here we briefly discuss three possibilities. Particle acceleration in the outer magnetosphere and associated production of γ-rays is discussed in more detail by Lamb *et al.* (39).

Consider again the picture of the velocity and magnetic fields shown in the top panel of Figure 2.1. Twisting of the stellar magnetic field causes the magnetosphere to balloon outward. At the same time, a localized region of high azimuthal magnetic pitch develops above and below the disk plane (86,87,35). This region of high pitch produces a region of high azimuthal current density. If the current density becomes sufficiently large, current-driven instabilities will produce an anomalously high resistivity in this region (see [68]). Depending on whether or not the instability is self-adjusting, the free energy of the twisted magnetic field may be released fairly steadily or in a large flare. While the resistance is high, a large potential drop will develop across the resistive region. The resulting strong electromotive force

$$\mathcal{E}_{\rm tot} \approx \mathcal{E}_{\rm disk} - \mathcal{E}_{\rm star} \approx \frac{1}{c}(\Omega_{K0} - \Omega_s)B_0 r_0^2 \sim 10^{15} \ \text{Volts} \qquad (4.1)$$

may accelerate charged particles along the magnetic field. The time development of such a circuit can often be described by equivalent circuits with lumped circuit elements, like those shown in the bottom panel of Figure 2.1.

A second possibility is that double layers may develop within the magnetosphere (again see [68]). Such laminar space-charge layers trap a large fraction of the current-carrying electron population and accelerate the remainder. They can accelerate particles to high energies and can be modeled by an equivalent circuit having a capacitor and a resistor parallel to the magnetic field lines; however, the capacitance and resistance must be treated as highly nonlinear functions of the electric field in the layer.

A third possibility is that the energy stored in the twisted stellar magnetic field is released by reconnection, as suggested by GL. In fast rotators, the azimuthal field reverses sign at $r_c \approx r_0$. The resulting current sheet may tear, releasing the stored magnetic energy. Reconnection near the inner edge of the disk has recently been discussed in more detail by Aly and Kuipers (2) and Kuipers (29).

Figure 4.1 shows a possible scenario for producing energetic γ-rays with the right beam direction by accelerating protons in a resistive region, double layer, or reconnection zone within the magnetosphere. The protons enter the disk at an oblique angle where the highly twisted magnetic field from the acceleration region threads the disk. Collisons of the energetic protons with protons in the disk produce π_0's which then decay, generating a beam of γ-rays close to the disk plane. If the acceleration is electrodynamic, only those stars with $\boldsymbol{\mu} \cdot \boldsymbol{\Omega}_s > 0$

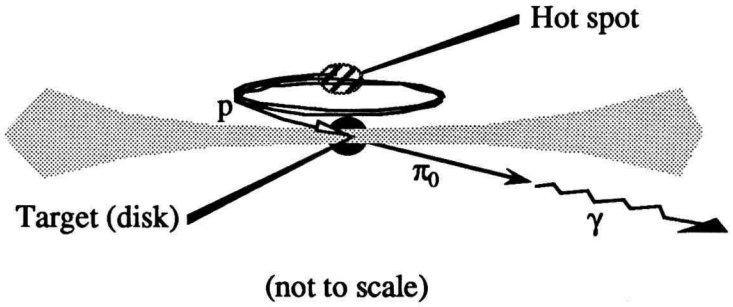

Fig. 4.1.—Perspective schematic view of γ-ray production by a magnetic neutron star accreting from a disk. Protons are accelerated in a resistive region, double layer, or reconnection zone within the magnetosphere. They then enter the disk at an oblique angle where the highly twisted magnetic field from the acceleration region threads the disk. The accelerated protons collide with protons in the disk, producing energetic π_0's. When the π_0's decay, they generate a beam of γ-rays close to the disk plane.

can produce γ-rays in this way, since only such stars will accelerate protons toward the disk.

Because the potential drop across the acceleration region necessarily leads to differential rotation within the magnetosphere, we do not expect these mechanisms to produce γ-radiation that oscillates in intensity at *exactly* the stellar spin frequency. Indeed, unless the energy release is relatively steady and the magnetosphere is quiescent, the spread in pattern frequencies is likely to be comparable to the spread in the Keplerian frequencies of the disk plasma that is threaded by the magnetic flux from the acceleration region. However, the long-term average of the frequencies of any oscillations in the intensity of the γ-rays should be equal to the stellar spin frequency.

5. REFERENCES

1. Alpar, M. A., and Shaham, J. 1985, *Nature*, **316**, 239.
2. Aly, J.-J., and Kuipers, J. 1990, *Astron. Ap.*, **227**, 473.
3. Bai, T. 1980, *Astrophys. J.*, **239**, 334.
4. Becker, R. H., *et al.* 1977, *Astrophys. J.*, **214**, 879.
5. Bhattacharya, D., and van den Heuvel, E. P. J. 1991, *Phys. Rep.*, in press.
6. Björnsson, G. 1990, Ph.D. Thesis, University of Illinois at Urbana-Champaign.
7. Björnsson, G., and Svensson, R. 1991, *Astrophys. J.*, in press.
8. Chadwick, P. M., McComb, T. J. L., and Turver, K. E. 1990, *J. Phys. G*, **16**, 1773.
9. Cronin, J. 1990, in *Proc. XIV International Symposium on Lepton and Photon Interactions*, in press.
10. Cunningham, C. T. 1973, Ph.D. Thesis, University of Washington.
11. Fortner, B. F., Lamb, F. K., and Miller, G. S. 1989, *Nature*, **342**, 775.
12. Fortner, B. F., Lamb, F. K., and Miller, G. S. 1991a, *Ap. J.*, submitted.
13. Fortner, B. F., Lamb, F. K., and Miller, G. S. 1991b, in preparation.
14. Ghosh, P., and Lamb, F. K. 1978, *Astrophys. J.*, **223**, L83 (GL).
15. Ghosh, P., and Lamb, F. K. 1979, *Astrophys. J.*, **232**, 259 (GL).
16. Ghosh, P., and Lamb, F. K. 1979, *Astrophys. J.*, **234**, 296 (GL).

17. Ghosh, P., and Lamb, F. K. 1991, in preparation.
18. Hameury, J. M., Bonazzola, S., and Heyvaerts, J. 1980, *Astron. Ap.*, **90**, 359.
19. Hasinger, G. 1987, in *IAU Symposium* **125**, *The Origin and Evolution of Neutron Stars*, ed. D. J. Helfand and J. H. Huang (Dordrecht: Reidel), p. 333.
20. Hasinger, G. 1987, *Astron. Ap.*, **186**, 153.
21. Hasinger, G. 1988, in *Physics of Compact Objects*, ed. N. E. White and L. G. Filipov (*Adv. Space Res.*, **8**), p. 377.
22. Hasinger, G. 1988, in *Physics of Neutron Stars and Black Holes*, ed. Y. Tanaka (Tokyo: Universal Academy), p. 97.
23. Hasinger, G., Langmeier, A., Sztajno, M., Trümper, J., Lewin, W.H.G., and White, N. E. 1986, *Nature*, **319**, 469.
24. Hasinger, G., Priedhorsky, W. C., and Middleditch, J. 1989, *Astrophys. J.*, **337**, 843.
25. Hasinger, G., and van der Klis, M. 1989, *Astron. Ap.*, **225**, 79.
26. Hasinger, G., van der Klis, M., Ebisawa, K., Dotani, T., and Mitsuda, K. 1990, *Astron. Ap.*, **235**, 131.
27. Kennel, C. F., and Coroniti, F. V. 1975, in *The Magnetospheres of the Earth and Jupiter*, ed. V. Formisano (Dordrecht: Reidel), p. 451.
28. Kennel, C. F., and Coroniti, F. V. 1977, *Ann. Rev. Astron. Astrophys.*, **15**, 389.
29. Kuipers, J. 1990, in *Active Close Binaries*, ed. C. Ibanoğlu and I. Yavuz (Dordrecht: Kluwer Academic Publ.), in press.
30. Kusunose, M., and Takahara, F. 1988, *Pub. Astr. Soc. Japan*, **40**, 435.
31. Kusunose, M., and Takahara, F. 1989, *Pub. Astr. Soc. Japan*, **41**, 263.
32. Kusunose, M., and Takahara, F. 1990, *Pub. Astron. Soc. Japan*, in press.
33. Lamb, F. K. 1988, in *Physics of Compact Objects*, ed. N. E. White and L. G. Filipov (*Adv. Space Res.*, **8**), p. 421.
34. Lamb, F. K. 1988, Talk presented at the Los Alamos Workshop on QPOs, La Cienega, N.M., September 1988.
35. Lamb, F. K. 1989, in *Timing Neutron Stars*, ed. H. Ögelman and E.P.J. van den Heuvel (Dordrecht: Kluwer), p. 649.
36. Lamb, F. K. 1989, in *Proc. 14th Texas Symp. on Relativistic Astrophysics*, ed. E. J. Fenyves (*Ann. NY Acad. Sci.*, **571**), p. 347.
37. Lamb, F. K. 1989, in *Proc. 23rd ESLAB Symp. on X-Ray Astronomy*, ed. N. E. White (ESA SP-296), p. 215.
38. Lamb, F. K. 1991, *Ap. J.*, in press.
39. Lamb, F. K., Ghosh, P., Hamilton, R., and Miller, M. C. 1991, in preparation.
40. Lamb, F. K., Pethick, C. J., and Pines, D. 1973, *Astrophys. J.*, **184**, 271.
41. Liang, E.P.T. 1979, *Astrophys. J.*, **234**, 1105.
42. Lightman, A. P. 1990, personal communication.
43. Lightman, A. P., and Eardley, D. M. 1974, *Astrophys. J. (Letters)*, **187**, L1.
44. Middleditch, J., and Priedhorsky, W. C. 1986, *Astrophys. J.*, **306**, 230.
45. Miller, G. S.1990, *Astrophys. J.*, **356**, 572.
46. Miller, G. S., and Lamb, F. K. 1988, Talk presented at the Los Alamos Workshop on QPOs, La Cienega, N.M., September 1988.
47. Miller, G. S., and Lamb, F. K. 1991, in preparation.
48. Mitsuda, K. 1988, in *Physics of Compact Objects*, ed. N. E. White and L. G. Filipov (*Adv. Space Res.*, **8**), p. 391.
49. Mitsuda, K. 1988, in *Physics of Neutron Stars and Black Holes*, ed. Y. Tanaka (Tokyo: Universal Academy), p. 117.

50. Mitsuda, K. 1989, in *Proc. 23rd ESLAB Symp. on X-Ray Astronomy*, ed. N. E. White (ESA SP-296), p. 197.
51. Mitsuda, K., and Dotani, T. 1989, *Pub. Astr. Soc. Japan*, **41**, 557.
52. Norris, J. P., and Wood, K. S. 1987, *Astrophys. J.*, **312**, 732.
53. Park, M.-G., and Miller, G. S. 1991, *Ap. J.*, in press.
54. Piran, T. 1978, *Astrophys. J.*, **221**, 652.
55. Priedhorsky, W. C., Hasinger, G., Lewin, W.H.G., Middleditch, J., Parmar, A., Stella, L., and White, N. 1986, *Astrophys. J. (Letters)*, **306**, L91.
56. Pringle, J. E. 1976, *Mon. Not. R. astr. Soc.*, **177**, 65.
57. Pringle, J. E., Rees, M. J., and Pacholczyk, A. G. 1973, *Astron. Ap.*, **29**, 179.
58. Ruderman, M. 1989, Talk presented at the NASA EGRET Symposium, Greenbelt, Maryland.
59. Ruderman, M. 1990, Proc. XIV International Symposium on Lepton and Photon Interactions, in press.
60. Schreier, E. J., *et al.* 1972, *Astrophys. J.*, **172**, L79.
61. Schulz, N. S., Hasinger, G., and Trümper, J. 1989, *Astron. Ap.*, **225**, 48.
62. Shakura, N. I. 1972, *Astron. Zh.*, **49**, 921 [Engl. transl. *Sov. Astron.–AJ*, **16**, 756].
63. Shakura, N. I., and Sunyaev, R. A. 1973, *Astron. Ap.*, **24**, 337.
64. Shakura, N. I., and Sunyaev, R. A. 1976, *Mon. Not. R. astr. Soc.*, **175**, 613.
65. Shapiro, S. L., Lightman, A. P., and Eardley. D., M. 1976, *Astrophys. J.*, **204**, 187.
66. Shibazaki, N., and Lamb, F. K. 1987, *Astrophys. J.*, **318**, 767.
67. Slane, P., and Fry, W. F. 1989, *Astrophys. J.*, **342**, 1129.
68. Spicer, D. S. 1982, *Space Sci. Rev.*, **31**, 351.
69. Spiegel, E. A. 1976, in *Physique des Mouvements dans les Atmosphères Stellaires* (Paris: CNRS), p. 19.
70. Spiegel, E. A. 1977, in *IAU Colloq.* **38**, *Problems of Stellar Convection*, ed. J. Ehlers, K. Hepp, R. Kippenhahn, H. A. Weidenmüller, and J. Zittartz (Berlin: Springer-Verlag), p. 19.
71. Srinivasan, G. 1989, *Astron. Ap. Rev.*, **1**, 209.
72. Stella, L., and Rosner, R. 1984, *Astrophys. J.*, **277**, 312.
73. Stenger, V. J. 1984, *Astrophys. J.*, **284**, 810.
74. Szuszkiewicz, E. 1990, *Mon. Not. R. astr. Soc.*, **244**, 377.
75. Taam, R. E., and Lin, D. N. C. 1984, *Astrophys. J.*, **287**, 761.
76. Tritz, B., and Tsuruta, S. 1989, *Astrophys. J.*, **340**, 203.
77. van den Heuvel, E.P.J. 1989, in *Timing Neutron Stars*, ed. H. Ögelman and E.P.J. van den Heuvel (Dordrecht: Kluwer Academic Publ.), p. 523.
78. van der Klis, M. 1989, *Ann. Rev. Astr. Ap.*, **27**, 517.
79. van der Klis, M., Jansen, F., van Paradijs, J., Lewin, W.H.G., Sztajno, M., and Trümper, J. 1987, *Astrophys. J. (Letters)*, **313**, L19.
80. van der Klis, M., Jansen, F., van Paradijs, J., Lewin, W.H.G., van den Heuvel, E.P.J., Trümper, J., and Sztajno, M. 1985, *Nature*, **316**, 225.
81. Wang, Y.-M. 1982, *Astron. Ap.*, **112**, 24.
82. Weekes, T. C. 1988, *Phys. Rep.*, **160**, 1.
83. White, N. E., and Stella, L. 1987, *Mon. Not. R. astr. Soc.*, **231**, 325.
84. White, T. R., and Lightman, A. P. 1989, *Astrophys. J.*, **340**, 1024.
85. White, T. R., and Lightman, A. P. 1990, *Astrophys. J.*, **352**, 495.
86. Zylstra, G. 1988, Ph.D. thesis, University of Illinois at Urbana-Champaign.
87. Zylstra, G., Lamb, F. K., and Aly, J.-J. 1991, in preparation.

A. M. Hillas

Some messages from PeV Gamma-ray Astronomy

There is still no single strong and enduring observation of undeflected PeV radiation from a cosmic source, but the reports strongly indicate pulsed and variable fluxes. Episodic emission of PeV radiation reported from Hercules X-1 seems to indicate a narrow wandering beam of PeV protons, such as would result from guidance by a very plausible magnetic field. Cygnus X-3 is still a puzzle: both it and the Crab can seemingly accelerate particles above 1 PeV without being powered by accretion.

1. INTRODUCTION

The "PeV" range of gamma-ray astronomy refers to observations of photons of energies of 10^{14} - 10^{16} eV, or 0.1 - 10 PeV — in X-ray terms this is 10^{11} - 10^{13} keV, emphasizing how far the spectrum extends beyond the well-studied X-ray domain. And there are less well established claims that the spectrum of neutral radiation extends to 3000 PeV. All these photons must surely derive from charged particles, most probably protons, of even higher energy that have been accelerated in these sources, and the possibility of learning how protons do indeed acquire such energies is one of the motivations for studying these radiations. A second aspect of these sources that has attracted attention is the possibility that a large part of their total energy output may appear initially as PeV particles. Astonishing estimates of the ultra high energy proton luminosity, exceeding the X-ray luminosity, could be derived from the supposition that the short episodes of gamma-ray detection marked the brief interposition of a gas target which generated gamma-rays from a quasi-isotropic proton beam, but this implausible luminosity can be avoided by not requiring widespread emission of the protons.

A third feature attracting great interest to these objects, but also great scepticism, is still a major problem: are the radiations photons? The particles or quanta detected from the direction of the sources Cyg X-3 and Her X-1 must be uncharged to be undeflected, and in the case of TeV radiation, the observation of a 12 ms pulsation (Turver's talk) from Cyg X-3, not smeared out on a 40,000-year journey, requires very high Lorentz factors, and a rest mass < 1 MeV/c^2. (Even the 1.24 second pulsation from Her X-1 sets a limit below the pion rest mass.) And yet the particles do not interact like neutrinos (they deposit their energy in the upper atmosphere), but produce showers that are broader than photonic showers, looking like proton showers. At PeV energies similar problems appear: the showers are rich in muons, and are even broader than proton showers, instead of being narrower, as gamma-initiated showers should be. How this serious problem will be resolved is not yet apparent, and I shall have to ignore it in the following discussion.

Gamma ray astronomy at energies beyond those accessible to satellites, has been divided into two domains — TeV and PeV — by the capabilities of two different detection techniques. All gamma rays above GeV energies initiate electron-photon cascades in the upper atmosphere. Around 1 TeV, these die out before reaching the ground, but the Cerenkov radiation emitted by the particles in the upper atmosphere can be detected by

large light collectors on the ground, and the incident directions of the primary quanta can be found to ~1°. When the initial particle energy reaches about 50 TeV (0.05 PeV), enough shower particles reach 1500-3000m altitudes for the showers to be detected efficiently by arrays of scintillators, and the time at which different scintillators are struck by particles in the (slightly fuzzy) shower front makes it possible again to measure arrival directions to ~1°. Counting rates have been much lower in the PeV experiments, because the flux falls off with increasing energy as always, and the collecting area of many scintillator arrays is less than that of a Cerenkov detector (the Cerenkov light from a shower falling in a pool of radius ~150 m), though the huge CASA installation of >1000 scintillators will notably increase the rate. There has been one exception: the Salt Lake City group has operated Cerenkov detectors of smaller aperture to detect 0.1 PeV showers by the Cerenkov technique (both with occasional special runs of their "Fly's Eye" detector, and by deployment of additional small-mirror telescopes).

With the scintillator arrays of smaller area the low counting rate makes it impossible to study pulsation or burst structure of the radiation: flux is integrated over weeks or months.

Sources have to be detected as an excess of counts in some window of ~1-2° radius, relative to with the number of background counts (due to proton and nuclear showers) in similar nearby windows.

Bearing in mind the remaining difficulty in getting absolutely clear and convincing demonstrations of PeV flux levels from such sources, the very variable nature of the apparent emission making it necessary to wait for a few years before the new improved experiments can clarify the situation, what picture should we form of these sources on the basis of present reports? Cygnus X-3 has received most attention, but is still baffling, so the emphasis here will be placed on Hercules X-1, a very familiar and characteristic X-ray binary, where we have a good idea of the geometry. The state of the evidence on Cygnus X-3 will be outlined later, and finally, the astonishing reports that, as usual, the Crab emits every conceivable type of radiation will be touched on.

2. HERCULES X-1 AS A PROTOTYPE SOURCE

The u.h.e. luminosity is at least a considerable fraction of the accretion luminosity, so the site of acceleration must not be very far from the neutron star if enough gravitational power is to be available. It will be argued below that the magnetic field structure is constrained by the requirement that the luminosity is not absurdly high (i.e. that the output is beamed). (Apart from the magnitude of the u.h.e. luminosity, another striking feature of the TeV observations is the report from several observers that an unusual pulsation periodicity sometimes takes over, differing by ~0.2% from the neutron star spin frequency.)

Reported PeV flux: The Fly's Eye experiment was operated in the Cerenkov mode on certain occasions, making it record showers of lower energy than usual, and on five nights (July 10-14) in 1983 Hercules X-1 was suitably placed for observation, and the data could be tested for a periodicity of 1.23779 seconds, as expected from X-ray data (each event time being corrected to the orbital barycentre). One night (July 11, 1983) showed such a signal (3). The non-uniformity of the count rate, folded with the assumed period, was largest (largest chi-squared) in the first half (40 minutes) of the run — although there appeared to be a weaker pulsed component present for a more extended duration — and maximized when the assumed period was in close agreement with that extrapolated from X-ray data, as shown in Figure 1(a). Figure 1(b) shows the very sharp peaking of the count rate with respect to the 1.2377-second phase, the signal peak in phase appearing significant at the 99.98% confidence level, allowing for the overall number of tests made. (The source of the radiation had also to be very close to the position of the neutron star in

its orbit in order that the barycentre time-of-flight corrections gave the sharp periodic signal (8).) The mean energy of the showers was 0.5 PeV, and the flux averaged over 40 minutes corresponded to 40% of the cosmic ray background in a 7° square window, corresponding to an energy flux ~6×10^{-9} erg cm^{-2} s^{-1} per decade of energy, at the Earth. The Durham group, observing at the same time at TeV energies, detected no activity: the spectrum must have been very hard (integral energy exponent ≤0.6, say, in contrast to 1.6 found for galactic cosmic rays). At the time of these observations, X-ray emission was suffering an unusual extended obscuration.

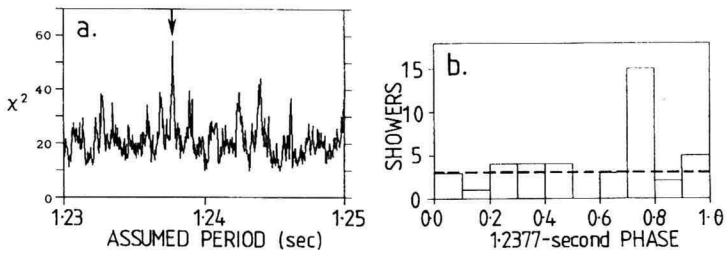

Figure 1. Periodicity of signals recorded by the Fly's Eye from Her X-1 during the first half of the run on July 11 1983: (a) non-uniformity of phase distribution plotted against assumed period in the range 1.23 to 1.25 sec (arrow marks X-ray period); (b) phase dependence of arrival times, folded with 1.23778-sec period.

The Los Alamos group (7) examined daily counts of showers recorded by their CYGNUS scintillator array over 340 days starting in April 1986, looking for days with an improbably high count and a significantly non-random distribution during the observing time. They found such an occurrence on July 23: their standard 2.3° square window surrounding Hercules X-1 contained 17 counts where 6 were expected with a non-random distribution during the observing interval: this included two bursts — each of about 7 extra events in about an hour (using a somewhat larger window for this count). Though the analysis needed to reveal significant bursts is a little tricky, the probability that these bursts (in 340 days) are spurious is estimated as 0.01%. The number of showers detected would correspond to a flux of ~7×10^{-9} erg cm^{-2} s^{-1} $decade^{-1}$ during the burst, at the energy of 0.2 PeV which would normally be the average energy of detected showers, though in fact the events in the bursts had a median energy of 0.5 PeV — again a hard spectrum — so the energy flux might have been ~1.8×10^{-8} erg cm^{-2} $s^{-1}$$decade^{-1}$. Bursts may have occurred often at slightly lower levels, but no further analysis has been presented. The strange periodicity claimed to be present within these runs will be taken up later.

Arrays with smaller collecting area or higher energy threshold would not have the sensitivity to detect such bursts.

The long-term average flux is hard to determine. The Baksan array must be best able to make such an estimate: an average over several years has been quoted (2), equivalent to 1% of the cosmic-ray background in a sky area of 20 square degrees: this would correspond to an average flux of 1.7×10^{-10} erg cm^{-2} s^{-1} $decade^{-1}$ at ~0.2 PeV. The Fly's Eye observers quote a mean flux about 40 times less than the 40-minute burst flux (8), but this is based on a short total run. The Leeds group (GREX array) have quoted an average flux equivalent to ~2.7×10^{-10} erg cm^{-2} s^{-1} $decade^{-1}$ at 1.2 PeV (4b), but with only 1.7σ significance, and later unpublished work makes this flux level look doubtful.

Thus the intensity during bursts seems to be about 40 times the mean flux, and the simplest interpretation of these very sketchy figures would be that bursts of radiation are present for about 2% of the time, the long-term average flux being very roughly ~2×10^{-10} erg cm^{-2} s^{-1} $decade^{-1}$ at ~0.2 PeV. (One may have to reduce the burst frequency if much

of the long-term average is contributed by a very low-level flux, which is probably present some of the time). This is rather like the pattern seen at TeV energies: the burst durations may be 5 min to 1 hour — typically ~20 minutes. At TeV energies a rather lower power per decade is required, as though the integral flux over the range TeV to PeV varies as $E^{-0.7}$, rather than the standard $E^{-1.0}$ characteristic of shock acceleration, or $E^{-1.6}$ characteristic of galactic cosmic rays. The "burst" events picked out at Los Alamos did have a very flat energy spectrum. (The fluxes are still near the threshold of detectability, which of course has led to some suspicions that the "signal" is really entirely noise. In this case the the apparent spectrum might well be of the nature that is reported!)

What would be the power of the source? The long-term average energy reaching the Earth is at least 3×10^{-10} erg cm^{-2} s^{-1}, if the spectrum extends to about 2 PeV, and most of the energy is confined to about 1.5 decades. If one guesses that the beam covers ~3 steradian (1/4 of the sky) — why do we see these objects if the beam size is much less? — the emitted power in u.h.e. gamma rays is

$$L_\gamma \approx 3\times10^{-10} \times (5\ \text{kpc})^2 \times 3 \approx 2\times10^{35}\ \text{erg s}^{-1}.$$

Presuming that the accelerated PeV particles are protons, because of the difficulty of getting electrons to such energies against radiation loss in the very strong field near the neutron star ($B \approx 5\times10^{12}$ gauss at the surface in Her X-1) and the presumption that the gamma rays must be produced far from the neutron star because they would be unable to penetrate fields of more than $\sim10^3$ gauss — and supposing that 50% of the protons interact in a target they will convert 1/4 of their energy into gamma rays (via $\pi^o \rightarrow \gamma$ and $\pi^{+-} \rightarrow \mu \rightarrow e \rightarrow \gamma$ decays) Hence

$$L_{proton} \sim 8\, L_\gamma \approx 1.6\times10^{36}\ \text{erg s}^{-1} \sim 8\%\ \text{of}\ L_X.$$

This of course is very approximate.

But what are the implications of this power being received in "bursts", say typically of 20 minutes, of 40 times the average power?

Assuming that we are not privileged observers, and that any other observers situated over about 1/4 of the sky surrounding Hercules X-1 would see very similar effects, we can compare three alternative interpretations of these episodes.

(a) All observers see the burst at the same time: the accelerator thas a duty ratio of 1/40 and generates a flux over 1/4 or the whole of the sky. In this case, while the accelerator is turned on, $L_{proton} \sim 40 \times 0.08\, L_X \sim 3\, L_X$ — or $13\, L_X$ if the flux is actually isotropic.

This seems most implausible: we require the accelerator to supply the peak flux, in all directions, for minutes to an hour. The energy emitted in such an episode would be ~ 5×10^{41} erg, which is much greater than the available energy stored in the magnetic field beyond ~ 100 km from the neutron star, so we cannot appeal to the release of accumulated energy to do this.

(b) A favoured hypothesis has been that the accelerator is always working, emitting protons in all directions, but a gas target is interposed in our line of sight for only 2% of the time. (This picture has been used initially in discussions of Cygnus X-3.)

The power is then 40 times greater than in (a), if the accelerator is on all the time!

(c) However, our different equivalent observers might see an outburst at different times. We could suppose that the accelerator is always working at a few percent of L_X but produces a narrow wandering beam. Figure 2 indicates the geometry: As the neutron star spins, it throws out a cone-shaped narrow beam of PeV protons (and hence gamma rays), the solid angle containing the beam being 1/40 of (say) 3 steradian. In the course of time the beam will be supposed to move up and down, covering a total solid angle of (say) 3

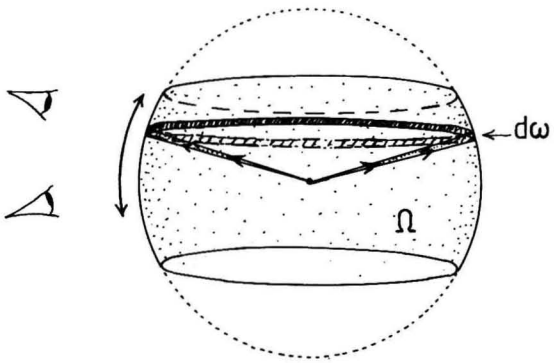

Figure 2. Suggested beam pattern from Her X-1. The spinning neutron star sweeps the beam round a narrow strip dω of the sky, but the strip wanders over a solid angle Ω 40 x dω as the star and the accretion disc precess.

steradians. Any one observer sees the beam as it passes into his line of sight.

This has the most reasonable power requirement — $L_p \sim 0.08\ L_X$ very roughly — and it accounts for the episodic observations. The wandering may be related to a precession of the neutron star, or to whatever causes the 35-day variations in the accretion disc geometry. Presumably the episodes should be related to the 35-day cycle in this case.

How might we get a collimated beam? Diverging field lines could well cause collimation in a beam of protons accelerated by some means near the neutron star: as protons moved away, their pitch angles would become small and even 10 PeV protons would be guided to follow the field lines for $r \leq 200\ r_*$ (r_* being the neutron star radius). Then the magnetic field pattern will determine the directions in which the beam is seen. The considerable tilt of the magnetic axis from the rotation axis in Hercules X-1 will have an important effect on the field pattern, and I believe that this will dominate any beaming pattern, so, as an alternative to the nearly-closed magnetosphere structures considered for modelling many X-ray phenomena, it seems appropriate here to take as a starting point the field of a tilted dipole surrounded by a perfectly diamagnetic accretion disc, as shown in Figure 3. On the left, the easily calculable field with a plane disc is shown: on the right is the likely form of the adjustment due to the vertical $\mathbf{j} \times \mathbf{B}$ forces acting on the inner edge of the disc, which excludes vertical B but has a radial B in its surface. (The inner edge of the disc is rotating in equilibrium with the neutron star: a little further out the disc matter orbits a little more slowly, and pieces of gas here will have a slow up-and-down motion superimposed on their orbital rotation, as they follow the warped disc shape. At certain distances there can be vertical resonances disturbing the disc.)

If the very large power in particle acceleration derives from accretion energy, it has to tap this energy source at a distance where r/r_* is not very large. It may occur through plasma processes in the infalling stream or by generation of large potentials in some vacuum gap close to the accretion stream — it is difficult to find a source of particles far from the stream — so the accelerated particles may be expected to emerge roughly where indicated in Figure 3; thus, if we assume that some magnetic field lines do enter the disc, protons will be guided into the disc where a gamma-ray beam will be generated, and can aim in roughly the direction of the observer. (We view the system within about 10° of the orbital plane, though the angle relative to the inner accretion disc will vary during the 35 day

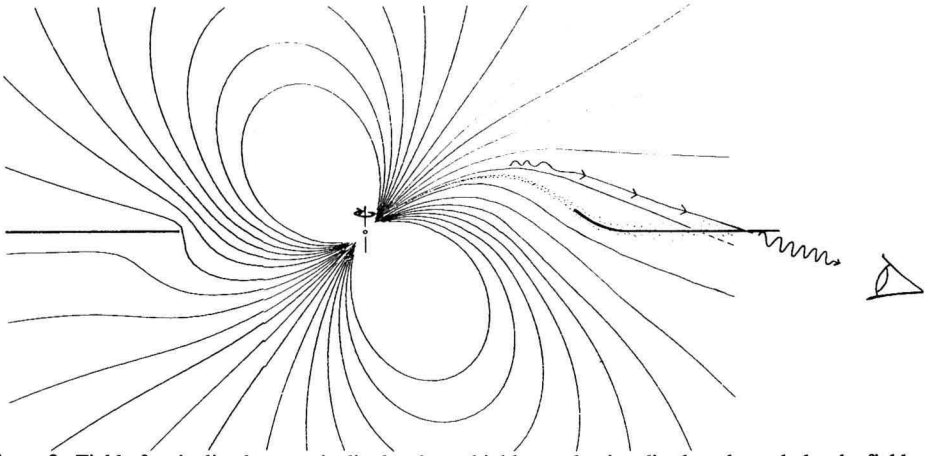

Figure 3. Field of an inclined magnetic dipole when a highly-conducting disc largely excludes the field component penetrating the disc. On the left the disc is assumed plane; on the right, the probable response to the upward magnetic force on the inner edge of the disc is shown. (The warp would be downwards on the other side of the star.) The accretion stream is marked by stippling. Any accelerated protons emerging above the accretion stream would be directed by the field into the disc, where they could generate gamma rays aimed towards the observer. (Field pattern: P. A. Johnson, private communication.)

cycle.) Even monoenergetic protons entering the disc could generate a reasonable spectrum of photons in the disc (12) especially if the spectrum has to be flatter than the canonical shock-acceleration spectrum. A precessing neutron star and a waving disc can then lead to a wandering direction of a narrow emergent beam.

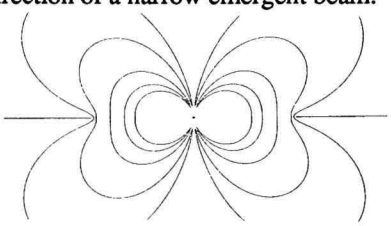

Figure 4. A closed magnetosphere that would not direct a beam towards the observer, through the disc.

It is worth remarking that the field lines must point towards the observer where the beam enters the target: a magnetic field of the form shown in Figure 4 would not do this. Another possible mode of particle acceleration which has been considered for some objects of this class involves the formation of a sub-relativistic outward-moving jet from a magnetic pole, which then strikes ambient gas much further out, forming a shock wave which is the main site of acceleration (24,15). However this would generate isotropic protons, and the distant field would not be strong enough to collimate and guide them to a target.

The conclusion is that if PeV protons are generated in the region indicated previously, the formation of a narrow wandering gamma-ray beam is quite natural.

Anomalies: strange period; muons

Many episodes of TeV gamma-ray emission have been reported with pulsations at exactly the X-ray periodicity 1.2377 seconds. At PeV energies the statistics are weaker, but the

first report (3) was in agreement. However, there have been several reports of detection of TeV pulsations from Hercules X-1 with a faster period (typically faster by about 1 part in 600), and the Los Alamos detection of bursts from Hercules X-1 at ~0.2 PeV, though comprising rather few events overall, was found to be consistent with a steady pulsation period of this same faster period. (A recent report from Ooty (11) of phase locking over 4 months does not sem to be statistically valid, though, according to private communication (Biller).)

These episodes of faster pulsation last for 40min to 1 hour (or even longer if the Los Alamos report that bursts are in phase is not an accident). In 40 minutes the apparent emitting source for the gamma rays has caught up 3 whole rotations relative to the X-ray emitter, so one cannot interpret the frequency shift by a drifting target or window within a normal beam rotating at the neutron star frequency, or the normal frequency would also be present (very strongly) in the fourier spectrum, which it is not.

Like the Kiel showers from Cygnus X-3, these were not deficient in muons, contrary to expectation for gamma-induced showers, according to standard theory of photons. Also, an upper limit to the flux of muon-poor showers from Hercules X-1 has been set by the large muon-shower array of the Michigan-Utah collaboration, at a level 20 times lower than the mean flux quoted above for all showers (6).

3. CYGNUS X-3

This was the first point source of PeV cosmic rays to be reported by an experiment with high angular resolution, when an excess in the general flux of cosmic rays was detected in the Kiel air shower experiment (26), and then identified with Cygnus X-3 when the excess signal was found to have a strong dependence on the phase of the 4.8 hour orbit of Cygnus X-3. The records of the long-running Haverah Park air shower experiment were then examined and an excess of showers found similarly closely defined in phase (though

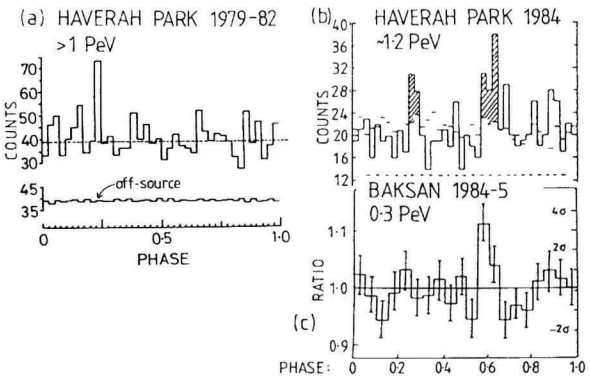

Figure 5. Change in phase pattern of PeV radiation from Cygnus X-3: (a) Pre-1983 data from Haverah Park, with peak near 0.25; (b) 1984 data from the GREX experiment at Haverah Park — emissions near phase 0.25 and 0.63; (c) Baksan data 1984-5 — main signal near phase 0.6.

the angular resolution was not so high and a much higher background count was present in the viewing window, so noise would hide an absolute excess of count rate.) Since then, several other shower arrays have been used to detect PeV radiation from that part of the sky, and it has appeared that the radiation can appear at two phases of the (presumed) binary orbit, but there have been switches in the relative prominence of these two. There has also been a long-term change in the overall intensity of the source. Figure 5 illustrates

the phase pattern seen in the first Haverah Park observations (19) (1979-83) and in 1984 (17) (with better angular resolution), where the switch from a phase near 0.25 to 0.6 was occurring, and also the observations from the experiment at Baksan (1) in late 1984, which now shows only the later peak. (The Baksan experiment has a high counting rate, but with a median energy of 0.3 PeV as against ~1.2 PeV for Haverah Park.)

The newer experiments set up to observe PeV radiation from Cygnus X-3 have found much lower fluxes than were reported earlier, and in many cases only upper limits could be set. The change over the years is shown in Figure 6. (Experiments selecting showers containing very few muons, as expected from primary gamma rays — marked by crosses in the diagram — have set much lower fluxes than those not thus restricted, or merely upper limits, keeping alive the anomaly first reported by Samorski and Stamm. The Ooty experiment (30) reported a much higher flux in 1984-5 than those shown, but this has been questioned by Sinha et al. (27).)

Figure 6:

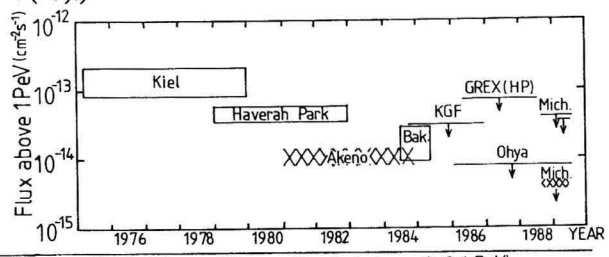

Figure 7(a)

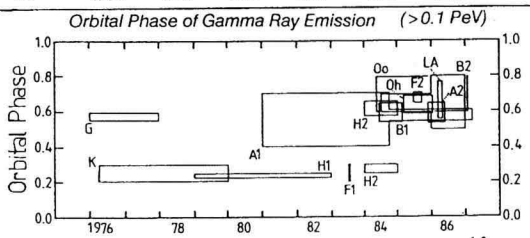

Figure 7(b):

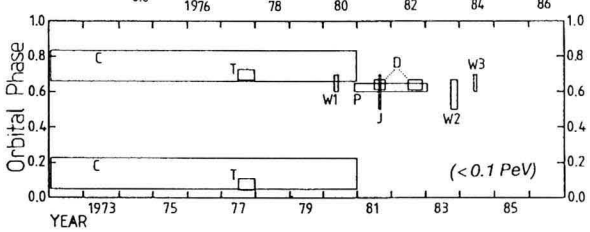

Figure 6. History of the flux of showers above 1 PeV from Cygnus X-3. XXXX marks data for showers containing very few muons. References: Kiel (26), Haverah Park (19), Akeno (14), Baksan (1), GREX (4), Ohya (20), Michigan (6), KGF (27).

Figure 7. 4.8-hour phases at which signals have been reported from Cygnus X-3 in various years, (a) above 0.1 PeV, and (b) near 1 TeV, as compiled by Protheroe. See (22,21) for references.

Before interpreting this failure to substantiate the original flux as evidence that the source is not real, it is relevant to examine the history of the orbital phase at which the emissions have been reported. Protheroe has assembled (22,21) all the reports on the phases at which gamma-ray emission had been detected (phase 0 being the minimum of the 4.8-hour X-ray profile): (a) for energies >0.1 PeV, and (b) for lower energies, ~TeV: these are shown in Figure 7. The time scales for figures 6 and 7 are aligned. There has been some

difficulty in agreeing on the "phase 0" to be used as the reference point in different years: Protheroe has attempted to correct for different choices, but some small phase discrepancies may still remain.

Boxes of very long duration in Figure 7 indicate observations summed over very long periods, and these may hide temporary switches in phase. Bearing this in mind, there seems to be very good agreement that there are two preferred parts of the orbit from which gamma rays can be detected; their relative prominence changes with time, and there may be some modest drifts. The consistency of these miscellaneous observations seems to be the strongest evidence that radiations from Cygnus X-3 really have been detected.

We obviously want very clear strong signals from a single experiment, rather than having to appeal to the consistency of several experiments (each with somewhat different energy sensitivity), and the most important requirement in this field will be to obtain a long exposure from the larger shower arrays which have been constructed recently; but the reason why we still await definitive observations is seen in Figure 6, showing the decline in the estimated flux of PeV showers from Cygnus X-3 over recent years. If one has mistaken noise for signal, and Cygnus X-3 emits no gamma-rays (but why are the phases then not random?), one would expect the apparent flux to decline as sensitivity improved, and only good exposures with very powerful arrays can resolve all doubts.

However, accepting at face value the evidence from Fig 7 that real radiations are detected, the system has evidently been changing gradually. One could envisage long-term drifts in the prominence of the two phase peaks in terms of changes in the geometry of viewing if the orbit precesses. Although the evidence for an orbital precession from non-linear terms in the epoch of phase 0 (31) is now less strong, the effect of geometrical changes can be illustrated by considering the stellar-wind opacity model for explaining the X-ray light curve. Figure 8 shows one version of this derived by Giler (9).

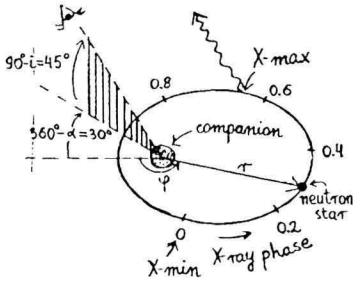

Figure 8. An illustrative model for the geometry of Cygnus X-3, due to Giler, in which viewing through varying column density of stellar wind is responsible for the variation in X-ray flux. The observer views the system from above the orbital plane. In this case, the line of sight might graze the atmosphere of the companion somewhere near phase 0.2, and precession could alter the closest angular separation of the two stars near phase 0.2, and hence alter the strength of a gamma ray signal.

One notes that near phase 0.2 (the gamma ray peak which went away) the neutron star would be seen passing behind and above the companion — so this peak could be attributed to the interposition of a denser outer atmosphere of the companion in the line of sight, generating gamma rays if protons emerge roughly radially from the neutron star. As the observer views from well above the orbital plane, a precession of the orbit would alter the angular separation at inferior conjunction, so the target might no longer be dense enough to generate detectable gamma rays. This merely illustrates the possibility of geometrical changes. The reason for a burst of gamma rays being received from the neutron star at phase 0.63 is not at all apparent at present.

The appearance of gamma rays at particular phases of the orbit might be explained by

the availability of a gas target for a proton beam to pass into at some special locations — such as having the beam graze the atmosphere of the companion star at some point, as mentioned above. This is a development of the original suggestion by Vestrand and Eichler (32) that gamma rays could be seen when the neutron star enters and emerges from eclipse, and is briefly seen through an atmosphere, though this does not fit the separation between the two favoured phases, and X-ray profiles suggest that the neutron star is never eclipsed. Cygnus X-3 probably does not accelerate particles in the same way as Hercules X-1, as will be argued below, so we may assume initially that the beam direction is unrelated to the position of the companion star, the target position rather than the beam determining the orbital phase of the radiation, and protons are emitted into a wide solid angle Ω. It was shown in Hillas (12) that an economical model for generating the whole spectrum of gamma rays would be to have 100 PeV protons enter a gas cloud of depth 2 radiation lengths or more, containing a magnetic field > 50 gauss that would speed up the generation of an electron-photon cascade. (Protons generate π°s which decay to γs: these produce pairs which rapidly dump their energy into gamma-ray synchrotron radiation.) Then one required a proton luminosity of

$$L_{proton} = 10^{39} \text{ erg s}^{-1} \times (\Omega/2\pi) \times (0.05/\Delta\text{phase})$$

to account for the fluxes reported at the time of the 1984 observations, if Δphase is the duty cycle of the gamma burst. (A distance of 12 kpc was assumed.) It is not so easy to see how the position of the companion could control the direction of a 100 PeV hadron beam from the neutron star (though if the magnetic field of the companion dominates that of the neutron star in the region of the accretion disc this might possibly happen (23)), so we want a wide beam to hit a localized target: Ω will not then be very small.

Can accretion be the power source? The likely magnitude of the proton luminosity indicated above would make this unlikely: it is appreciably greater than L_X. Moreover, the Durham group have made repeated observations of a 12.6 ms pulsation period in many of the more intense bursts of TeV gamma rays, which surely must indicate that a fast-spinning pulsar is emitting the high energy radiation. Using the Durham figures forand $d\omega/dt$, it would dump energy into the surroundings at a rate $-I\,\omega\,d\omega/dt = 5\times10^{38}$ erg s^{-1} , and this rate of slowing would be obtained if $B_{surface} > 0.6\times10^{12}$ gauss. Thus it is quite possible to derive the required luminosity from the rotational energy of a pulsar although it would be surprising if this energy went directly into u.h.e. particles. But apart from a pulsar being adequate as an energy source, such a high rotation speed would make make Cygnus X-3 an ejector rather than an accreter, so accretion does not seem to be available as an energy source here, if the 12.6 ms period is correct. (It is thus of great importance to get adequate sensitivity and observing time in other experiments to verify the 12.6 ms pulsation.) We may thus picture Cygnus X-3 as having a neutron star surrounded by an outer accretion disc, with the inner edge being blown away by jets or winds. It is still not clear what are the targets available at special phases — especially at phase 0.63, when the X-rays seem to suffer a shallow minimum in absorption.

Does the spectrum extend to near 10^4 PeV? The Kiel and Haverah Park observations indicated a fall-off in the flux near 10 PeV, but recently the Fly's Eye experiment has reported that summing their observations over several years, it sees an excess of showers of a few thousand PeV in a region of sky centred near Cygnus X-3. The large Akeno shower array also sees an excess in this region (29), but it occurs in showers of somewhat lower energy. Haverah Park does not see this excess. At this energy it would be difficult for gamma rays to escape from a magnetic field (if > 3 gauss) without suffering pair absorption, but the radiation could consist of neutrons: above 1000 PeV time dilation would allow many neutrons to arrive without decaying.

Although this report has attracted great interest, it is far from being established that there is such a radiation from Cygnus X-3. Even if the experimental disagreements can be resolved, there is another plausible explanation for a peak in the flux of ordinary 10^{18} eV cosmic ray protons in about that direction, as the direction coincides so far as we know with the direction of the galactic magnetic field, and protons running almost along the field would be trapped longer within the galaxy, resulting in an enhanced flux from that direction. Figure 9 shows some of the predicted intensity plots derived by Karakula et al. (13) for certain models of galactic field structure. The position of the maximum almost coincides with the direction of Cygnus X-3 (and the exact large-scale field directions are not precisely known) for protons of 1 to several EeV (thousand PeV) but not at lower energies. I think, therefore, that we do not yet have to find models to accelerate particles to 10^{19} eV in Cygnus X-3.

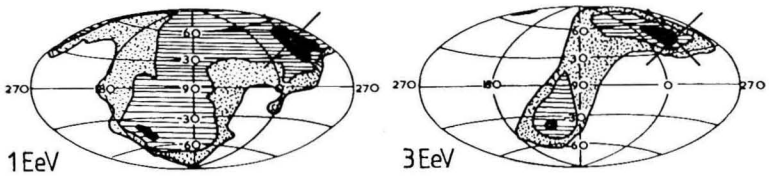

Figure 9. Intensity peaks in galactic cosmic rays that might result from longer paths of protons having small pitch angles with respect to the galactic magnetic field, according to one magnetic field model of Karakula, Osborne and Roberts (13). The large cross marks the position of Cygnus X-3. At energies below 1 EeV (10^{18} eV) the pronounced peak in this region does not occur.

4. THE CRAB NEBULA AND PULSAR

At TeV energies very steady, unpulsed radiation is seen (33), possibly from the nebula. The Durham group have reported detecting radiation related to the 33ms pulsar pattern, but this is not usually detectable. The luminosity is not high and the TeV radiation is quite unsurprising. Much more surprising is the fact that PeV gamma rays have been reported occasionally. If this is correct, it seems a lone pulsar can generate these u.h.e. particles, without requiring accretion.

The most notable occasion of such reports was on February 23 1989. The Baksan shower experiment records counts from the vicinity of several interesting objects every day, and it found an unusually high count on this day (2). The records of the KGF array in India (28) and the EAS-TOP array in Italy and the HEGRA array in the Canary Islands, which have similar energy response, were then examined for that day, and the first two reported excess counts.

Brief counting rate excesses seen successively at 3 different air shower arrays on February 23, 1989, from the direction of the Crab nebula/pulsar.

	UT on meridian	Off-source count	On-source count	Excess	Mean energy
KGF	14.1 h	17.8	35	4.1 σ	0.1 PeV
Baksan	16.5 h	31.1	57	4.4 σ	0.2 PeV
EAS-TOP	18.4 h	25.5	38	2.3 σ	0.2 PeV
HEGRA	21 h			none	

This gives the appearance of a flux lasting for a few hours, $\sim 10^{-11}$ cm^{-2}s^{-1} above 0.2 PeV at its peak, or $\sim 7\times10^{-9}$ erg cm^{-2}s^{-1}decade^{-1}, very similar (by chance) to the burst flux from

Hercules X-1. So, does the Crab pulsar also emit PeV gamma rays in a narrow wandering beam?

If there was a selection of showers, to enhance the signal, the significance of the confirmatory excesses may turn out to be less than appears from the table.

0.2 PeV showers recorded from the direction of the Crab at Ooty, in India, when averaged over a long period, show a small excess when folded with the 33ms pulsar period (using an ephemeris provided by Lyne), coinciding with the time of the radio interpulse (10). The flux would correspond to about 3×10^{-10} erg $cm^{-2}s^{-1}decade^{-1}$, averaged over all time. This is 15 times larger than the upper limit set by the Whipple observatory for the pulsed component of the TeV signal from the Crab.

REFERENCES

1. Alexeenko, V. V., et al., 1985. 19th Int. Cosmic Ray Conf., La Jolla, 1, 91-4.
2. Alexeenko, V. V. et al., 1989, International Workshop on VHE and UHE Gamma-Ray Astronomy, Crimea (ed. M. C. Cawley, D. J. Fegan and A. A. Stepanian), 187-91
3. Baltrusaitis, R. M. et al., 1985. Astrophys. J. Lett., 293, L69-72.
4. Bloomer, S. D., et al., 1090. 21st Int. Cosmic Ray Conf., Adelaide, 2, 39-42

4b.Bloomer, S. D., et al., 1990. 21st Int. Cosmic Ray Conf., Adelaide, 2, 334-8

5. Cassiday, G. L., et al., 1988. Phys. Rev. Lett., 62, 383-6
6. Ciampa, D., et al., 1990. 21st Int. Cosmic Ray Conf., Adelaide, 2, 35-8
7. Dingus, B. L., et al., 1988. Phys. Rev. Lett., 61, 1906-9
8. Elbert, J. W., 1986. Rencontre de Moriond
9. Giler, M. 1989. International Workshop on VHE and UHE Gamma-Ray Astronomy, Crimea (ed. M. C. Cawley, D. J. Fegan and A. A. Stepanian), 91-5
10. Gupta, S. K., et al., 1990. 21st Int. Cosmic Ray Conf., Adelaide, 2, 162-5
11. Gupta, S. K. et al., 1990. Astrophys. J. Lett., 354, L13-16
12. Hillas, A. M., 1984. Nature, 312, 50-52.
13. Karakula, S., et al., 1972. J. Phys. A, 5, 904-15.
14. Kifune, T., et al., 1986. Astrophys. J., 301, 230-4
15. Kiraly, P, and Meszaros, P., 1988. Astrophys. J., 333, 719-28.
16. Lamb, R. C., et al., 1988. Astrophys. J. Lett., 328, L13-16.
17. Lambert, A., et al., 1985. 19th Int. Cosmic Ray Conf., La Jolla, 1, 71-4
18. Lawrence, M. A., et al., 1989. Phys. Rev. Lett., 63, 1121-4
19. Lloyd-Evans, J., et al., 1983. Nature, 305, 784-7.
20. Muraki, Y., et al., 1990. 21st Int. Cosmic Ray Conf., Adelaide, 2, 56-9
21. Nagle, D. E., et al., 1988. Ann. Rev. Nucl. Part. Sci., 38, 609-57.
22. Protheroe, R. J., 1987. 20th Int. Cosmic Ray Conf., Moscow, 8, 21-44.
23. Protheroe, R. J., and Stanev, T., 1987. Nature, 328, 136-8
24. Quenby, J. J., and Lieu, R., 1987. 20th Int. Cosmic Ray Conference, Moscow, 2, 252-5
25. Resvanis, L. K., et al., 1988. Astrophys. J. Lett., 328, L9-12.
26. Samorski, M, and Stamm, W, 1983. Atrophys. J. Lett., 268, L17-21.
27. Sinha, S., et al., 1990. 21st Int. Cosmic Ray Conf., Adelaide, 2, 51-4
28. Sinha, S., et al., 1990. 21st Int. Cosmic Ray Conf., Adelaide, 2, 366-9
29. Teshima, M. et al., 1990. Phys. Rev. Lett., 64, 1628-31.
30. Tonwar, S. C., et al., 1988. Astrophys. J. Lett., 330, L107-11
31. van der Klis, M., 1990. Nuclear Physics B: 14B, 107-116.
32. Vestrand, W. T. and Eichler, D., 1982. Astrophys. J., 261, 251-8.
33. Weekes, T. C., et al., 1989. Astrophys. J., 342, 379-95.

A. M. Hillas, Physics Department, University of Leeds, Leeds LS2 9JT, U.K.

M. Ruderman

Energetic Gamma-rays from Accreting Compact Objects

ABSTRACT

Mechanisms are discussed for possible very high energy γ-ray emission from strongly magnetized accreting neutron stars in binaries and for possible low energy γ-ray emission by weakly magnetized neutron stars in low mass X-ray binaries (LMXB's). These are compared to proposed γ-ray emission mechanisms from the only two positively identified sources, the Crab and Vela radiopulsars.

1. INTRODUCTION

Among the very well established point-like γ-ray emitters in our Galaxy only two, the Crab and Vela radiopulsars, are already known sources. The great majority of such emitters are still unidentified. These consist of several families:

1) Cos B sources (1). These are very strong $10^2 - 10^3$ MeV γ-ray emitters ($L_\gamma \sim 4 \cdot 10^{35} - 5 \cdot 10^{36}$erg s^{-1}) of which about half seem to be interstellar clouds forming cosmic ray beam dumps. Most of the γ-ray emission is from the decay of π^0-mesons.
2) Galactic center region electron-positron pair annihilation γ-rays (2). The $e^\pm$ production has been variously ascribed to a $10^6 M_\odot$ black hole, an X-ray pulsar (3), and one or more low mass X-ray binaries (4).
3) Gamma-Ray Burst sources (5). These are transients among which are the brightest sources yet observed (probably because they are the closest). At times other than the brief γ-ray burst interval (10^{-1} to 10^3 s)) they are invisible.

It is likely that almost all of these faimilies, and perhaps all, involve neutron stars. Whether some, or even most, are accreting compact objects is less certain. In this category there are several well known accreting X-ray pulsars in binaries, but their γ-ray emission, mainly in the 10^{12}eV (TeV) and 10^{15}ev (PeV) regimes, still needs wider confirmation (7,8). That such puslars form the major group of TeV – PeV source candidates is expected because of the importance of *a priori* knowledge of some system periodicity in identifying a source's γ-ray signal in the usually much higher cosmic ray associated background. Moreover, such systems

would be high energy γ-ray candidates because of properties they seem to share with the Crab and Vela pulsars which do support very high energy accelerators. In the accreting binaries we have some necessary ingredients for a powerful very high voltage dynamo: a strongly magnetized neutron star (or White Dwarf) coupled through its magnetic field to a conducting disk rotating at a somewhat different rate. In the Crab and Vela radiopulsars the neutron star and its corotating magnetosphere are similarly coupled to the more slowly rotating environment beyond the pulsar light cylinders. An important difference, however, between the isolated radiopulsar neutron star and the neutron star in the accreting binary is the plasma environment. In the former it is mainly a very low density charge separated plasma in which accelerator electric fields may survive relatively easily limited only by $e^{\pm}$ pair production. In the latter it is dense conventional plasma which usually is effective in quenching such fields.

Several important general questions emerge from all of the γ-ray observations and source candidates.

a) Why are there so many different source families in each of which a neutron star (or, perhaps sometimes a magnetized White Dwarf) becomes a powerful particle accelerator?
b) Why are the accelerators so efficient? For the Crab radiopulsar about 10^{-3} of the total pulsar spin-down energy loss is carried off as hard X-rays and γ-rays (assuming a fan-beam emission geometry). For the Vela radiopulsar this fraction rises to 10^{-2}. With the accreting X-ray pulsar TeV/PeV γ-ray source candidates the needed ratio of γ-ray luminosity to total accretion power is of order 10^{-2} for Her X-1 and 10^{-1} for Cyg X-3.
c) Are the incident TeV/Pev γ-rays, which are detected by the $e^{\pm}$ air showers they initiate in the atmosphere really canonical γ-rays? Do these showers have the muon to electron ratio and the spatial size expected from QED (and for PeV muons, QCD)? Where such criteria have been applied, binary candidate TeV/PeV "γ-rays" seem to resemble incident charged background cosmic ray nucleons in their atmospheric interactions (8, 9, 10).

2. ACCRETING X-RAY PULSARS AS VERY HIGH ENERGY GAMMA-RAY SOURCES

Observations of transient γ-ray emission events (lasting several $\cdot 10^3$s) in the TeV/PeV regime would require the following properties for an accelerator in the emitting system:

1) A potential drop $\Delta V > 10^{12} V$ for TeV γ-ray emission. The γ-rays could come from TeV electrons or from the decay of π^0-mesons made in collisions of even higher energy nucleons.
2) A potential drop $\Delta V > 10^{16} V$ for PeV γ-ray emission. Because of inverse Compton drag by the intense X-ray flux and also radiaiton reaction from curvature radiation in orbits along curved $\boldsymbol{B}$-field lines, PeV electrons are

probably not plausible sources for PeV γ-rays. Instead an accelerator would need proton (or ion) injection.

3. An extremely high efficiency. If the accelerator is powered by accretion down to the outer boundary of Her X-1's corotating neutron star magnetosphere, the efficiency for converting that accretion power into very high energy γ-rays is of order unity, and of order 10^{-2} if all the accretion energy down to the surface can be mobilized.
4. Accelerated hyper-PeV protons (ions) directed through a target layer whose thickness is in the range 50 to 500 gcm^{-2}. If thicker, the PeV γ-rays would not escape with sufficiently high probability; if thinner, too many protons would pass through the target without interacting. Parts of the accretion disk itself (probably especially thin regions) would seem to be the most plausible candidates.
5. Very steady pulse to pulse reproductibility at least in Her X-1. The γ-ray observations in the TeV/PeV regimes are generally obtained as power spectrum peaks very near the neutron star spin period. For Her X-1 this power peak is very narrow, compatible with a constant γ-ray pulse phase and not with one whose phase varies erratically from pulse to pulse (7, 8, 9).
6. A target for TeV/PeV γ-ray production at least 10^8cm away from a strong magnetized neutron star so that the TeV γ-ray can escape before conversion into an $e^{\pm}$ pair and even further out for PeV γ-ray emission.
7. Accelerator power put into a relatively small particle flow ($\ll 10^{16}$ amps) corresponding to a charged particle density $< 10^8\mathrm{cm}^{-3}$. at injection.
8. A reproducible period difference between that measured in X-rays and that measured in γ-rays of about one part in 10^3 (8, 10).

The above requirements may well be so constraining that no accretion measured accelerator model survives and one must look harder at other possible interpretations of the data. However, several kinds of accretion powered ultra high energy particle acceleration have been proposed.

a) Fermi acceleration in the stand-off accretion shock wave above the neutron star accretion cap. This has already been discussed by Achterborg in these *Proceedings*. One problem is the efficiency of such accelerators for TeV–PeV particles. They generally give a power law spectrum E^{-n} with $n \gtrsim 2$. This would imply a lower efficiency for TeV-PeV energy particle acceleration relative to that for producing much lower energy particles and would lead to a conflict with requirement 3) above. The Fermi stochastic acceleration is accomplished by scattering an Alfven waves before and behind the shock. One limit to the maximum energy which can be achieved is reached where the accelerator power given to particles is exceeded by their synchrotron radiation. This gives

$$E(\mathrm{proton}) < 10^{15} B_6^{-1/2} \mathrm{eV}. \qquad (1)$$

To reach the needed $E \sim 10^{16}$eV of requirement 2) above, $B \lesssim 10^4$G and the acceleration time exeeds 10 s. This accelerator must be much further than 10^8cm from the neutron star. The total accretion power available for the

accelerator is then too small to account for the needed γ-ray power. (Disk shock acceleration mechanisms are discussed in these *Proceedings* by Spruit.)

b) Recombination of magnetic field lines above the inner part of this disk as they are stretched by disk-star rotation (11). Problems with such a source for electric field acceleration include the needed pulse to pulse reproducibility of the above argument 5) in what is generally expected to be a rather chaotic process. In addition requirement 7) may be difficult to satisfy: typical canonical ambient plasma densities around the accretion disk are of order $10^{16}\mathrm{cm}^{-3}$, very far indeed from that suggested as needed if the accelerator power is not to be shared by so many particles that too few reach the required energy.

c) A steady dynamo with quasi-steady $E \cdot \hat{B}$ acceleration, similar to that suggested below for the main very high acceleration mechanism in the Crab and Vela radiopulsars (14, 15, 12a, 12b). Is there any possibility that an accelerator of this sort could survive in the expected relatively dense plasma of the disk-star environment? (The answer is, probably, not likely.) It is only to the extent that the TeV/PeV data seems persuasive that a closer look at unlikely models may be warranted: all models, at this time, seem unlikely.

A toy model which gives a time indpendent $\boldsymbol{E} \cdot \hat{\boldsymbol{B}}$ accelerator is sketched in Fig. 1.

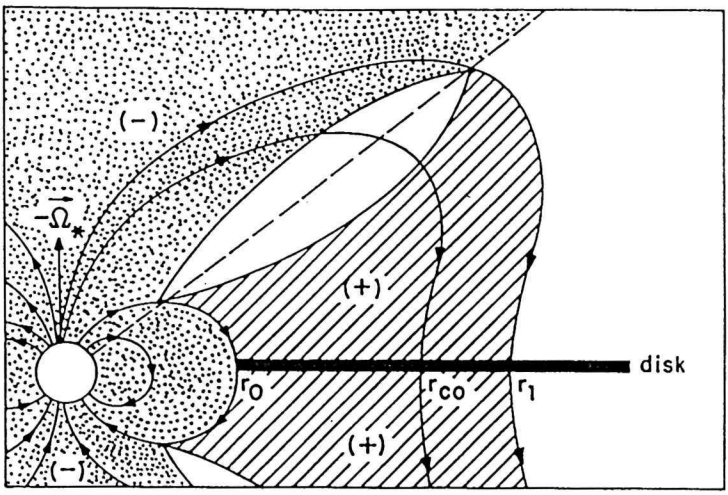

Figure 1. Geometry of a (closed) gap above a Keplerian disk when the disk $\Omega(r_0) > \Omega_*$ and the corotation radius r_{co} where the disk and star corotate is not far beyond r_0 (ref. 12b).

An aligned neutron star with an axially symmetric magnetic field is surrounded by a differentially rotating conducting disk. Each ring of the disk rotates at its Keplerian speed. From the inner edge of the disk at $r = r_0$ to the corotation radius at $r = r_{co}$ the disk rotates with an angular speed $\Omega_d(r) > \Omega_*$, the neutron star spin rate. The neutron star's magnetic field also threads the disk.

The disk-star dynamo EMF ($\oint \boldsymbol{E} \cdot d\boldsymbol{s}$ for a path along $\boldsymbol{B}$ from the star to r_0, along the disk to r, back along the connecting $\boldsymbol{B}$ flux line between r and the star and, finally, connecting through the star to its initial emergence point) changes sign as it passes through zero at $r = r_1$. The dotted part of a change separated magnetosphere corotates with the star ($\Omega = \Omega_*$). In the diagonally hatched region above and below the disk, charge separated plasma, of opposite sign to that around the star's polar caps, rotates with the angular speed of that part of the disk to which it is linked by $\boldsymbol{B}$. Between r_0 and r_1 the entire disk-star EMF is balanced by a potential drop along $\boldsymbol{B}$ in an empty plasma "gap" around the $\boldsymbol{\Omega}_* \cdot \boldsymbol{B} = 0$ surface. Beyond r_1 no such time independent solution exists: here there is the canonical region of stretching and reconnecting magnetic flux lines above the disk driven by the different rotational speeds of the star and that part of the disk to which it is linked by $\boldsymbol{B}$ (12a, b).

In the charge separated regions separated by the plasma gap the total force on the surviving charge, the sum of those from the electric field, gravity, and centripetal acceleration, satisfies $\boldsymbol{F}_{+(-)} \cdot \hat{\boldsymbol{B}} = 0$. This is not true for the opposite charge which is driven out of these regions away from the gap toward the star or the disk. The energy needed to lift the wrong charge from the star into the charge separated plasma above it is of order 10^2MeV $\sim 10^6$eV. Therefore, if established the gap might possibly survive, at least temporarily, despite the dense plasma on neighboring $\boldsymbol{B}$ flux lines which could quench it or prevent its formation. Such a gap could accelerate protons (ions) toward the target disk with enough energy and power to be a candidate for that needed to account for Her X-1's reported TeV γ-ray luminosity. Because of $e^{\pm}$ pair production processes in the gap which can limit the potential drop for particle acceleration by it, it is less plausibe as a PeV γ-ray source.

An accreting neutron star can be replaced by a magnetic White Dwarf in the above TeV γ-ray source model candidates. With $r_0 = 5 \cdot 10^9$cm and $B_* = 10^5$G for AE Aqr, TeV luminosities similar to those reported at this meeting by de Jager are obtained in the accelerator gap model.

3. LMXB's AS LOWER ENERGY GAMMA-RAY SOURCES (4)

A weak magnetic field strongly accreting neutron star has, typically $B_* \rightarrow 3 \cdot 10^8$G and $r_0 \rightarrow R_* = 10^6$cm. If a putative TeV/PeV accelerator in Her X-1 is powered by disk spin or turbulence or the interaction between the disk and the stellar magnetosphere, the expected very high energy γ-ray emission from a weak field LMXB would differ in two important ways from that reported from Her X-1. First, the available dynamo power, instead of being a small fraciton ($R_*/r_0 \sim 10^{-2}$) of the total accretion power ($L_x \sim 10^{37} - 10^{38}$erg s^{-1}), would be comparable to it. Second, even the weak field neutron star accelerator did produce TeV/PeV γ-ray emission near the interface of the disk and the stellar magnetosphere, such very high energy γ-rays could not escape before $\gamma \rightarrow e^+ + e^-$ conversion in the local magnetic field: $B(r_0) \sim B_* \sim 3 \cdot 10^8$G in an LMXB, a field strength 10^2 times greater than $B(r_0)$ in a strongly magnetized binary like Her X-1 with $B_* \sim$

$4 \cdot 10^{12}$G. These $e^{\pm}$ pairs will, in turn, synchrotron radiate lower energy γ-rays. The γ-rays will make further $e^{\pm}$ by direct conversion on the local $\boldsymbol{B}$ which they traverse or from $\gamma + X \rightarrow e^- + e^-$ on the intense LMXB X-ray flux. The resulting pairs can synchrotron radiate or up-scatter X-rays into γ-rays (inverse Compton scattering). A very rough analysis of the net γ-ray emission gives the result of Fig. 2. In addition, this LMXB would be a source of about 10^{43} $e^{\pm}$ pairs per second. How many would escape from the magnetic field around the accelerator, to contribute a narrow $e^{\pm} \rightarrow \gamma + \gamma$ annihilation line from positron annihilation far from the accelerator, has not been calculated. If it is substantial, the 10^{37} to 10^{38}erg s^{-1} $e^{\pm}$ annihilation line, together with the similarly luminous continuum radiation of Fig. 2, would resemble the observed Galactic center radiation whose origin is still unknown.

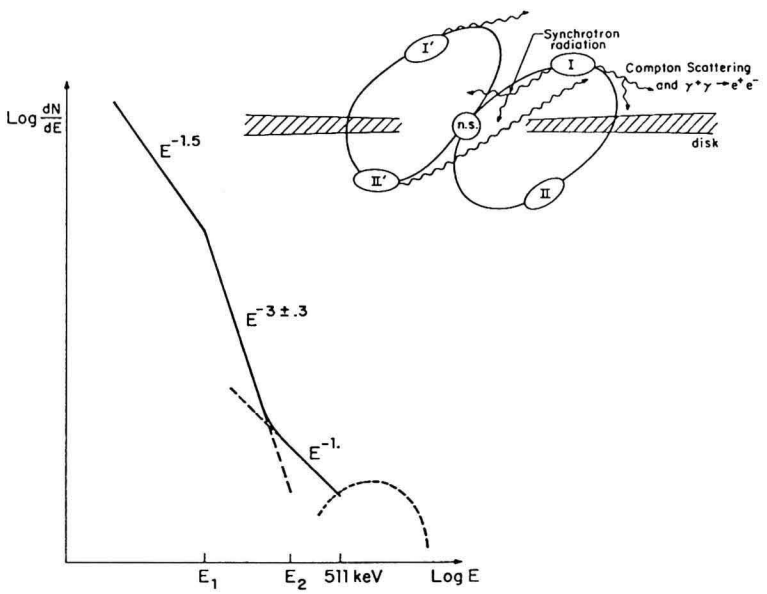

Figure 2. The theoretical X-ray/γ-ray spectrum of some accreting LMXB's. (It is similar to the HEAO-3 galactic center region spectrum.) The MeV bump (dotted line) may occur in only a subset of systems exhibiting the broken power-law (solid line) spectrum. The detailed shape of the bump has not been computed. The spectrum below $E_2 \sim 10^2$keV is due to synchrotron radiation, the part between E_2 and $\sim$ 511 keV is due to Compton scattering of $\sim$ 100 MeV photons (whose emission is also predicted, but which are not shown in the figure). The break at E_1 may occur anywhere between $\sim$ 10 keV and $\sim$ 100 keV. Inset: the geometry of the emitting region. The placement of the presumed accelerator(s) (ovlas I, II, ...) is shown, as well as representative magnetic field lines (solid curves) and photon trajectories (wiggly lines). From Ref. (4).

4. RADIOPULSARS AS GAMMA-RAY SOURCES

We consider next the two radiopulsar γ-ray sources for which neutron star parameters and also observations of γ-rays and most other parts of the electromagnetic

spectrum are known with certainty. Here there are significant clues in the observed data from these two pulsars which suggest properties and locations of their accelerators (13). In the Crab radiopulsars the pulsed radiation from optical to GeV and perhaps even to 10^{12}eV is coincident to within subpulse peak location measurement accuracy. If the emission source lies within the pulsar's magnetosphere or in the neighborhood of the light cylinder radius (1.5×10^8cm for the Crab pulsar) the emission source position for all of this radiation is probably coincident to within less than 10^4cm, very much less than the magnetosphere radius. Three arguments then suggest that this position, the same for all energetic emission and the non-precursor part of the radio emission, must be very much more than 10 neutron star radii above the stellar surface. Most likely is a source near the light cylinder.

i) There is evidence (19) that the Crab Pulsar's pulsed γ-ray spectrum extends to at least 10^{12}eV. Such energetic γ-rays could not cross a magnetic filed larger than several $\times 10^6$G without conversion to $e^{\pm}$ pairs. A magnetic field satisfying the constraint for 10^{12}eV γ-rays to escape is not found within the Crab pulsar's magnetosphere at a radius less than about half the distance to its light cylinder.

ii) The location of the Crab's optical emission, and, by inference, the X-ray and γ-ray emission coincident with it, is constrained by limits on the efficiency of those emission processes which can give optical light. The observed optical intensity (assuming a beam shape almost fully extended in latitude as argued below) implies that the optical luminosity efficiency ($\hat{f}$) satisfies

$$\hat{f} \equiv \frac{L_{\rm opt}}{L_{\rm KE}} > \frac{L_{\rm opt}}{I\Omega\dot{\Omega}} \sim 10^{-5} \tag{2}$$

with $L_{\rm opt}$ the optical luminosity, $L_{\rm KE}$ the rate at which energy is pumped by the spinning star into the kinetic energy of particles which emit the light, and $I\Omega\dot{\Omega}$ the total Crab pulsar spindown power inferred from its measured angular spin frequency (Ω), decay rate ($\dot{\Omega}$) and calculated moment of inertia (I). Acceleration of e^- (or e^+) along $\boldsymbol{B}$ gives optical radiation with $\hat{f}_{||} \ll 10^{-6}$.

For curvature radiation of photons with energy $\hbar\omega$ from centripetal acceleration

$$\hat{f}_{\rm curv} \sim \frac{\hbar\omega}{m_e c^2}\,\frac{e^2}{\hbar c} \sim 10^{-8}. \tag{3}$$

For synchrotron radiation by electrons with Lorentz factor γ and pitch angle θ in a magnetic field $\boldsymbol{B}$,

$$\hbar\omega \sim \frac{\gamma^2 eB}{\sin\theta m_e c} > 10^5 \left(\frac{R_*}{r}\right)^3 \text{ eV}. \tag{4}$$

Here the Crab pulsar magnetic field is approximated as dipolar and expressed in terms of the ratio of stellar radius (R_*) to radial coordinate r. To achieve the needed strong luminosity at optical frequencies the distance $r \gg 10R_* \sim 10^7$cm. Finally, inverse Compton scattering into the optical regime is hugely

suppressed in the presence of the large neutron star magnetic field. Any $e^-(e^+)$ near the star moves along $\boldsymbol{B}$ (because of very rapid synchrotron loss). In the electron's rest frame the soft photon to be up-scattered to optical energies moves almost parallel to $\boldsymbol{B}$. The Thomson cross section for photon scattering (σ_T) to angular frequency ω is then reduced to

$$\sigma \sim \sigma_T \left(\frac{\omega m_e c}{eB\gamma}\right)^2 \sim 10^{-15}\sigma_T \tag{5}$$

near the star. This cross section is much too small for up-scattering of microwave photons to be an important contributor to the Crab pulsar's optical luminosity. Thus only sychrotron radiation from electrons at distances r approaching the light cylinder radius survives among the canonical incoherent processes for optical photon emission from a pulsar magnetosphere.

iii) The absolute magnitude of the Crab pulsar's energetic radiation luminosity also constrains the emission source location. The maximum net magnetospheric current along (open) magnetic field lines through any pulsar accelerator should not itself give a magnetic field which significantly exceeds the neutron star's own magnetic field anywhere along current flow lines (along $\boldsymbol{B}$) between the polar cap ($B \equiv B_*$) and the light cylinder. This limits the net particle flow through any accelerator which accelerates e^- and e^+ in opposite directions to

$$\dot{N} \lesssim \frac{\Omega^2 B_* R_*^3}{ec} < 10^{34}\ \mathrm{s}^{-1}. \tag{6}$$

If the accelerator is near the stellar surface pair production in the 10^{12}G magnetic field limits the potential drop (ΔV) along $\boldsymbol{B}$ to

$$\Delta V \lesssim 10^{12}\ \text{Volts}. \tag{7}$$

The total power $e\dot{N}\Delta V \lesssim 10^{34}\mathrm{erg\ s}^{-1}$. This is much smaller than the $5 \cdot 10^{35}\mathrm{erg\ s}^{-1}$ from the Crab pulsar in the X-ray – GeV spectral interval (for a beam shape that gives a similar time averaged observed luminosity from almost all directions). Only for $r > 10^7$cm could local B be low enough to allow ΔV to exceed 10^{14} Volts.

We assume (and it is a consequence or assumption of most models) that the electrons and/or positrons injected into the the Crab's dominant magnetospheric particle accelerators are locally produced. For an accelerator close to the stellar surface these pairs could originate in the conversion of 10^2MeV curvature γ-rays to $e^\pm$ pairs in the huge stellar magnetic field. However, for accelerators as far from the star as indicated above $\gamma + \gamma \rightarrow e^+ + e^-$ is a much more important pair production mechanism. If there is strong $e^\pm$ production and acceleration of e^-/e^+ in the Crab magnetosphere where $r \gg R_*$, the associated radiation from these electrons (or their progeny) has several properties which are not dependent upon the detailed way in which the acceleration and radiation are achieved.

1) Because intitially accelerated e^-/e^+ move relativistically along local $\boldsymbol{B}$ most of the primary energetic radiation is emitted parallel to the $\boldsymbol{B}$ at the accelerator.

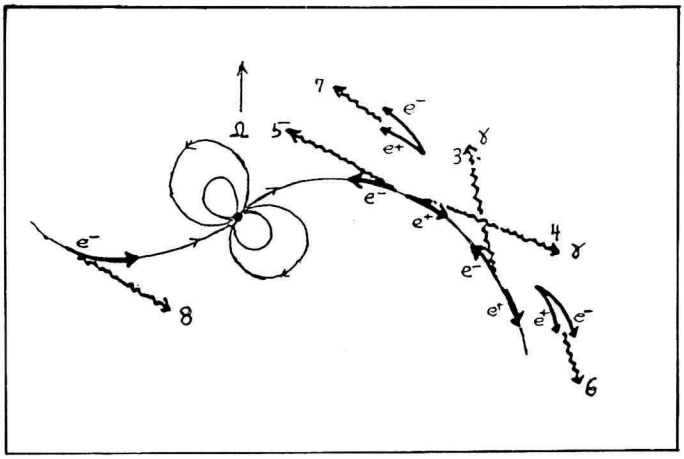

Figure 3. The geometry for photon emission from outer-magnetosphere accelerators which accelerate e^-/e^+ along local $\boldsymbol{B}$ with an electric field component $\boldsymbol{E}\cdot\boldsymbol{B}$ within the accelerator. The resulting radiation from curvature radiation, synchrotron radiation, or inverse Compton scattering is a fan covering almost all latitudes. Similar beams go outward (4, 6) and inward (3, 7). Because of dipolar symmetry the observer who sees outward moving photons (4) in one subpusle will also see inward moving photons (8) from the other side of the star in a later arriving second subpulse as the star rotates. Gamma-ray beam crossing such as shown for 3 and 4 will sustain $e^{\pm}$ production around the accelerator (ref. 13).

The flow of $e^-(e^+)$ accelerated toward the star will be approximately matched by $e^+(e^-)$ flowing away from it. The same is true for any $e^{\pm}$ pairs created by γ-rays from the accelerator in locations where $e^{\pm}$ are not separated by local electric fields along $\boldsymbol{B}$. It follows from this that the emission from around these $e^- - e^+$ symmetric accelerators must consist of four beams of similar strengths (cf. Figure 3). First, a beam from outward (i.e., moving along $\boldsymbol{B}$ away from the neutron star) moving $e^-(e^+)$ or $e^{\pm}$ paris. Second, an almost equivalent beam from inward (i.e., moving along $\boldsymbol{B}$ toward the star) moving $e^+(e^-)$ or $e^{\pm}$ pairs. Finally phenomena on open $\boldsymbol{B}$-field lines connected to the star at a polar cap should be matched by very similar ones on $\boldsymbol{B}$-field lines from the opposite polar cap. Because the radiation source is so far from the stellar surface all of the radiation ultimately escapes through the light cylinder. (For near surface accelerators inward directed beams could be blocked.)

2) These four beams (only two of which would be visible to any observer) should have a very large longitudinal spread. This follows because the needed accelerator potential drop in the Crab magnetosphere ($\Delta V > 10^{14}$ Volts) and the associated electric field along $\boldsymbol{B}$ ($\boldsymbol{E}\cdot\hat{\boldsymbol{B}} > 10^6$ Volts cm^{-1}) are so large that accelerated e^-/e^+ quickly achieve energies that are radiation reaction limited (by curvature radiation if inverse Compton scattering on abundant soft photons does not limit accelerated e^-/e^+ energies first). As a result the primary radiation, and that from secondary pairs, is determined by the accelerator

$\boldsymbol{E}\cdot\hat{\boldsymbol{B}}$ which tends to be flat through the accelerator (rather than the potential drop which grows monotonically from one end to the other). The very large ΔV needed in the outer magnetosphere can be achieved only in a very long accelerator. Therefore similar γ-ray emission is expected for great distances along a downward (upward) curving $\boldsymbol{B}$-field line through the relevant accelerators. One consequence is a large probability that any observer would see two beams of energetic radiation from the accelerator no matter what the angle between the pulsar's spin ($\boldsymbol{\Omega}$) and its dipole moment or the direction to the observer. This suggested geometry (Figure 3) receives some support from two features of the observed optical, X-ray and γ-ray radiation from several young pulsars. First, searches of the Crab and Vela supernova remnants and also that containing PSR 0540-693 for such young pulsars did indeed discover them. If the rotating beams were cone-like with lattitudinal widths comparable to their observed widths in latitude such a success rate would be highly improbable. The *a priori* probability for intercepting both the Crab and Vela energetic radiation beams would not have exceeded about 1/25. Longitudinally extended fan-like beams (or very wide angle hollow cones) are more plausible alternatives. A second consequence is that all three pulsars should have a double beam structure. While the large 140° subpulse separation of the Crab and Vela pulsars might suggest successive observation of North and South magnetic poles, the very much smaller 80° separation observed in PSR 0540 (21) argues against such an interpretation. However these separations are quite compatible with the geometry of Figure 3 where aberration and time of flight differences would give observed subpulse phase separations which can vary greatly for different viewing or tilt angles (e.g., photons 4 and 8 of Figure 3 would arrive at any observer with a time separation comparable to the time of flight difference across the light cylinder, i.e., Ω^{-1}).

3) Because radiation reaction limits the e^-/e^+ energy achieved in the accelerator essentially the full potential drop energy $e\Delta V$ is radiated away from the accelerator. Thus the magnetosphere accelerator is almost 100 percent efficient as a radiation source.

4) Finally, the expected accelerator geometry has crossing γ-ray beams in the outer-magnetosphere (e.g., beams 3 and 4 of Figure 3) which gives copious $e^{\pm}$ production from $\gamma + \gamma \rightarrow e^- + e^+$ (or $\gamma + X \rightarrow e^- + e^+$ with $10^2 - 10^3$ MeV γ-rays on KeV X-rays).

5. AN EMISSION MODEL (13)

It has been argued (14, 15, 24) that expected current flow in many young pulsar magnetospheres can lead to charge deficient regions ("gaps") in which $\boldsymbol{E}\cdot\hat{\boldsymbol{B}}$ grows until limited by pair production processes. For short period pulsar outer-magnetosphere parameters a series of processes can give self-sustained $e^{\pm}$ production and associated energetic radiation:

a) Any $e^{\pm}$ produced in an accelerator gap is instantly separated by large $\boldsymbol{E}\cdot\hat{\boldsymbol{B}}$. Because of magnetic field line curvature each oppositely accelerated lepton radiates multi-GeV curvature γ-rays.

b) These γ-rays collide with KeV X-rays, from d) below, to make $e^{\pm}$ pairs. Pairs created in the accelerator gap itself repeat process a) above.

c) In the Crab magnetosphere pairs created beyond the gap boundary lose their energy to optical-MeV synchrotron radiation and also to higher energy γ-ray creation when they inverse Compton scatter on the same X-ray flux which was responsible for their creation.

d) The X-ray flux from synchrotron radiation is also that which originally caused materialization of the curvature γ-rays of b) and the inverse Compton scattering of c). Because of the beam crossing of Figure 3, $e^{\pm}$ and γ-rays interact mainly with the crossing X-ray flux radiated by the oppositely directed pairs.

e) A further generation of $e^{\pm}$ paris from crossed γ-ray fluxes of c) radiates soft photons extending down to far IR for Vela (15). Some of this passes through the accelerator gap where it can be inverse Compton scattered by primary gap accelerated e^{-}/e^{+}.

This cyclic chain a) – e) of processes bootstraps a self-sustained emission of radiation with calculated self-consistent spectra shown in Figures 4 and 5 for Crab and Vela parameters.

The calculated break in the Vela spectrum which greatly suppresses the X-ray part of the spectrum is a direct consequence of the limited time (τ) spent by synchrotron radiating $e^{\pm}$ pairs in the outer-magnetosphere. Those pairs moving inward are reflected in the converging $\boldsymbol{B}$-field and join with outward moving pairs in passing out through the light cylinder. The critical synchrotron radiation frequency (ω_c) achieved by the $e^{\pm}$ pairs before this happens has a τ and local B dependence (15)

$$\omega_c \propto \tau^{-2} B^{-3} \propto \tau^2 \Omega^{-9} \propto \Omega^{-7}. \tag{8}$$

A spectral break calculated to occur at around 40 eV in the Crab spectrum would be at 10^2 keV in Vela's if additional corrections relating to initial pitch angle are neglected.

The rough agreement of calculated spectra and subpulse features from such outer-magnetosphere accelerator models with those observed (Figures 4 and 5) may support using such models to predict the dependence of γ-ray luminostiy on pulsar period (P).

Calculated γ-ray luminosities of Crab-Vela type γ-ray pulsars ($B_* \sim 3 \cdot 10^{12}$G) as a function of a pulsar period is given in Figure 6 (17, 18). For $P < P_{\rm crab}$, B in the outer-magnetosphere is greater than that of the Crab pulsar at the same fractional distance ot its light cylinder. One consequence is that it is much easier to limit the growth of outer-magnetosphere accelerator gaps by pair production. The γ-ray luminosity, which equals the accelerator power needed to achieve this limit, is roughly proportional to P in this regime. The Vela pulsar has a much different mix of the processes a) – e) above than that in the larger (local) $\boldsymbol{B}$ of the Crab outer-magnetosphere. A much larger fraction (f) of its total spin-down power appears in $L_\gamma (f \sim 10^{-2})$ than was the case for the Crab ($f \sim 10^{-3}$). As the pulsar period grows beyond Vela's, local B decreases and ω_c increases well above an MeV so that the efficiency for $\gamma + \gamma \rightarrow e^- + e^-$ is diminished: an increasing f and L_γ are then required to sustain needed outer-magnetosphere $e^{\pm}$ production.

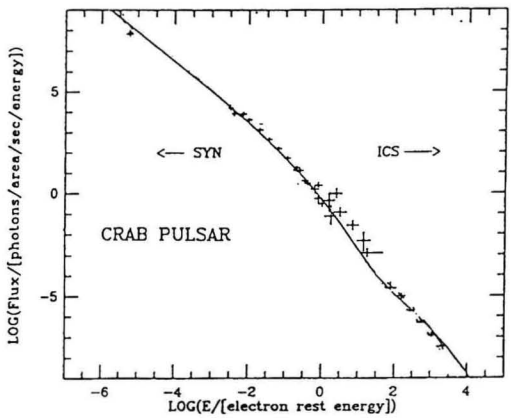

Figure 4. Comparison of Crab pulsar observations and a model prediction for an outer-magentosphere gap. (The normalization is adjusted arbitrarily.) SYN refers to synchrotron radiation and ICS to inverse Compton (from ref. 15).

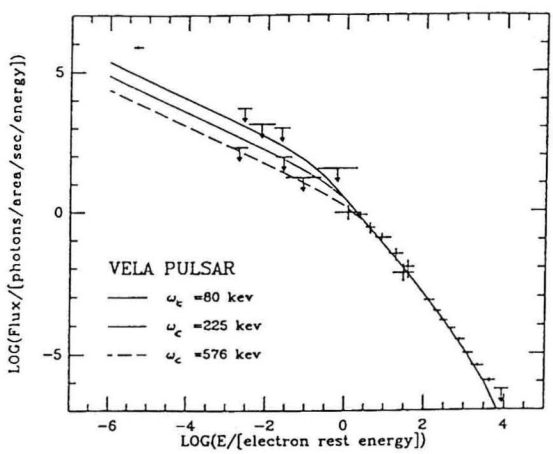

Figure 5. Comparison of Vela pulsar observations and model predictions from ref. (15). The ω_c refer to Eq. (8).

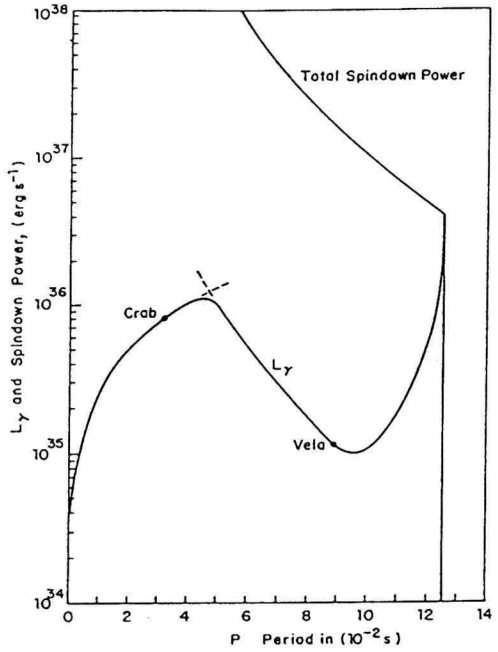

Figure 6. Model calculations for the evolution of the γ-ray luminosity (L_γ) of a strongly magnetized ($B_* \sim 3 \cdot 10^{12}$G) pulsar as a function of pulsar period (P) (ref, 18).

L_γ grows until it somewhat exceeds 10^{36}erg s^{-1} and $f \to 1$. No further growth is then possible and self-sustained outer-magnetosphere accelerator pair production ceases for still longer P. The estimated number ($\sim$ 40) and luminosity of such intense γ-ray sources are of the same order as those of the still unidentified strong Cos B sources. It is tempting to propose that these Cos B sources are indeed dying Vela type γ-ray pulsars. Even if various outer-magnetosphere accelerator details do not survive, the general argument that lengthening P beyond Vela's will increase f (a growth already apparent in the transition from the Crab to Vela pulsars) may be expected to be quite robust so that the predicted growth in L_γ and subsequent γ-ray turn-off should remain valid.

Strong γ-ray sources may also be achieved for much smaller P when B_* is small enough. The magnetospheres of many members of the millisecond pulsar family resemble the outer-magnetosphere of the Vela family so that many of them may be detectable as strong γ-ray pulsars.

The crucial question of how canonical radio pulsars may continue to be radio emitters even if strong outer-magnetsophere $e^\pm$ production is quenched has been discussed elsewhere (17, 18).

6. POSSIBLE EXO-MAGNETOSPHERIC ORIGINS FOR ADDITONAL CRAB PULSAR MeV AND TeV RADIATION

Because the Crab model calculations and observations agree roughly over a spectral

interval of 10 orders of magnitude and a photon flux spanning 20 the log-log plot of Figures 4 and 5 show a rather promising fit. The data theory comparison in Figure 7 (20) more clearly emphasizes the differences between theory and observations.

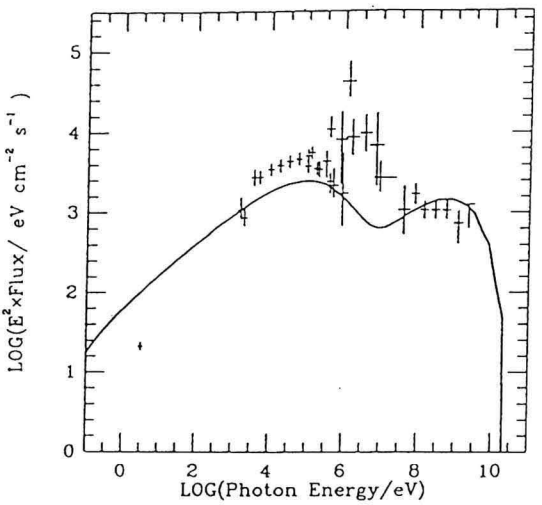

Figure 7. Emitted energy per decade of photon frequency for the Crab pulsar (ref. 20).

We note first that the calculated synchrotron light is almost an order of magnitude larger than that observed. However, the Crab model calculation does not exploit the spectral break of Equation 8 which is predicted to be near optical frequencies for the Crab outer-magnetosphere. Its inclusion can very significantly reduce model predictions. The failure of the model to reach observed intensities around an MeV raises more serious questions. The data themselves have been acquired in a variety of different programs and show considerable scatter and lack of consistency. The largest observed excesses over model calculations are generally those from long term observations from satellites; rocket, and balloon flight data have been closer to theoretical predictions (cf. 16, 22). It is, perhaps, possible that much of the excess is in transient activity usually missed in shorter time observations. A spectrally broad (transient) excess around an MeV may possibly have a very different kind of origin from the rest of the Crab pulsar emission. Most of the Crab spin-down power is probably carried beyond the magnetosphere light cylinder as a 30 Hz (electro-)magnetic field spun off by the rotating dipole of the neutron star and a TeV – PeV $e^{\pm}$ wind. The pairs are created within the magnetosphere but receive most of their ultimate energy beyond it from acceleration by the rotating magnetic dipole. This ultra-relativistic $e^{\pm}$ wind (whose power may approach $5 \cdot 10^{38}$erg s^{-1}) can inverse Compton scatter on the pulsar's radio and optical emission. Near the magnetosphere where there is still a significant angle between the wind direction and that of the radiation photons (both approach exact radial flow only far from the magnetosphere) inverse Compton scattering of the

very abundant photons at the low end of the pulsar's radio emission spectrum may convert enough of these into MeV γ-rays to give a dominant contribution to the observed pulsed γ-ray photons in that spectral region. A large additional pulsed inverse Compton contribution by the Crab pulsar's exo-magnetospheric outgoing $e^{\pm}$ wind would then also be expected from inverse Compton scattering on the abundant optical emission coming from within the magnetosphere. These up-scattered photons should acquire up to the full TeV–PeV energy of the wind electrons. Transient pulsed 10^{14}eV γ-rays from the Crab have indeed been reported recently (22) in simultaneous observations by the Kolar Gold Field air-shower group in India and the Baksan group in the USSR. Both the high luminosity (3×10^{36}erg s^{-1} if isotropic) and γ-ray energy would make a magnetospheric origin for this radiaiton implausible (10^{14}eV γ-rays cannot traverse $B \gtrsim 10^4$G).

It is a pleasure to thank Professors E. van den Heuvel, J. van Paradijs and the Astronomical Institute Anton Pannekoek for their warm hospitality. This research has received support from NSF AST89-01681. This work is contribution number 435 of the Columbia Astrophysics Laboratory.

REFERENCES

(1) Bignami, G., in *High Energy Phenomena around Collapsed Stars*, ed F. Pacini, *NATO ASI; Cargese 1985)* (Reidel, 1987).
(2) Levinthal, M., in *13th Texas Symposium on Relativistic Astrophysics*, ed M. Ulmer (World Scientific, Singapore, 1987), p. 382 and references therein.
(3) McClintok, J., and Levinthal, M. *Ap.J.* (1989), in press.
(4) Kluźniak, W., Ruderman, M., Shaham, J., and Tavani, M. 1988, *Nature*, **336**, 558 and *IAU Symposium 136*, ed. M. Morris.
(5) *Gamma Ray Bursts*, ed. E. Liang and V. Petrosian (AIP Conf. Proc. 141) and references therein.
(7) Protheroe, R. in *Proceedings of 20th International Cosmic Ray Conference* (Moscow, 1987) and references therein.
(8) Weekes, T., in *Proc. of 14th Conference on Relative Astrophysics*, ed. E. Feneyes (World Scientific, Singapore, 1989) and references therein.
(9) Weekes, T., Cawley, M., Fegan, D., Gibbs, K., Hillas, A., Kowk, P., Lamb, R., Lewis, D., Macomb, D., Porter, N., Reynolds, P. and Vacanti, G., *Ap.J.*, in press.
(10) Dingus, B., Alexandreas, D., Allen, R., Burman, R., Butterfield, K., Cady, R., Chang, C., Ellsworth, R., Goodman, J., Gupta, S., Haines, T., Karakaver, D., Lloyd-Evans, J., Nagle, D., Potter, M., Sandberg, V., Talaga, R., Wilkinson, C., and Yodh, G. 1988, *Phys. Rev. Lett.*, **61**, 1906.
(11) Ghosh, P. and Lamb, F. 1979, *Ap.J.*, **234**, 296.
(12a) Cheng, K., and Ruderman, M. 1990, *Ap.J.*, submitted.
(12b) Cheng, K., and Ruderman, M. 1989, *Ap.J. (Letters)*, **337**, L77.
(13) Ruderman, M., 1989 in *Gamma Radiation from Radiopulsars*, NASA 1989 Egret Symposium Proc., ed. F. Stecher (Sections 4, 5 and 6 of this paper are largely taken from this reference).

(14) Cheng, K., Ho, C., and Ruderman, M. 1986, *Ap.J.*, **300**, 495.
(15) Cheng, K., Ho, C., and Ruderman, M. 1986, *Ap.J.*, **300**, 522.
(16) Graser, U. and Schönfelder, V. 1982, *Ap.J.*, **263**, 677.
(17) Ruderman, M., in *13th Texas Symposium on Relativistic Astrophysics*, 1986, ed. M. Ulmer (World Scientific, Singapore, 1987) p. 448.
(18) Ruderman, M. and Cheng, K. 1988, *Ap.J.*, **355**, 306.
(19) Dowthwaite, J., Harrison, A., Kirkman, I., McCrae, H., McComb, T., Oxford, K., Turner, K., and Walmsley, M. 1984,, *Ap.J. (Letters)*, **286**, L35.
(20) Ho, C. 1989, *Ap.J.*, **342**, 396.
(21) Middleditch, J., and Pennypacker, C. 1985, *Nature*, **313**, 659.
(22) White, R. *et al.* 1955, *Ap.J. (Letters)*, **299**, L93.
(23) Rao, M. 1989, *IAU Circular No. 4883* (Oct. 23, 1989).
(24) Ruderman, M., in *Timing Neutron Stars* in *Proceedings of NATO Advanced Study Institute*, Cesme, 1988, ed. H. Ogelman and E. van den Heuvel (North Holland, Amsterdam, 1989).

AUTHOR'S ADDRESS:

Astronomical Institute
University of Amsterdam

and

Department of Theoretical Physics
University of Oxford

Permanent address:

Department of Physics
Columbia University
New York, N.Y. 10027, USA

K. E. Turver

TeV Gamma-rays from X-ray Binary Pulsars

Abstract: A number of categories of celestial very high energy (> 0.2 TeV) gamma ray sources has now been established including X-ray binary sources containing pulsars. We here briefly describe the ground based atmospheric Cerenkov light technique used to detect such very high energy (VHE) gamma rays, and review the evidence for their emission from X-ray binary pulsars. An initial attempt is made to establish patterns in the observed emissions as an aid to understanding of gamma ray production.

1. INTRODUCTION

It is now about 20 years since the first claims were made for the detection of very high energy (VHE) gamma rays from celestial sources. These early results suggested that the Crab pulsar (56) and nebula (45), the enigmatic object Cygnus X-3 (104) and the active galaxy Centaurus A (57) all emitted gamma rays of energy around 1000 GeV. All of these observations depended, as do the more recent results, on the use of the atmospheric Cerenkov light technique pioneered by Jelley (49) and reviewed by Turver (98) and Weekes (106).

It came as something of a surprise in 1983 that a classical X-ray binary pulsar (XRB) - Hercules X-1 - was observed as a source of VHE gamma rays showing an excess of counts which were periodic at the X-ray rotational period (41). Since then other XRBs have been identified as VHE gamma ray emitters with a range of statistical significance. Some identifications are quite firm, some are marginal and it is possible that some of the claims for sources may be ultimately proved to be erroneous. Nevertheless, a review of the evidence for VHE gamma ray emission from X-ray binaries as a basis for the development of models for its production is timely.

In this review we outline the atmospheric Cerenkov light technique which underpins all the VHE observations, report the evidence for emission of VHE photons from XRBs and search for any pattern in these emissions.

2. THE ATMOSPHERIC CERENKOV LIGHT TECHNIQUE

2.1 Cerenkov light in the atmosphere

A celestial high energy gamma ray striking the top of the atmosphere initiates a cascade of electrons and photons which reaches a maximum of development at altitudes of around 10 km above sea level. The electrons - about 1 for every GeV of incident gamma ray energy - produce a brief optical flash through the Cerenkov

process in the medium (air). This lasts for a few ns and penetrates with little attenuation to produce a pool of visible light at ground level. For a primary gamma ray with energy 1000 GeV the pool covers an area of ~ 10000 m^2 with typical densities of 50 optical (blue) photons m^{-2}. This brief flash of visible radiation may be readily detected by a simple flux collector which focuses the light onto a photosensor. Due to the width of the light pool, a detector of small physical area (typically a few m^2) will have a large effective collecting area so enabling the low intrinsic VHE gamma ray rate to be translated into a worthwhile rate of detection. Unfortunately this simple and economic technique suffers from a serious background problem owing to the presence of a dominant isotropic background of cosmic ray particles (mainly protons). These produce atmospheric Cerenkov light signatures which are very similar to the gamma ray initiated events. The fraction of gamma-rays is typically a few percent of this background. Recently attempts to overcome these limitations have been made involving different approaches to identify the signatures due to gamma rays (22, 11, 99).

2.2 Atmospheric Cerenkov light telescopes

The simplest Cerenkov telescope comprises two flux collectors and two light detectors (photomultipliers (PMTs) have always been used to date). The fast coincidence between the light flashes detected by the two collector systems ensures that a genuine Cerenkov light flash is detected and a low threshold energy for detection can be attained. Such simple systems were typical of the first Cerenkov telescopes. In recent years more ambitious telescopes have been built and operated. For example, the Whipple collaboration (25) has pioneered a new technique to enhance the proportion of gamma rays in a dataset by using a high resolution camera comprising more than 100 PMTs at the focus of a single large area high quality mirror and exploiting the information in the shape of the Cerenkov light image. The Haleakala collaboration (91) has pursued an alternative approach based on the combination of carefully chosen low noise PMTs and matched mirror areas (¾ in PMTs viewing 60 cm mirrors operated in typically 7-fold coincidence) to provide a fast (sub ns) sample of the Cerenkov photons at the single photoelectron level. The Durham group (10) has developed a range of conventional telescope designs incorporating threefold fast coincidence between photon samples. Recent versions of their telescopes have involved 11 m^2 mirrors, viewed by clusters of 7 PMTs at each prime focus used for rejecting off-axis (background proton) events on the basis of arrival direction.

Since many of the results to be reported here have been obtained with the Durham telescopes they will be briefly described.

2.3 The University of Durham VHE gamma ray telescope

The University of Durham Mark III VHE gamma ray telescope has been operating in Narrabri, NSW, Australia since September 1986. It consists of three paraxial dishes of approximately 11 m^2 effective area and each is formed from 44 smaller spherical mirrors deployed as a close-packed array (see Figure 1).

Each flux collector is viewed by a detector package containing seven 46 mm diameter photocathode PMTs operated in triple fast coincidence between the three dishes. Within each detector package, the central PMT views the area of sky along the telescope's axis, while the other six PMTs view adjacent areas of sky offset by 2° from the central channel. This allows simultaneous measurements of a suspected source region and six surrounding background regions. This type of detector also

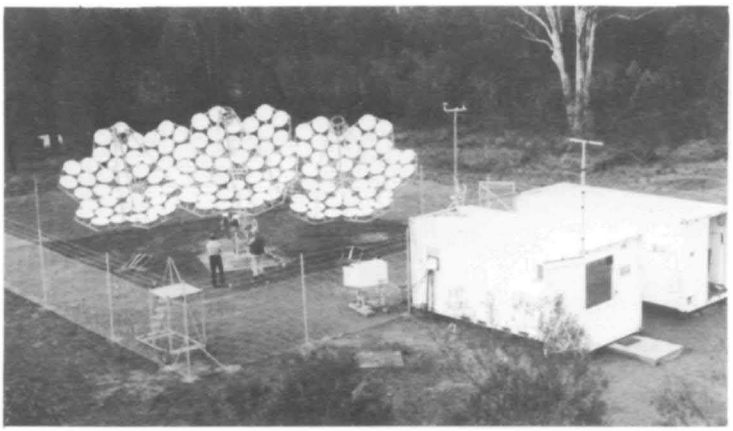

Figure 1. The University of Durham Mark III gamma ray telescope at Narrabri, NSW, Australia.

enables a worthwhile enhancement of the gamma ray to background proton counting rate to be made by rejecting those events recorded by the central (on-source) PMT and any of the guard ring PMTs (11). Such events originate from directions away from the source and have been shown to be predominantly background cosmic ray events.

The time of arrival of each Cerenkov flash is recorded to an accuracy of 1 μs, along with the detail of the detector responses and the charge registered by each PMT. Close to the zenith, a count rate of > 2 Hz per square degree (i.e. per channel) is achieved. A detailed description of the Mark III telescope is given in Brazier *et al* (10); the Mark IV telescope, which was used in 1988/89 in La Palma, Canary Islands and is now operational at Narrabri, is similar in all respects except that the flux collectors are each of area 6 m^2.

3. VHE GAMMA RAYS FROM X-RAY BINARY PULSARS

3.1 Introduction

Table 1 shows a list of the known X-ray binaries which include a pulsar; they are listed in order of increasing rotational period. The objects in Table 1 for which gamma ray observations have been made are summarized in Table 2, where an indication of the status of the search for VHE gamma ray emission is given. The evidence from each gamma ray measurement will now be considered in detail, dealing first with high mass X-ray binaries (HMXRB) and then with the low mass X-ray binaries (LMXRB).

The analysis of the typical weak signal in VHE gamma ray observations of binary systems (a few % of the cosmic ray count rate) requires special treatment of the data. For example, the rotational period of the pulsar after Doppler shifting due to the orbital motion cannot be directly observed, in contrast with the case in X-ray observations. Rather, the effects of the binary motion of the source region for VHE gamma rays must be accurately allowed for by transforming the time of each recorded Cerenkov flash to the rest frame of the binary system. This is followed by a test for uniformity of phase. Such a routine is necessary if a weak signal in a large dataset spanning a wide range in orbital phase is to be recovered. In most cases the sensitivity of this analysis to the assumed parameters of the orbit is not critical; the binary orbital

Table 1. The known X-ray binary pulsars.

Name	Pulsar period (s)	Orbital Period (days)	Classification
1E1024-57	0.061		
A0538-66	0.069	16.7	Massive Be
SMC X-1	0.714	3.89	HMXRB
Her X-1	1.24	1.70	LMXRB
H0850-42	1.78		
4U0115+63	3.61	24.3	Massive Be
V0332+53	4.38	34.25	Massive Be
Cen X-3	4.84	2.09	HMXRB
1E1048.1	6.44		Massive Be
1E2259+59	6.98	0.03 (?)	LMXRB
4U1626-67	7.68	0.03	LMXRB
2S1553-54	9.30	30.6	Massive Be
LMC X-4	13.5	1.41	HMXRB
2S1417-67	17.6		Massive Be (?)
GS1843+00	29.5		
OAO1653-40	38.2		HMXRB
EXO2030+37	41.8	45-47	Massive Be
Cep X-4	66		
4U1700-37	67.4 (?)	3.4	HMXRB
GS1836-04	81.1		
GS1843-02	94.8		
A0535+26	104	111	Massive Be
Sct X-1	111		
X0021.8-72	120.2		LMXRB (?)
GX1+4	122	304	LMXRB
4U1230-61	191		
GX304-1	272	133	Massive Be
Vela X-1	283	8.96	HMXRB
4U1145-61	292	188	Massive Be
1E1145.1	297	5.6 (?)	HMXRB
A1118-61	405		Massive Be
GPS1722-36	414		
4U1907+09	438	8.38	HMXRB
4U1538-52	529	3.73	HMXRB
GX301-2	696	41.5	HMXRB
4U0352+30	835	580	Massive Be

parameters (known from X-ray or optical observations) are usually of sufficient accuracy to allow a satisfactory transformation. Similarly, any uncertainty due to assuming a common origin for the X-ray (or optical) and VHE photons is in most cases acceptable.

3.2 SMC X-1

This X-ray binary consists of a highly magnetized neutron star in a 3.9 d orbit about a B0.5 I supergiant. It is one of the most powerful of the known X-ray binaries with high state X-ray luminosities in excess of 10^{39} erg s^{-1}. The pulsar spin period is 0.7 s and the X-ray observations over an 18 year period indicate that the pulsar is being spun up uniformly.

Table 2. Summary of VHE gamma ray observations

Object	Status of VHE observations		
	Source	Possible source	Flux limit
Cyg X-3	X		
A0538-66			X
SMC X-1		X	
Her X-1	X		
4U0115+63	X		
V0332+53			X
Cen X-3	X		
1E1048.1			X
1E2259+59		X	
4U1626-67		X	
LMC X-4		X	
2S1417-62			X
X0021.8-72		X	
GX1+4			X
Vela X-1	X		
4U1145-61		X	
1E1145.1			X
4U0352+30			X
A0535+26			X

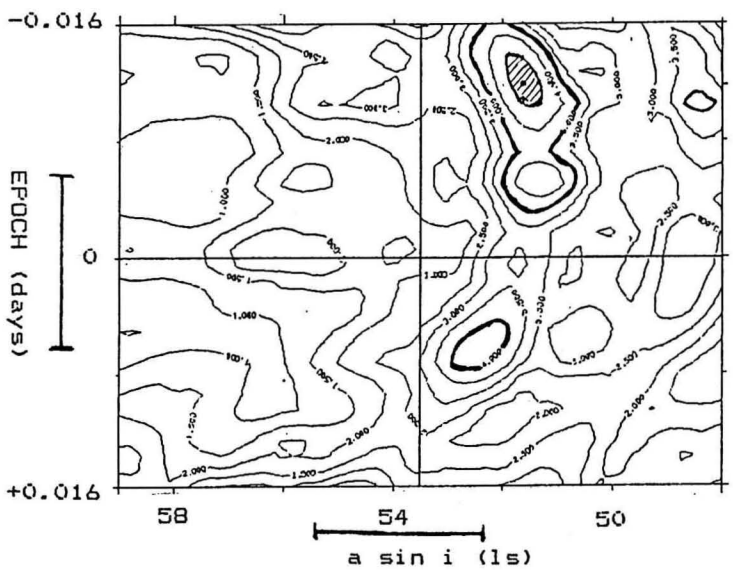

Figure 2. A contour plot for the 1987 July dataset from SMC X-1 taken with the University of Durham telescope at Narrabri . The contours represent the chance probability at the X-ray period plotted as a function of the epoch of mid-eclipse and *a sin i*. The heavy line represents the contourof a chance probability 10^{-4}; the hatched area has chance probability $< 10^{-5}$. × denotes the orbital parameters expected from X-ray measurements. The error flags show the bounds for "sampling" intervals in epoch and *a sin i*.

The only VHE observations of SMC X-1 are those made for a total of 333 hrs on 101 nights between 1986 October 3 and 1989 December 1 with the Durham University Mark III telescope at Narrabri (12, 69). This is the largest dataset for any XRB observed in the Durham program; however the analysis of the data poses problems when attempting to allow for the Doppler shifting of the period because of the short rotational period (0.7 s) and semi-major axis of the binary orbit (53 ls). It is necessary to consider the effects of "sampling" in the dataset not only of the value of the pulsar period but also the values of the semi-major axis *(a sin i)* and the epoch of mid-eclipse. We show in Figure 2 a contour plot of the probability of uniformity in phase according to a Rayleigh test as a function of epoch and *a sin i*. (The test for uniformity at the X-ray period was made on a sample of 9 observations each of typically 3 hrs duration made in an elapsed interval of 10 days in 1987 July; the data from each observation were analysed independently and the probability quoted is derived by combination of the results of tests of the individual datasets). The minimum probability (6×10^{-6}) increases to about 6×10^{-4} when allowance is made for the range of values of pulsar period and orbital parameters tested, and for the effects of oversampling. Similar data are available from later observations.

3.3 Centaurus X-3

Centaurus X-3 is a 4.8 s pulsar in a 2.1 d orbit. The X-ray emission is well studied, with recent observations from the *Ginga* and *Mir-Kvant* spacecraft. VHE gamma-ray emission from Cen X-3 was first reported by the Durham group using the Narrabri telescope (20). The total data set consisted of 207 hours of observations and spanned the whole of the orbit. This is an example of a case where the orbital paparameters from X-ray observations allow an adequate correction for Doppler shifting of the period to be made. Evidence was found, significant at the 10^{-6} chance level, for pulsed emission at the expected X-ray period but the emission is found to be confined to data recorded in a 5% wide orbital phase band around the ascending node - see Figure 3.

Independent confirmation of VHE emission from this object has come from the Potchefstroom group (79). Analysing 71 hours of data accumulated during 1986 May

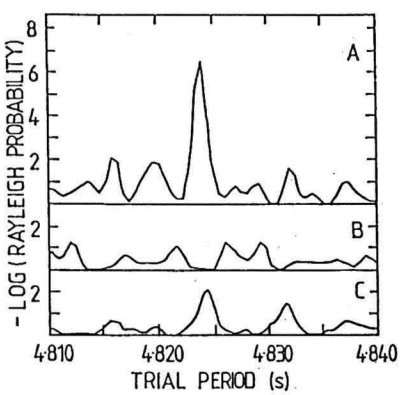

Figure 3. The variation of chance probability with period for data taken in the orbital phase range 0.77 - 0.82 from Cen X-3. (a) uses events which triggered the central detector only, (b) uses events which triggered both the central detector and an outer guard-ring detector and (c) comprises events which triggered an outer guard-ring detector only. The data are from the University of Durham telescope at Narrabri.

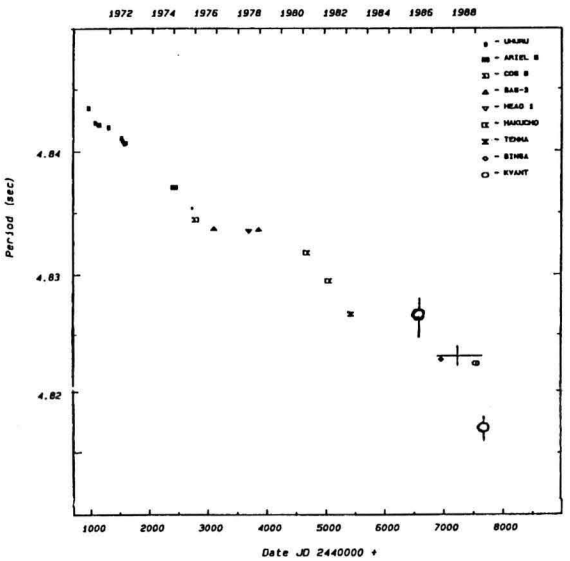

Figure 4. The pulse period history of Cen X-3 based on X-ray measurements from the compilation of Gilfanov *et al* [51]. Legend

o Potchefstroom VHE gamma ray measurements (79)

\+ Narrabri VHE gamma ray measurements (20)

1 - 1989 April 5, they found evidence for pulsed emission, also confined to orbital phases 0.7 - 0.8 only, at a chance probability level of 2×10^{-4}. However, the large value of the period derivative hinted at by these results contrast with small values demonstrated by the contemporary X-ray and the Durham VHE gamma ray measurements - see Figure 4.

3.4 LMC X-4

The fourth X-ray source in the Large Magellanic Cloud was discovered by Giacconi *et al* (50), using data from the *Uhuru* satellite. Photometric and spectroscopic observations of the optical counterpart revealed the binary nature of the source, the orbital period being 1.408 days. Occasional X-ray flaring episodes have been observed from this object, and a pronounced 30.5 day periodic modulation in the hard X-ray flux has also been observed, similar to that of Hercules X-1. This modulation is also seen in photometric data. The pulsar period is 13.5 s, and it has been measured with the *SAS 3*, *EXOSAT* and *GINGA* satellites (59, 60, 80). Ultra high energy gamma ray data from the direction of this object, taken with the Buckland Park array show modulation with the characteristic 1.4 d orbital cycle which is significant at the 3.2 σ level (82).

The only VHE measurements to date have been made by the University of Durham group. Over 107 hr of data on LMC X-4 were taken with the University of Durham Mark III telescope on 36 nights between 1987 January 26 and 1989 November 29 (12). The first data, from observations in 1987 January and February, were tested for the pulse period expected from the X-ray measurements. Some evidence for periodic behaviour was found in the data recorded at orbital phases 0.5 - 0.7. The pulsed strength for this dataset was found to be 3.8% of the cosmic ray background, corresponding to a VHE gamma ray flux of 2.0×10^{-10} cm^{-2} s^{-1}, with a Rayleigh probability of 2.2×10^{-4}, after correcting for all degrees of freedom. Further

observations of the object were made and the data analysed in the same way. These showed no evidence for pulsed emission. A possible explanation of this apparent variable VHE gamma ray emission may lie with the 30.4 day cycle observed in optical measurements. However observations made in 1989 November at approximately the same phase in the 30.4 day optical cycle as those of 1987 January/February showed no periodicity.

3.5 Vela X-1

Vela X-1 is a 283 s pulsar in an 8.96 d binary orbit. X-ray observations show that the pulse period history is complex, with epochs of spin-up and spin-down behaviour (see Figure 5). At UHE energies, there have been reports of the detection of a signal (81, 96, 103); the first reported detection at VHE energies was by North *et al* (78), using the Nooitegedacht telescopes of the Potchefstroom group. During 1986, they observed pulsed emission which persisted throughout the binary orbit. They also observed a strong outburst of pulsed emission which occurred in phase with the persistent pulsed effect but which lasted for only a few pulsar rotations around the time of entrance to the X-ray eclipse. However, there is a puzzle; the period found in both these observations (282.82 s) is inconsistent with the value provided by later X-ray and gamma-ray measurements. Subsequent observations (85, 86) using the Potchefstroom telescopes in 1987 and 1988 confirmed the persistent emission and the bursts, which were confined to about half the orbit around eclipse. Moreover, the period observed in these later measurements was in accord with that from measurements using the *Ginga* X-ray satellite (69). Observations have been made with the University of Durham telescope at Narrabri during 1986 - 1988 (21). These provided evidence for a persistent emission at the X-ray period throughout the binary orbit, but no evidence for episodes of enhanced emission on a time scale of a few pulsar rotations was found. Observations from the White Cliffs experiment (34) and the JANZOS experiment (9) have produced upper limits for VHE emission which are consistent with the reported fluxes. The VHE gamma ray observations and the measured fluxes are summarised in Table 3. (It should be noted that there are discrepancies between the procedures used for the estimation of fluxes from the Durham and Potchefstroom experiments (31) and that the apparent flattening of the energy spectrum below 1 TeV may not be real).

Persistent emission of VHE gamma rays from Vela X-1 seems well established, corresponding to a source luminosity of $\sim 3.6 \times 10^{34}$ erg s^{-1} for gamma ray energies above 300 GeV. However, the episodes of enhanced emission remain to be confirmed.

3.6 4U1145-619

4U1145-619 is a 292 s X-ray pulsar in a binary system with an orbital period of 186.5 d. X-ray observations show that outburst episodes, lasting ~ 10 d, occur every 186.5 d. It is assumed that this latter value is the period of a binary orbit of undetermined radius. During these outburst episodes, the pulse period is observed to change very rapidly, with a period derivative of $\sim -1.8 \times 10^{-7}$ s s^{-1} observed during the 1985 January outburst (35). This is attributed to the Doppler shifting due to the orbital motion of the pulsar.

The Durham University group observed 4U1145-619 with the Narrabri telescope for 45 hours during 1987 April and 1988 April and June (13). The 1987 April measurements, made exactly 4.5 orbital periods after an X-ray measurement (35), showed evidence for periodicity at the expected X-ray period (292.4 ± 0.5 s) with a chance probability of 1.5×10^{-4}. These data also indicated a value of period derivative of $+ 1.9 \times 10^{-7}$ s s^{-1} (significant at the 2 σ level) , which is equal in magnitude but

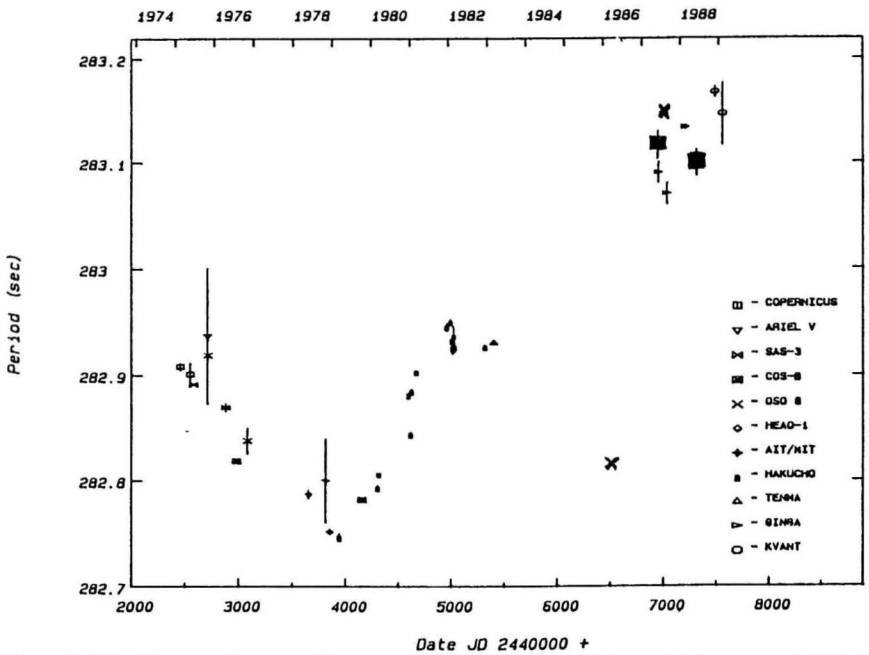

Figure 5. The X-ray pulse period history of Vela X-1 adopted from Gilfanov *et al* (51). The VHE gamma-ray measurements in 1986 - 1988 are shown .

■ Carramiñana *et al* (21)

× North *et al* (78, 86)

Table 3. VHE gamma ray observations of Vela X-1. (a) denotes fluxes for persistent pulsed emission, (b) denotes pulsed fluxes observed during episodes of enhanced emission, (c) denotes a DC measurement.

Telescope	Observation Dates	Period (s)	Integral Flux (10^{-11} cm^{-2} s^{-1})	Energy (GeV)	Reference
Nooitgedacht	1986 Apr 2 - 1986 May 10	282.82	2.0 ± 0.4 (a) 78 ± 9 (b)	3000	(78)
Nooitgedacht	1987 Apr 29 - 1987 May 30	283.14	1.5 ± 0.4 (a)	3000	(85)
Nooitgedacht	1988				(86)
Narrabri	1986 Nov 1987 Mar - 1987 Apr 1988 Mar - 1988 May	283.15 283.115 283.09	7.4 ± 1.5 (a)	300	(21)
JANZOS	1989 Mar - 1989 Apr		< 2.5 (95% CL)	1000	(9)

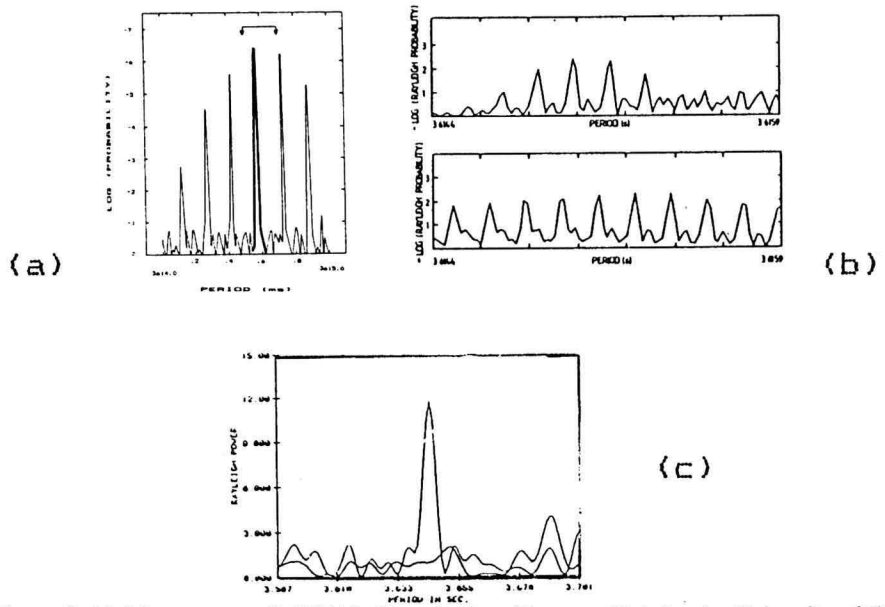

Figure 6. (a) Measurement of 4U0115+63 made from Dugway, Utah by the University of Durham telescopes (26).

(b) Measurements of 4U0115+63 made from La Palma by the University of Durham telescope (14).

(c) Measurements of 4U0115+63 made by the Gulmarg group (83).

opposite in sign to that shown by the X-ray data at a position on the opposite side of the (assumed) orbit. The further observations in 1988 April (1.9 orbital cycles after the 1987 April detection) and 1988 June (2.2 orbital cycles later) showed no evidence for VHE emission.

In a recent report (48) the suggestion has been made that an excess in the shower count rate measured by the SPASE PeV gamma ray project could be due to this source (or the close-by source 1E1145-61).

3.7 4U0115+63

This transient X-ray binary has a pulse period of 3.61 s and an orbital period of 24.3 d. The system is also known to show transient optical activity. Following the discovery of VHE gamma rays from Her X-1, 4U0115+63 was chosen as a candidate gamma-ray source by the Durham group working at Dugway, Utah. This object resembles Her X-1 in many ways (similar period, period derivative, luminosity and probable cyclotron line emission) but differs in at least two marked features - the mass of the companion and the mechanism for mass transfer. Data were accumulated over 8 consecutive nights in 1984 September (26). Due to a lack of a contemporary X-ray ephemeris, the parameters of the orbit used in the analysis had to be relaxed, as well as searching over a small range in pulsar period. Evidence was found, at a chance probability level of 10^{-5}, for VHE emission at the expected pulsar period (see Figure 6(a)). This corresponds to a gamma ray flux at energies > 1000 GeV of $(7 \pm 1.4) \times 10^{-11}$ cm^{-2} s^{-1}. No evidence for variation of the gamma ray flux through the range of orbital period sampled was found.

It has been suggested (63) (on the basis of positional association) that 4U0115+63 is the VHE gamma ray source Cas Gamma-1 detected in DC measurements by the

Crimean group in 1971 and 1972 (94).

Confirmation that 4U0115+63 is a VHE gamma ray emitting object was provided by the Whipple and Haleakala VHE telescopes (64, 90). The Whipple telescope observed this source between 1985 September - 1986 January and identified one three-day interval which showed evidence for the 3.6 s period at a threshold energy of 600 GeV. Further data collected by this group during 1986 September - 1987 February showed no evidence for pulsed emission (23). The Haleakala observations were made from 1989 August - December and showed evidence for three episodes of sporadic emission. The Durham group, using their La Palma telescope, made observations of 4U0115+63 during two 7 day periods in 1988 September - October. Evidence for persistent emission throughout each of these observations was found, leading to a gamma ray flux of 4.4×10^{-10} cm^{-2} s^{-1} for an energy threshold of 400 GeV (14) (see Figure 6(b)). The Gulmarg group (83) report one episode of pulsed emission, lasting for ~ 1950 s on 1987 Nov 14, from ~ 40 hours of observation (see Figure 6(c)). The Tata group working at Pachmarhi (1) have also accumulated ~ 40 hours data from 4U0115+63 during 1987 and 1988, but report no evidence for pulsed emission.

4U0115+63 can thus be regarded as an established, but possibly sporadic VHE gamma ray emitter, with a luminosity of about 1.7×10^{36} erg cm^{-2} above an energy of 400 GeV.

3.8 1E2259+586

1E2258+586 is a 7 s X-ray pulsar coincident with the remnant of a supernova explosion. It is thought to be a member of a binary system but there is no strong evidence of orbital effects; there are some indications of a 2300 s periodicity in the X-ray observations of Fahlman and Gregory (44), and indirectly from IR observations (74). A recent paper (60) tentatively suggests an orbit with period 2120 s and *a sin i* of 0.038 ls. Other studies have provided flux limits in this range of values.

VHE gamma ray observations have concentrated on searches for the pulsar period in the data. Observations with the Whipple telescope in 1985 September - 1986 January and 1986 September - 1987 February failed to detect any persistent pulsed emission and established an upper limit (95% CL) to the flux above 600 GeV of 9.0×10^{-10} cm^{-2} s^{-1} (23). Further measurements with the Whipple telescope in 1987 and 1988 led to a flux limit of 2.2×10^{-10} cm^{-2} s^{-1} (without imaging enhancement) and 2.7×10^{-11} cm^{-2} s^{-1} (using the imaging technique) (24). Similar flux limits have been reported by the Haleakala group (107). The Durham group, using the La Palma telescope, observed this source in 1988 October and 1989 September (18). The 1988 data show evidence (significant at the 10^{-4} level) for periodic emission at the second harmonic of the expected X-ray period, leading to a flux ($E > 400$ GeV) of $(2.0 \pm 0.8) \times 10^{-11}$ cm^{-2} s^{-1}. Similar observations in 1989 failed to detect any persistent emission and give a 3σ flux limit of $(2.0 \pm 0.8) \times 10^{-11}$ cm^{-2} s^{-1} at a similar energy threshold.

The observations indicate that 1E2259+586 may be a variable gamma ray source over time scales of years or months; further observations of this unconfirmed VHE source are required.

3.9 Hercules X-1

The LMXRB Hercules X-1 displays a wide range of well-measured X-ray periods: a 1.24 s pulsation associated with the pulsar rotation period, a 1.7 day variation due to the orbit of the pulsar, and a 35 day period. The origin of the 35 d period has attracted a number of explanations. Trümper *et al* (97) have suggested that it is due to precession of the neutron star, while others (58) have argued that it is due to

precession of the accretion disc. In addition, the X-ray source sometimes enters an extended low state, lasting between months and years.

VHE gamma rays from Her X-1 were discovered during observations using the Dugway atmospheric Cerenkov telescopes in 1983 (41). A 3 minute outburst of VHE emission was observed, and was found to be periodic at the contemporary X-ray pulsar period. At the time of the outburst, the X-ray pulsar in the binary system was at the ascending node in the orbit, and the "switch on" of the 35 day cycle was imminent. Following this discovery, more observations of Her X-1 were made by the Durham group at Dugway. Evidence was obtained for persistent, weak periodic emission during 1983 July (17, 28). Observations were made using the University of Durham Mark IV telescope on La Palma in 1988 July; a short burst of pulsed activity was observed on 1988 July 16, similar in all aspects to that first noted in 1983. Once again this occured close to the ascending node and at a time close to turn on in the 35 d cycle.

Independent confirmation that Her X-1 is a source of VHE gamma rays came from observations made with the Whipple Observatory in 1984 March-May (53). These initial observations showed 3 episodes of pulsed emission, occurring on timescales of a few hours or less. An extension of these observations resulted in a total of 8 episodes of pulsed emission being observed by the Whipple group (52, 65).

The first instance of pulsed VHE gamma ray emission observed with the Whipple telescope occurred on 1984 April 4, when Her X-1 was in the HIGH ON state in its 35 day cycle. At the same time, observations of Her X-1 were made using the University of Durham telescopes at Dugway, Utah (29). Both the Whipple and Durham measurements detected the X-ray period of 1.2376 ± 0.0004 s. This represents the first simultaneous detection of a VHE gamma ray source by two independent sets of telescopes.

A burst of pulsed VHE gamma ray emission observed with the Whipple telescope on 1985 June 16 is also remarkable (54). The observed emission took place just after the neutron star had passed behind its companion and entered X-ray eclipse. If the effect is real, this indicates that the site of at least some of the VHE gamma ray production differs from that of the X-rays.

Observations of Hercules X-1 with the Haleakala VHE gamma ray telescope started in 1985, when Hercules X-1 was observed for 29 hours (89). During this time, three bursts of pulsar activity were observed, all of which were in the LOW ON portion of the 35 day cycle. One episode of pulsed emission was observed at ingress to X-ray eclipse.

Further observations of Hercules X-1 were made by the Haleakala group in 1986 (92). On 1986 May 13 a burst of approximately 15 minutes duration was detected, with a pulse period of 1.23593 ± 0.00018 s. This period differs significantly from the period expected from X-ray and optical observations, being 0.15% lower. However, this period is in good agreement with an observation made at the Whipple Observatory in 1986 June (65) and with an episode of pulsed emission observed at energies above 10 TeV with the Cygnus Air Shower Array in 1986 July (39). A further detection of such a blue-shifted period was made by the Haleakala group in 1987 June (4), in agreement with the 1986 observations. The observed period shift is two orders of magnitude greater than the transient changes observed in X-rays, and 2.8 times the maximum orbital Doppler shift possible in the Her X-1 system. A convincing explanation for these detections of an anomalous period remains to be found.

A 15 minute burst of VHE gamma ray emission was observed with the Gulmarg gamma ray telescope on 1988 June 12 (87). The period is indistinguishable from that expected from the X-ray measurements, and is compatible with the period observed 34 days later in July of the same year by the Durham group. However, observations made

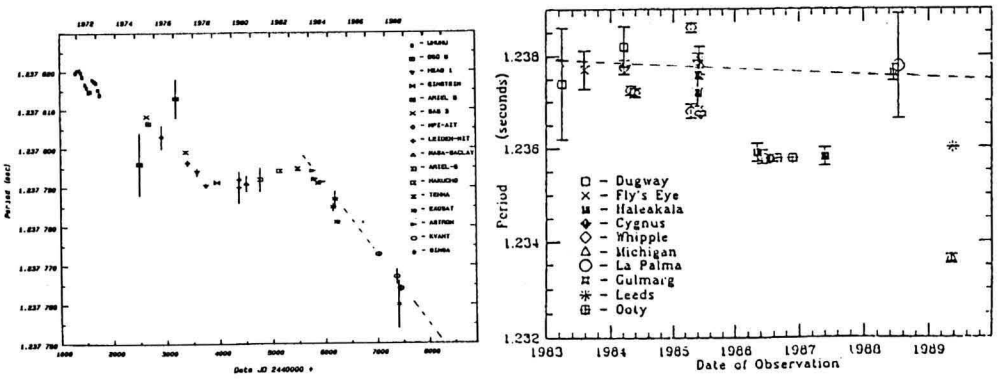

Figure 7. (a) The X-ray pulse period history of Hercules X-1 after Gilfanov *et al* (51).
(b) The VHE gamma ray period history. The broken line depicts the X-ray period measurements from Figure 7(a).

with the Pachmarhi telescopes in 1987-1989 show no evidence for any bursts of pulsed emission from Her X-1 (7). A further negative result for bursts of pulsed emission has been reported by the γ^* experiment (2), which observed Her X-1 from 1988 May to 1989 June. No evidence for bursts of periodic emission at the X-ray period was found.

The largest bursts of VHE emission from Her X-1 was observed by the Pachmarhi group on 1986 April 11, early in the life of this experiment (105). A burst of events, resulting in a 54% increase in the cosmic ray counting rate and lasting for 14 minutes was seen, corresponding to an excess significant at the 42 σ level. Unfortunately, there were problems with the recording equipment during the observation which precludes a meaningful search for pulsar periodicity in these data.

In Figure 7, we show the time evolution of the X ray period from Her X-1 and the VHE gamma ray periods measured between 1983 and 1989.

3.10 4U1626-67

4U1626-67 is an X-ray pulsar with a period of 7.68 s. The X-ray data has not revealed an orbital period but optical observations have given indications of a period of around 42 min (73). There is some uncertainty in the precise value of the orbital period from optical measurements but the best estimate is 2485 s. X-ray measurements indicate that the projected semi-major axis, *a sin i*, is very small, less than 13 lt s, which implies that the binary is being viewed at a very high angle of inclination (67). This is an unusual situation and an implication of this for VHE gamma ray observations is that correction of the data for the effects of orbital motion may not be necessary for periodicity to be detected.

The Durham group, using the Narrabri telescope, have made observations of this object during 1987 April - July and 1989 May (13). The longest single observation (a 9 hr observation taken on 1987 June 1) shows evidence for periodicity at the period expected from the X-ray data (7.664 s) throughout the observation with a chance Rayleigh probability of 2×10^{-5}. The other datasets show no evidence for periodicity at a similar period. This result is interpreted as a time-averaged 3 sigma flux limit for 300 GeV gamma ray emission of $(7.6 \pm 1.3) \times 10^{-11}$ cm^{-2} s^{-1}.

3.11 X0021.8-7221

This is a transient X-ray source with a period of 120.2 s in the globular cluster 47 Tucanae (3). The nature of the source is unclear from the X-ray observations, a low mass X-ray binary or a cataclysmic variable being possible. The Potchefstroom group have detected the X-ray period in VHE gamma ray data taken between 1989 July 7 and September 3 (38), with a chance probability of 3×10^{-4}. The VHE emission was found to be highly variable, with a peak luminosity of about 10^{36} erg s^{-1} at a threshold of about 5 TeV suggesting that this object is a low-mass X-ray binary observed at high inclination and is not a cataclysmic variable. Observations made by the Durham group at Narrabri on four occasions in 1988 and 1989 show evidence that on two occasions (in 1988 July and October) emission was detected (70). In 1989 July an indication of a periodicity at 118.5 ± 0.02 s was obtained significant at the 10^{-5} level; in 1988 October a signal at a period of 117.87 ± 0.01 s was obtained with chance probability 3×10^{-7}. In both these datasets there were indications that the period was decreasing rapidly suggesting a period derivative of -1.3×10^{-7} s s^{-1}. We interpret this as a consequence of Doppler shifting in an orbit. The observations in 1989 October and November (when the object was observed at a large zenith angle) provided a small dataset and no evidence for a periodic signal.

3.12 Scorpius X-1

Sco X-1 is the brightest continuous X-ray source in the sky. It is accepted as a LMXB with an orbital period of approximately 0.787 d and is thought to be a candidate for a system including a millisecond pulsar, but no clear evidence for pulsation yet exists. Candidate periods of 4.53 ms (75) and 2.93 ms (66) have been suggested from X-ray data, but these remain to be confirmed. There have been reports of detection at UHE energies (72).

In view of the lack of a confirmed X-ray pulsar period, VHE gamma ray observations have concentrated on a search for DC emission. The Potchefstroom group have reported a flux of $(1.7 \pm 0.2) \times 10^{-11}$ cm^{-2} s^{-1} for energies greater than 1000 GeV (37). This measurement was made without a system of background light stabilisation and so a correction for varying background light conditions was made. The Durham group observed this object in 1988 May - June and 1989 May, using the chopping technique with background light stabilisation (16). A time-averaged DC signal, significant at the 3.1 sigma level in each measurement was seen, corresponding to a flux of $(1.2 \pm 0.4) \times 10^{-10}$ cm^{-2} s^{-1} for energies greater than 300 GeV. The emission appears strongest at orbital phase around 0.35 although the significance is marginal.

Searches for millisecond periodicity in the VHE gamma ray data have been made . Using the Rayleigh test, the candidate periods of 2.93 and 4.53034 ms were investigated but no evidence for periodicity was found. The Potchefstroom group have also searched for evidence of the QPO seen in X-rays, with an upper limit of 0.9×10^{-11} cm^{-2} s^{-1} being established for such oscillations in VHE gamma rays (84).

Unpulsed VHE gamma ray emission from Sco X-1 has been detected by two experiments, leading to a VHE gamma ray luminosity of $(2.3 \pm 0.7) \times 10^{34}$ erg s^{-1}. Further observations of this object are required to confirm the detection, to investigate the orbital variation of the flux and also with the hope of detecting short bursts of enhanced VHE emission upon which a sensitive *ab initio* search for millisecond periodicity could be performed.

3.13 Cygnus X-3

This remarkable object has been the subject of many detailed reviews, e.g. (33, 106). We here confine ourselves to a review of the TeV gamma ray observations.

Cygnus X-3 was first detected as a VHE gamma ray source by a Soviet group working at the Crimean Astrophysical Observatory in 1972, just after the first known radio outburst from this object. The 4.8 hr. X-ray period was identifiable: initially, two equal gamma ray maxima were observed, one at phase 0.15 - 0.2, and the other at 0.6 - 0.8. (These data were analysed using a definition of X-ray minimum due to Canizares *et al* (19), which was not used in later measurements either by the Crimean group or by others). Further observations and a new analysis of data from 4 years of observation showed the phase 0.2 peak to be stronger (95). Sporadic bursts were observed, specifically in September 1973, August 1974 and October 1980, the last observation being preceded by a radio outburst (47). The Crimean detection was followed by confirmation by a group in T'ien Shan using a similar telescope (77).

Further VHE gamma ray detections of Cygnus X-3 came in 1981 from the collaboration between University College, Dublin and the Harvard-Smithsonian Center for Astrophysics working at Mt. Hopkins, Arizona (36). The data were also found to show 4.8 hr. periodicity, with the maximum emission between phase 0.7 and 0.8. This phase was determined using an ephemeris derived from the Crimean observations. If the data are analysed using the 4.8 hr. ephemeris of Van der Klis and Bonnet-Bidaud (101), which rapidly became the standard for VHE gamma ray observations of this object in the 1980s, the emission is found to be at phase 0.6 - 0.7. The few observations made at other phases showed no significant excess.

Observations made by Lamb *et al* (62), using two 11 m solar concentrators of the Jet Propulsion Laboratory's Solar Energy Facility at Edwards Air Force Base as a VHE gamma ray telescope, showed an excess of events from Cygnus X-3 between phase 0.5 - 0.7 of the 4.8 hr. cycle.

Data taken during 1981 - 3 by the Durham group operating at Dugway, Utah, showed a 4.4σ excess lasting for about 10 min at phase 0.64 ± 0.03 with respect to the Van der Klis and Bonnet-Bidaud 1981 ephemeris, after allowing for the non-uniform background in the Cygnus region (40). Table 4 gives a summary of these and other results from Cygnus X-3.

Cygnus X-3 has long been suspected to contain a fast pulsar (92 - 96). However, the high column density of hydrogen in the region of Cygnus X-3 (it lies almost directly along a spiral arm of the galaxy) represents a severe limitation on searches for

Table 4. Fluxes from Cygnus X-3.

Group	Energy (TeV)	Flux (photon cm^{-2} s^{-1})	Phase	Epoch
Crimean Astrophys. Obs.	2	1.6×10^{-11} to 1.6×10^{-10}	0.15 - 0.2	1972 - 80
Tien Shan	5	1.6×10^{-10}	0.15 - 0.2	1977 - 78
Whipple Observatory	2	1.5×10^{-10}	0.6 - 0.7	April - June 1980
	0.8	$(5.1 \pm 1.1) \times 10^{-10}$	0.58 - 0.67	October 1983
ISU-JPL-UC	0.5	8×10^{-11}	0.5 - 0.7	Aug - Sept 1982
Durham	1	3×10^{-10}	0.625	1981 - 82

short period pulsation in the radio region due to the effects of frequency dispersion. This is not a problem for pulsed high energy radiation. However, the search for a fast pulsar in sparse VHE gamma ray data does present two problems:

(i) In the case of Cygnus X-3, the orbital parameters are unknown, so it is impossible to adjust event arrival times to remove the effect of the motion of the pulsar about a companion. The data must therefore have been taken over a short time interval and be searched for a Doppler shifted period.

(ii) As the pulsar period is obviously unknown, many trial periods must be searched.

It follows that a large number of events is required if any detection is to be statistically significant, and since from (i) the data must be taken over a short period of time, it is necessary to observe a strong burst of events from the object if a pulsar search is to be worthwhile.

During observations made in 1983 August - October with the Durham University telescopes, just such a burst was observed. On 1983 September 13, a count rate excess was noted, lasting for 7 minutes and representing an excess of 20% in the number of counts above the background. The events within the burst were tested for periodicity between 10 and 50 ms using the Rayleigh test. The resulting probability distribution was in agreement with chance, with the exception of one trial period: 12.5908 ms, which had a probability of chance origin of 4.8×10^{-8}. Six other datasets taken within one month were also tested for periodicity; one observation (1983 October 2) showed 12.5908 ms periodicity during the corresponding 7 minutes in the 4.8 hr cycle (27). Further, weaker evidence for 12.59 ms periodicity was found from analyses of data taken with the Dugway telescopes before 1983 (the telescopes were less sensitive prior to this), and also from analysis of data taken in 1985 October and November using a single, sensitive telescope (30). These results suggested that the pulsar was spinning down with a period derivative of $(2.8 \pm 0.4) \times 10^{-14}$ s s^{-1}. A new telescope (the Mark IV) was operated by the Durham group at the Spanish Observatorio del Roque de los Muchachos of the Instituto de Astrofisica de Canarias on the island of La Palma during 1988 June - October. Observations of Cygnus X-3 made in 1988 June/July and September (15) showed 12.59 ms periodicity in data taken in a 600 s interval close to the maximum of the X-ray cycle as defined by the most recent X-ray ephemeris (102). The period and period derivative observed were compatible with the earlier Dugway measurements (30). No related periodicity was detected in observations in 1988 October. On the basis of these observations it was possible to predict the interval of activity and the pulse period appropriate to 1989 observations.

The discovery of a 12.59 ms pulsar in Cygnus X-3 prompted searches for the pulsar by other VHE gamma ray astronomy groups. The database from the Whipple collaboration at Mt Hopkins, Arizona consists of observations made in the tracking mode, each of approximately 28 minutes duration (46). The data were taken between April 1983 and November 1986. Each scan was split into six 8 minute segments overlapping each other by 4 minutes. These were then subjected to periodicity analysis. It was noted that, although there is a "tail" of periods with low chance probabilities around 12.59 ms in the power spectrum, no significant evidence is found for periodic emission when the number of trials is taken into account. In this, and a later paper (68) indications of 12.6 ms pulsed emission is reported, significant at the 3×10^{-3} level. However, the lack of an increase in count rate coincident with the pulsed emission when compared with the count rate in earlier and later intervals is cited as counter evidence, relying on the assumption that all gamma ray emission is confined to the eight minute test segment showing strong periodicity. Marshak (71) has recently criticised the statistical analysis adopted by the Whipple group and concludes that the Whipple data do, in fact, provide some evidence for the 12.59 ms periodicity.

The telescope on Haleakala in the Hawaiian Islands operated by the Universities of Hawaii, Wisconsin and Purdue made observations of Cygnus X-3 for some 133 hrs during the Summer and Autumn of 1985. On 1985 October 12 (when a pulsar detection was made in Durham), a 60s burst of events was observed from the direction of Cygnus X-3, at phase 0.74 of the 4.8 hr X-ray cycle (88). While preliminary analysis of the data taken on October 12 showed some evidence for a 12 ms pulsar signal, a subsequent *ab initio* period scan of the events occurring within the burst showed no significant evidence for pulsar activity when the large number of degrees of freedom, consequent upon the wide range of periods searched (10 ms - 2.2 s), were taken into account.

The Tata Institute telescope at Pachmarhi accumulated 10 hr. of data in 1986 October-November covering the orbital phase range 0.2 to 0.8 (6). The whole data set has been tested for periodicity covering the period range 12.5850 - 12.5967 ms. No evidence for 12.59 ms periodicity was found when the large number of degrees of freedom were taken into account.

The above negative results must be treated with caution if they are to be considered as being in conflict with the University of Durham claim. The hyphothesis to be tested is that there is sporadic pulsed emission at a well defined period at specific parts of the 4.8 hr cycle on some but not all occasions. In many of the attempts at independent confirmation this precise hypothesis has not been tested.

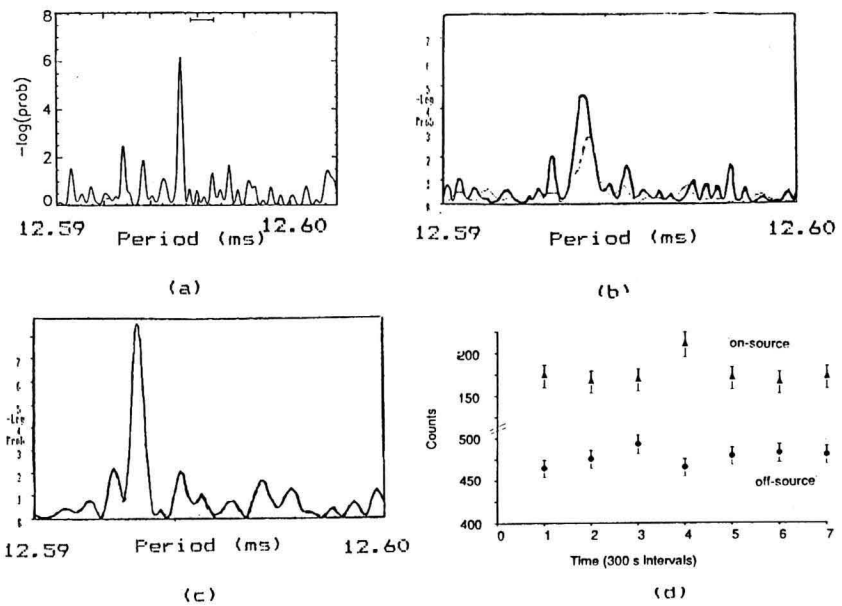

Figure 8(a) The chance probability for periodicity in the 600 s dataset in the observations of Cygnus X-3 at Woomera on 1989 September 1 and 2 (55).

Figure 8(b) The chance probability of periodicty in a corresponding 600 s dataset recorded during an observation of Cygnus X-3 on 1989 September 1 at La Palma (100) (broken line). The solid line shows the similar plot for a 300 s segment of data at the centre of the 600 s dataset.

Figure 8(c) The chance probability for periodicity in 300 s of data from an observation of Cygnus X-3 on 1989 September 7.

Figure 8(d) The count rate profile during the observation of Cygnus X-3 on Septemer 7. Interval #4 corresponds to the data set analysed in Figure 8(c).

Follow-up observations were made in La Palma in 1989 by the Durham group after the large radio outbursts in June and July. These observations failed to provide evidence at the period (12.5960 ms) in the specific window of the 4.8 hour cycle predicted from earlier results.

Observations of Cygnus X-3 were made by the University of Adelaide group using their VHE gamma ray telescope which is similar to the Durham Mk III telescope and is located at Woomera, South Australia. These were the first measurements using the large zenith angle technique suggested by Elbert and Sommers (93). The data showed no evidence for pulsed VHE gamma radiation in 1989 August/September at the period and phase in the 4.8 hr cycle suggested by (15). However they did observe periodicity in their data (55). The most significant effect they observed was a periodic signal in a 600 s window centred 950 s *before* the time predicted from the 1988 Durham observation in La Palma and at a period ~ 1 μs shorter. The strongest such episodes were during observations on the nights of 1989 September 1 and 2 with a chance probability $< 10^{-4}$ - see Figure 8(a). This result may provide the long-awaited independent confirmation of the 12.6 ms pulsar in Cygnus X-3 and also expose an interesting change in the pulsed emission and the orbital motion of the VHE emitting region. Corresponding 600 s segments of observations with the Durham telescope in La Palma were available on each night between 1989 September 1 - 7 (108). The observation made on 1 September at La Palma was two 4.8 hr cycles after that made at Woomera and referred to as September 1 and three 4.8 cycles before that referred to as September 2. For these data from La Palma in the *precise* 600 s in the 4.8 hr cycle identified by the Adelaide group a pulsed signal was noted at a period of 12.5939 ± 0.0004 ms - see Figure 8(b). In accord with our earlier results, which suggest that the interval of activity is no more than 400 s, we have investigated the distribution of the pulsed signal within the 600 s sample. We find that the emission lasts for about 300 s during which the pulsed signal is 23% of the cosmic ray background. We did not observe an accompanying increase in count rate. In addition, we find a second interval of emission lasting 300 s during an observation on September 7 on this occasion. The pulsed signal was 30 % of the background count rate and the period was 12.5930 ± 0.0004 ms - see Figure 8(c). A corresponding increase in count rate was detected on this occasion - see Figure 8(d). This 300s burst of emission occurred 250 s later in the 4.8 cycle than the activity noted at La Palma and Woomera on 1 - 2 September.

It may be helpful that X-ray observations using the Ginga spacecraft were made on 1989 Aug 31 - Sept 1 (61). The analysis of these data is awaited with keen interest; in particular we wish to know if the epoch of X-ray maximum has advanced since observations pre-1989, as appears to be the case for VHE gamma rays.

3.15 Other systems

A number of other X-ray binary systems with well established pulsar periods have been observed at VHE gamma ray energies without any detection of gamma rays. The flux-limits derived from the observations are summarised in Table 5.

4. PATTERNS IN VHE EMISSION

4.1 Introduction

It is quite likely that VHE emission from X-ray binaries, many of which show transient behaviour, is itself also highly variable. Here, we attempt to identify any pattern in the VHE emission, whilst acknowledging that for most observations the

Table 5. limits to VHE gamma ray emission from other X-ray binary pulsars.
(a) limited data sample prevents calculation of a meaningful flux limit.

Object	Telescope	Pulsar Period (s)	Flux Limit (10^{-11} cm^{-2} s^{-1}) (GeV)	Energy Threshold	Reference
V0332+53	Whipple	4.375	98 (95% CL)	600	(23)
4U0352+30	Whipple	835.64	(a)	600	(23)
A0535+26	Whipple	103.34	82 (95% CL)	600	(23)
GX1+4	Nooitgedacht Narrabri	93.4	7.7 (3σ) 7.2 ± 1.3 (3σ)	1000 300	(84) (13)
2S1417-62	Nooitgedacht	17.6	7.0 (3σ)	1000	(84)
1E1048.1	Narrabri	6.4	5.0 (3σ)	300	(100)

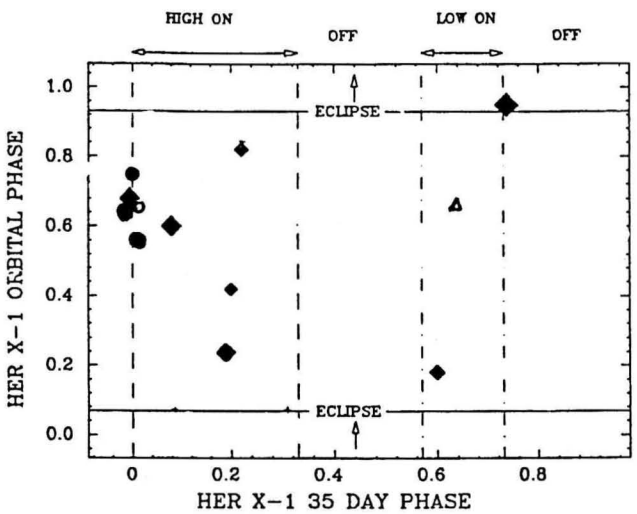

Figure 9. Distribution of VHE gamma ray measurements of Her X-1 in 1.7 day and 35 day phase.

identification of instances of strong emission is difficult, due to the difficulty of separating the statistical variation in telescope counting rate for a constant source from that of a source with truly varying VHE gamma ray luminosity.

4.2 Sporadic emission / long term variability

There are two objects for which clear evidence exists for sporadic or long-term variations in VHE emission - Cygnus X-3 and Hercules X-1.

Cyg X-3 is clearly not always producing VHE gamma rays; in the Durham observations it shows a probability of about 5 - 10% of being detected in any measurement at the most favourable part (X-ray maximum) of the 4.8 hour cycle. There is some evidence that there may be a 19.2 d cycle in the strength of the VHE emission (42).

For Hercules X-1 there is evidence for 35 d modulation of the VHE emission (see Figure 9). Episodes of bursts of VHE emission appear to be confined to the high on and low on parts of the 35 d X-ray cycle, with strong VHE emission being particularly favoured coincident with the 35 d "switch on" (and at the ascending node in the 1.7 d orbit - see Section 4.3).

The evidence for sporadic emission from 4U0115+63 is not clear. The Durham group detected emission lasting for periods of ~ 5 d apparently at a constant strength during three observations. However, detections made by other groups have been predominantly of short bursts of emission lasting for a few minutes or hours.

Insufficient data has so far been accumulated from studies of other XRBs to attempt to draw any firm conclusions about their long-term VHE gamma ray behaviour.

4.3 Orbital phase dependence of emission

The evidence for orbital phase dependence of VHE emission is well established in a number of sources, with Centaurus X-3 and Cygnus X-3 (if the 4.8 hour X-ray cycle is indeed orbital in origin) providing the best examples.

Cygnus X-3 has clearly shown the 4.8 hour modulation since its discovery in VHE gamma rays, with emission confined to regions close to X-ray phase 0.2 and 0.65 (in the past 10 years all observed effects have been close to X-ray maximum). Detection of the 12.6 ms periodicity has also been confined to regions close to X-ray maximum.

The observed VHE emission from Cen X-3 is confined to a narrow (5% wide) band of orbital phase, centred at X-ray phase 0.73, close to the ascending node.

The situation with Hercules X-1 is not so clear (see Figure 9). Emission occurs at all phases but there appears to be a clustering of bursts of VHE emission around orbital phase 0.6 - 0.7. The phase region corresponding to X-ray eclipse seems devoid of episodes of pulsed emission, except for two episodes which occur just after the onset of X-ray eclipse.

4U0115+63 is another well studied source, but evidence for any preferred orbital phases for emission is not obvious. Again, there is some evidence of bursts of emission being confined to the later portion of the orbit, but in this case this may be a selection effect.

If any broad hint of preferred orbital phase for emission exists it points to phase 0.6 - 0.7.

5. FUTURE PROSPECTS

Important advances in VHE gamma ray astronomy have been made through the 1980s, using telescopes of sensitivity such that most detections are just above threshold (a not unusual situation in the early stages of any new field). Although evidence has been built up for a number of X-ray binaries as VHE gamma ray emitters, it has not been possible so far to recognise clear patterns in VHE emission which may constrain the possible explanations so far advanced.

Methods of improving the signal to noise ratio by identifying the γ-rays (imaging, time structure of the signal) and by optimising the telescope design (larger collectors, smaller apertures) are continuing. Implementation of these ideas through the 1990s should provide further more significant and detailed evidence for VHE emission and a sound future for VHE gamma ray astronomy's studies of accreting binary systems. The prospect of simultaneous ground-based gamma ray observing and observation from space using *The Gamma Ray Observatory* in 1991/2 should ensure a continued and succesful evolution of the field.

ACKNOWLEDGEMENTS

It is a pleasure to acknowledge the efforts made by all colleagues in the University of Durham gamma ray group who have contributed to the collection and analysis of much of the data reported here during 5000 hours of observing at Dugway, La Palma and Narrabri. In particular, I am indebted to Drs Paula Chadwick and Lowry McComb who have assisted me in gathering material for this review.

REFERENCES

(1) Acharya, B. S. *et al*, 1990: In: *Proc. 21st Int. Cosmic Ray Conf.*, Adelaide, **2**, 319.
(2) Akerlof, C. *et al*, 1990. In: *Proc. 21st Int. Cosmic Ray Conf.*, Adelaide, **2**, 95.
(3) Auriere, M., Koch-Miramond, L. and Ortolani, S., 1989, *Astron. Astrophys.*, **214**, 113.
(4) Austin, R. *et al*, 1990. In. *Proc. 21st Int. Cosmic Ray Conf.*, Adelaide, **2**, 110.
(5) Basko, M. M., Sunyaev, R. A. and Titarchuck, I. G., 1974, *Astron. Astrophys.*, **31**, 249.
(6) Bhat, P. N., Ramana Murthy, P. V. and Vishwanath, P. R., 1988, *J. Astrophys. Astron.*, **9**, 155.
(7) Bhat, P. N. *et al*, 1990. In: *Proc. 21st Int. Cosmic Ray Conf.*, Adelaide, **2**, 108.
(8) Bignami, G. E., Maraschi, L. and Treves, A., 1977, *Astron. Astrophys.*, **55**, 155.
(9) Bond, I. A. *et al*, 1990. In: *Proc. 21st Int. Cosmic Ray Conference*, Adelaide, **2**, 271.
(10) Brazier, K. T. S. *et al*, 1989, *Experimental Astron.*, **1**, 77.
(11) Brazier, K. T. S. *et al*, 1990, *Nucl. Phys. B, (Proc. Suppl.)*, **14A**, 250.
(12) Brazier, K. T. S. *et al*, 1990, In: *Proc. 21st Int. Cosmic Ray Conference*, Adelaide, **2**, 300.
(13) Brazier, K. T. S. *et al*, 1990. In: *Proc. 21st Int. Cosmic Ray Conference*, Adelaide, **2**, 292.
(14) Brazier, K. T. S. *et al*, 1990. In: *Proc. 21st Int. Cosmic Ray Conf.*, Adelaide, **2**, 379.
(15) Brazier, K. T. S. *et al*, 1990, *Astrophys. J.*, **350**, 745.
(16) Brazier, K. T. S. *et al*, 1990, *Astron. Astrophys.*, **232**, 383.

(17) Brazier, K. T. S. *et al*, 1990, *Astrophys. J.*, submitted.
(18) Brazier, K. T. S. *et al*, 1990, *Astron. Astrophys.*, submitted.
(19) Canizares, C. R. *et al*, 1973, *Nature (Phys. Sci.)*, **241**, 28.
(20) Carramiñana, A. *et al*, 1989, In: *Timing Neutron Stars*, eds. H. Ögelman and E. P. J. van den Heuvel (Dordrecht: Kluwer Academic Press), 369.
(21) Carramiñana, A. *et al*, 1989, *Astrophys. J.*, **346**, 967.
(22) Cawley, M. F. *et al*, 1985. In: *Proc. 19th Int. Cosmic Ray Conf.*, La Jolla, **1**, 131.
(23) Cawley, M. F. *et al*, 1987. In: *Proc. 20th Int. Cosmic Ray Conf.*, Moscow, **1**, 240.
(24) Cawley, M. F. *et al*, 1989. In: *Proc. Int. Workshop on Very High Energy Gamma Ray Astronomy*, ed. A. A. Stepanian, D. J. Fegan and M. F. Cawley, 165.
(25) Cawley, M. F. *et al*, 1990. In: *Proc. 21st Int. Cosmic Ray Conference*, Adelaide, **2**, 224.
(26) Chadwick, P. M. *et al*, 1985, *Astron. Astrophys.*, **151**, L1.
(27) Chadwick, P. M. *et al*, 1985, *Nature*, **318**, 642.
(28) Chadwick, P. M. *et al*, 1985. In: *Proc. 19th Int. Cosmic Ray Conf.*, La Jolla, **1**, 251.
(29) Chadwick, P. M. *et al*, 1987. In: *Very High Energy Gamma Ray Astronomy*, ed. K. E. Turver, (Dordrecht: Reidel), 121.
(30) Chadwick, P. M. *et al*, 1987. In: *Very High Energy Gamma Ray Astronomy*, ed. K. E. Turver, (Dordrecht: Reidel), 159.
(31) Chadwick, P. M. *et al*, 1988, *Astrophys. J.*, **333**, L19.
(32) Chanmugam, G. and Brecher, K., 1985, *Nature*, **313**, 767.
(33) Chardin, G. and Gerbier, G., 1989, *Astron. Astropyhys.*, **210**, 52.
(34) Clay, R. W. *et al*, 1987. In: *Proc. 20th Int. Cosmic Ray Conference*, Moscow, **1**, 250.
(35) Cook, M. C. and Warwick, R. S., 1987, *Mon. Not. R. Astr. Soc.*, **225**, 369.
(36) Danaher, S. *et al*, 1981, *Nature*, **289**, 568.
(37) de Jager, H. I. *et al*, 1986, *S. Afr. J. Phys.*, **9**, 107.
(38) de Jager, O. C. *et al*, 1989, *I A U Circ. 4858.*
(39) Dingus, B. *et al*, 1987. In: *Proc. 20th Int. Cosmic Ray Conf.*, Moscow, ??.
(40) Dowthwaite, J. C. *et al*, 1983, *Astron. Astrophys.*, **126**, 1.
(41) Dowthwaite, J. C. *et al*, 1984, *Nature*, **309**, 691.
(42) Dowthwaite, J. C., 1986, *Ph D Thesis*, University of Durham.
(43) Eichler, D. and Vestrand, W. T., 1984, *Nature*, **307**, 613.
(44) Fahlman, G. G. and Gregory, P. C., 1983, In: *IAU Symposium 101, Supernova Remnants and Their X-ray Emission*, eds. P. Gorenstein and J. Danziger (Dordrecht: Reidel), 437.
(45) Fazio, G. G. *et al*, 1972, *Astrophys. J.*, **175**, L117.
(46) Fegan, D. J. *et al*, 1989, *Astron. Astrophys.*, **211**, L1.
(47) Fomin, V. P. *et al*, 1981. In: *Proc. 17th Int. Cosmic Ray Conf.*, Paris, **1**, 28.
(48) Gaisser, T. K. *et al*, 1990. In: *Proc. 21st Int Cosmic Ray Conference*, Adelaide, **2**, 283.
(49) Galbraith, W. and Jelley, J. V., 1953, *Nature*, **171**, 349.
(50) Giacconi, R. *et al*, 1972, *Astrophys. J.*, **178**, 281.
(51) Gilfanov, M. *et al*, 1989. In: *Proc. 23rd ESLAB Symposium on Two Topics in X-Ray Astronomy*, **1**, 71.
(52) Gorham, P. W. *et al*, 1986, *Astrophys. J.*, **308**, L11.
(53) Gorham, P. W. *et al*, 1986, *Astrophys. J.*, **309**, 114.
(54) Gorham, P. W. *et al*, 1987. In: *Very High Energy Gamma Ray Astronomy*, ed. K. E. Turver, (Dordrecht: Reidel), 125.
(55) Gregory, A. G. *et al*, 1990. In: *Proc. 21st Int. Cosmic Ray Conf.*, Adelaide, **2**, 279.

(56) Grindlay, J. R., 1972, *Astrophys. J.*, **174**, L9.
(57) Grindlay, J. *et al*, 1975, *Astrophys. J.*, **197**, L9.
(58) Katz, J., 1973, *Nature (Phys. Sci.)*, **246**, 87.
(59) Kelley, R. L. *et al*, 1983, *Astrophys. J.*, **264**, 568.
(60) Koyama, K. *et al*, 1989, *Publ. Astron. Soc. Japan*, **41**, 461.
(61) Koyama, K. and the Ginga team, 1989, private communication.
(62) Lamb, R. C. *et al*, 1982, *Nature*, **296**, 543.
(63) Lamb, R. C. and Weekes, T. C., 1986, *Astrophys. Letts.*, **25**, 67.
(64) Lamb, R. C. *et al*, 1987. In: *Very High Energy Gamma Ray Astronomy*, ed. K. E. Turver, (Dordrecht: Reidel), 139.
(65) Lamb, R. C. *et al*, 1988, *Astrophys. J.*, **328**, L13.
(66) Leahy, D. A., 1987, *I A U Circ. 4485*.
(67) Levine, A. *et al*, 1988, *Astrophys. J.*, **327**, 732.
(68) Lewis, D. A., 1989, *Astron. Astrophys.*, **219**, 352.
(69) Makino, F. *et al*, 1987, *IAU Circ.* 4459.
(70) Mannings, V. G., 1990, *Ph. D. Thesis*, University of Durham, in preparation.
(71) Marshak, M. L., 1990. In: *Proc. 21st Int. Cosmic Ray Conf.*, Adelaide, **2**, 6.
(72) Matano, T. *et al*, 1990. In: *Proc. 21st Int. Cosmic Ray Conf.*, Adelaide, **2**, 266 .
(73) Middleditch, J. *et al*, 1981, *Astrophys. J.*, **244**, 1001.
(74) Middleditch, J., Pennypacker, C. R. and Burns, M. S. 1983, *Astrophys. J.*, **274**, 213.
(75) Middleditch, J. and Priedhorsky, W. C., 1987, *Astrophys. J.*, **306**, 230.
(76) Milgrom, M. and Pines, D., 1978, *Astrophys. J.*, **220**, 272.
(77) Mukanov, J. B. *et al*, 1981. In: *Proc. 17th Int. Cosmic Ray Conf.*, Paris, **1**, 143.
(78) North, A. R. *et al*, 1987, *Nature*, **326**, 567.
(79) North, A. R. *et al*, 1990, In: *Proc. 21st Int. Cosmic Ray Conference*, Adelaide, **2**, 275.
(80) Pietsch, W. *et al*, 1985, *Space Sci. Rev.*, **40**, 371.
(81) Protheroe, R. J., Clay, R. W. and Gerhardy, P. R., 1984, *Astrophys. J.*, **280**, L47.
(82) Protheroe, R. J. and Clay, R. W., 1985, *Nature*, **315**, 205.
(83) Rannot, R. C. *et al*, 1990. In: *Proc. 21st Int. Cosmic Ray Conf.*, Adelaide, **2**, 315.
(84) Raubenheimer, B. C. *et al*, 1988, *S. Afr. J. Sci.*, **84**, 461.
(85) Raubenheimer, B. C. *et al*, 1989, *Astrophys. J.*, **336**, 394.
(86) Raubenheimer, B. C. *et al*, 1990, *Nucl. Phys. B*, in the press.
(87) Rawat, H. S. *et al*, 1990. In: *Proc. 21st Int. Cosmic Ray Conf.*, Adelaide, **2**, 104.
(88) Resvanis, L. *et al*, 1987, In: *Very High Energy Gamma Ray Astronomy*, ed. K. E. Turver, (Dordrecht: Reidel), 105.
(89) Resvanis, L. K. *et al*, 1987. In: *Very High Energy Gamma Ray Astronomy*, ed. K. E. Turver, (Dordrecht: Reidel), 131.
(90) Resvanis, L. *et al*, 1987. In: *Very High Energy Gamma Ray Astronomy*, ed. K. E. Turver, (Dordrecht: Reidel), 135.
(91) Resvanis, L. *et al*, 1987. In: *Very High Energy Gamma Ray Astronomy*, ed. K. E. Turver, (Dordrecht: Reidel), 225.
(92) Resvanis, L. K. *et al*, 1988, *Astrophys. J.*, **328**, L9.
(93) Sommers, P. and Elbert, J., 1987, *J. Phys. G*, **13**, 553.
(94) Stepanian, A. A. *et al*, 1972, *Nature (Phys. Sci.)*, **239**, 40.
(95) Stepanian, A. A. *et al*, 1977. In: *Proc. 15th Int. Cosmic Ray Conf.*, Plovdiv, **1**, 135.
(96) Suga, K. *et al*, 1985. In: *Proc. Workshop on Techniques in UHE Gamma-Ray Astronomy*, La Jolla, eds. R. J. Protheroe and S. A. Stephens, University of Adelaide, 48.
(97) Trümper, J. *et al*, 1986, *Astrophys. J.*, **300**, L63.

(98) Turver, K. E. (ed), 1987, *Very High Energy Gamma Ray Astronomy*, (Dordrecht: Reidel).
(99) Tumer, O. T. *et al*, 1990. In: *Proc. 21st Int. Cosmic Ray Conference*, Adelaide, **2**, 155.
(100) University of Durham VHE Gamma Ray group, 1990, unpublished.
(101) Van der Klis. M. and Bonnet-Bidaud, J. M., 1981, *Astron. Astrophys.*, **95**, L5.
(102) Van der Klis, M. and Bonnet-Bidaud, J. M., 1989, *Astron. Astrophys.*, **214**, 203.
(103) van der Walt, D. J. *et al*, 1987. In: *Proc. 20th Int. Cosmic Ray Conf.*, Moscow, **1**, 303.
(104) Vladimirsky, B. M. *et al*, 1975. In: *Proc. 14th Int. Cosmic Ray Conf.*, Munich, **1**, 113.
(105) Vishwanath, P. R. *et al*, 1989, *Astrophys. J.*, **342**, 489.
(106) Weekes, T. C., 1988, *Phys. Reports*, **160**, 1.
(107) Weeks, D. D., 1988, *Ph. D. Dissertation*, University of Hawaii, (unpublished).

K. E. Turver, Department of Physics, University of Durham, Durham, U.K.

R.M. Hjellming and W. Penninx

Radio emission and particle acceleration in compact accreting objects

ABSTRACT

We will show in this review that the observed radio emission of many compact accreting objects (in most cases X-ray binaries) comes from a relative large emission region with relativistic electrons. These compact accreting objects eject relativistic electrons at high velocities. The details of both the acceleration of the relativistic electrons and the production of bulk motion are still very unclear. In this review we will concentrate on reviewing the observations, discussing what they determine, and surveying the scenarios that seem to be reasonable possibilities.

1 INTRODUCTION

The compact accreting objects that are of interest for this conference are those for which observations of radio emission indicate the presence of particle acceleration. While this includes some cataclysmic variables (CV's), particularly the magnetic CV's, most of the interesting compact accreting objects are X-ray binaries (XRB's). In all cases there is a companion star ('mass donor') transferring matter to the accretion environment of the compact object (white dwarf, neutron star, or black hole). We will discuss the evidence indicating that compact accreting objects accelerate relativistic electrons and eject relativistic electrons at high velocities. The details, however, of both the acceleration of the relativistic electrons and the production of bulk motion are still very unclear. In some models one causes the other, and vice versa. For this reason we will concentrate on reviewing the observations, discussing what they determine, and surveying the scenarios that seem to be reasonable possibilities. Previous reviews on radio emission of X-ray binaries were given by Hjellming (1988) and Penninx (1989).

2 RADIO EMISSION PROCESSES

2.1 Evidence for Relativistic Electron Acceleration

For any observable radio source the first question is whether the basic emission mechanism for the radio photons is thermal or non-thermal. While the definition of these two options is often vaguely defined, the usual definition is that an emission process is thermal if the radiating particles are in thermal equilibrium. This means that their velocity distribution obeys a Maxwellian distribution with a well defined temperature. In radio astronomy, the most common thermal emission mechanism is bremsstrahlung where the radiating electrons are interacting with ions, so the electron-temperature and electron density completely

determine the appropriate emission and absorption processes. A thermal distribution of very-high-energy electrons interacting with magnetic fields will produce thermal emission described as gyro-resonance radiation. The brightness of these two thermal emission processes are limited by a maximum temperature of the plasma. Neither can produce the extremely bright emission seen in most cosmic radio sources.

The two best understood mechanisms for non-thermal radio emission involve either accelerating the electrons to very high energies with non-Maxwellian velocity distributions, or allowing plasma emission processes to provide emission feeding on waves in the plasma (see e.g. Zheleznyakov 1970). The latter are theoretically difficult to relate to observable emission, because the theory is complex, so it is the practice in radio astronomy to invoke plasma radiation only when all other alternatives fail. In practice, plasma radio emission tends to be related to very high time variability, hence there is an obvious observable symptom: short time scale variations. As we will discuss, some of the radio-emitting X-ray binaries are being found with variations on time scales as short as tens of minutes. In no case, yet, do these observations force one to abandon the first option (incoherent synchrotron emission) as the emission mechanism for radio-emitting accretion environments.

The most efficient known mechanism for production of intense radio emission from cosmic sources is the so-called synchrotron emission mechanism. Highly relativistic electron interacting with magnetic fields produces intense radio emission which tends to be linearly polarized. Under circumstances ranging from galactic background radio emission to the strong emission from quasars and radio galaxies, the observed radio emission can be reasonably explained by assuming there are simple (or complex) distributions of relativistic electrons, usually with a power-law energy distribution, interacting with ordered, or turbulent, distributions of magnetic fields. Because synchrotron emission explains most, if not all aspects of radio emission from compact accreting objects, the presence of intense non-thermal radio emission is taken as prima facie evidence for the presence of highly relativistic electrons mixed with magnetic fields. Particularly when one sees flaring, or highly time-variable radio emission this implies the need for acceleration of electrons in the environment of the object. Thus, radio emission is usually taken as evidence for particle acceleration. However, before addressing the question of production of relativistic electron plasma let us summarize some of the characteristics of synchrotron emission.

2.2 Synchrotron Emission Properties

Synchrotron emission theory as it is generally applied to the discussion of compact accreting objects is fairly simple and worth summarizing. An extensive discussion of synchrotron radiation theory can be found in Ginzburg and Syrovatskii (1965). The first important point is that the radio emissivity of an electron or ion interacting with magnetic fields is inversely proportional to the fourth power of its mass. Therefore, the relativistic electrons completely dominate the radio emission from any relativistic plasma. Unfortunately, that also means that after one has estimated the properties of the electron component one must arbitrarily assume an electron to proton ratio for the plasma. A popular assumption for this ratio is unity in order to preserve charge neutrality. In practice it is not known. Synchrotron emission over the observed frequency ranges of a few hundred MHz to a few tens of GHz require particle energies in the range of MeV to several tens of MeV, and it is common practice, consistent with the constraints of the observations, to assume a power law for the electron energy distribution. Thus we assume that if there are $N(E)dE$ electrons with energies between E and $E+dE$, then $N(E) = K \cdot E^{-\gamma}$, where γ is the energy spectral index, generally > 1, and K is a constant. Unless one knows the details about the geometry of particle motions and field distribution, most applications of synchrotron emission theory assume an average over finite volumes which have random

directions of motion and orientation of magnetic field. Under these circumstances all the emission and absorption properties can be described by simple emission and absorption coefficients, whereby the emission coefficient is given by

$$\epsilon_\nu = \epsilon_0(K/K_0)(H/H_0)^{(\gamma+1)/2}(\nu/\nu_0)^{-(\gamma-1)/2} \quad (1)$$

and the absorption coefficient k_ν is related to ϵ_ν by a so-called source function, which in this case is

$$\frac{\epsilon_\nu}{k_\nu} = \frac{\epsilon_0}{\kappa_0}(H/H_0)^{-1/2}(\nu/\nu_0)^{5/2}. \quad (2)$$

whereby H is the strength of the magnetic fields.
Later in this review we will discuss some of the models applicable to radio emission from compact accreting objects. Assuming that this simple model applies, the observations can be used to derive one or more (or a combination) of the parameters (H, K, γ, D and d). The apparent solid angle subtended by such a emittion region is $\Omega_s \approx (D/d)^2$. Defining the optical depth of the source by $\tau_\nu = k_\nu \cdot L$, whereby L is the size of the emission region, the observed radio flux density for such a source is

$$S_\nu = \frac{j_\nu}{k_\nu} \cdot (1 - e^{-\tau_\nu})\Omega_s. \quad (3)$$

If the angular size of the source, $\Theta_s \approx D/d$ is known (e.g. if the source is resolved), together d or D, one can determine some of the interesting parameters of the source. One of the interesting combinations of parameters determined for some X-ray binaries is $\Theta_s H^{-1/4}$, which is usually found to be the order of a few milli-arcseconds Gauss$^{-1/4}$. This indicates size scales of the order of milli-arcseconds since other consideration estimate the fields to be the order of milli-Gauss.

3 OBSERVED JETS AND LOBES AS INDICATORS OF BULK ACCELERATION AND EJECTION

Extended radio emission in the form of stationary structures or moving jets surrounding an X-ray binary is a direct indicator that relativistic electrons have been accelerated in the environment of the X-ray binary, and then ejected in bulk motion of mixed relativistic electrons, thermal plasma, and magnetic fields that we refer to as 'plasmoids' or 'jets'. Four X-ray binaries have exhibited resolved jets and/or lobes: Sco X-1, SS433, Cir X-1, and Cyg X-3.

3.1 The classic double radio source in an XRB: Sco X-1

Sco X-1 was first shown to be a triple radio source by Hjellming and Wade (1971). The central radio source, which is highly variable on time scales of minutes to hours (Bradt *et al.* 1975), is coincident with the position of the X-ray binary. Two companion radio sources lie 1.3′ NE and 2.0′ SW on opposite sides of Sco X-1. A VLA 5 GHz image of these sources with 1″ resolution is shown in Figure 1. At higher resolution the NE companion is still unresolved ($\lesssim$0.007 "; Geldzahler, Fomalont and Cohen 1988) while the SW companion is even more resolved than in appears in Figure 1 (Fomalont *et al.* 1983); successive epochs of high resolution have shown that the NE companion has a proper motion with respect to the

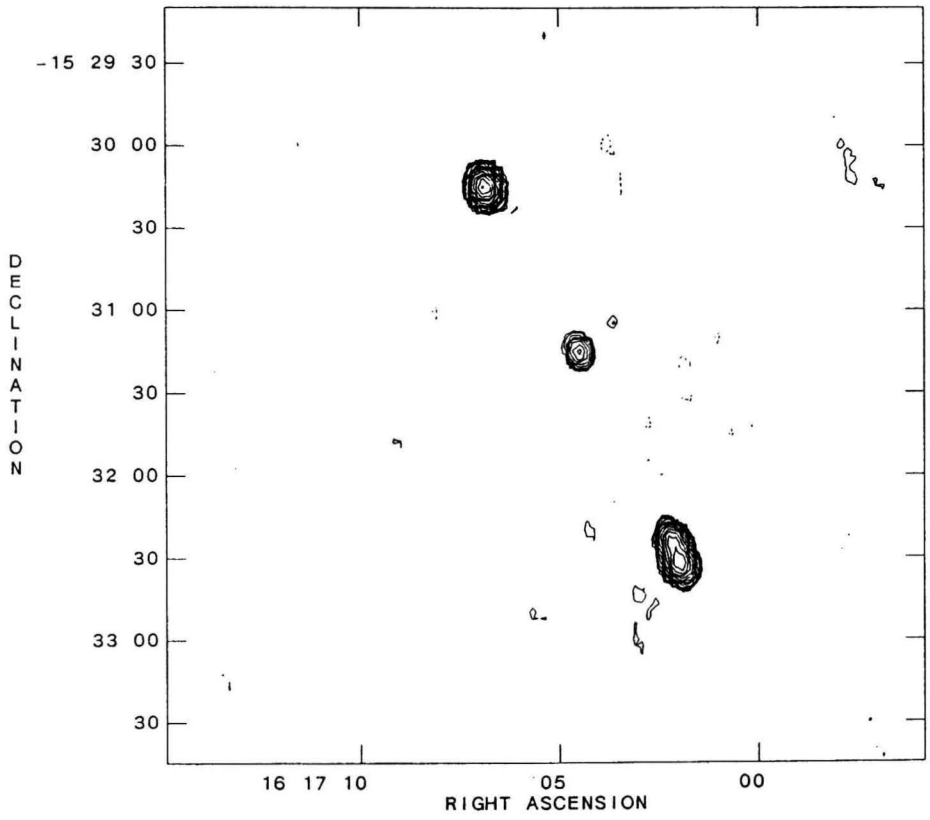

Figure 1: Deep 1.4 GHz VLA image of the Sco X-1 triplet

center 0.015″ per year, or 72 km/sec if the distance is 1 kpc (Geldzahler and Fomalont 1986).

The simplest interpretation of the double radio source surrounding Sco X-1 involves an un-seen jet in which energy and possibly non-radiating relativistic electrons move outward until they interact with material to at 'hot spots' which may then diffuse into resolved structures. These phenomena are commonly seen in triple radio sources associated with external galaxies and quasars (Kellermann and Owen 1988). It is unclear how the relative small proper motion of the lobes can be combined with the extremely small angular size of the NE component in this model.

3.2 The classic moving jet source: SS433

SS433 is a weak X-ray source at the center of a very large complex of radio (W50) emission (Königl 1983, Elston and Baum 1987), extended X-ray emission (Watson *et al.* 1986), and optical filaments (Margon 1984). However, its most striking characteristic is the essentially continuous ejection of matter at a velocity of 0.26c which is seen in the X-ray regime through Doppler shifts of iron lines, in the optical regime through Doppler-shifted emission lines of hydrogen and helium (Margon 1984), and in the radio regime through radio jets

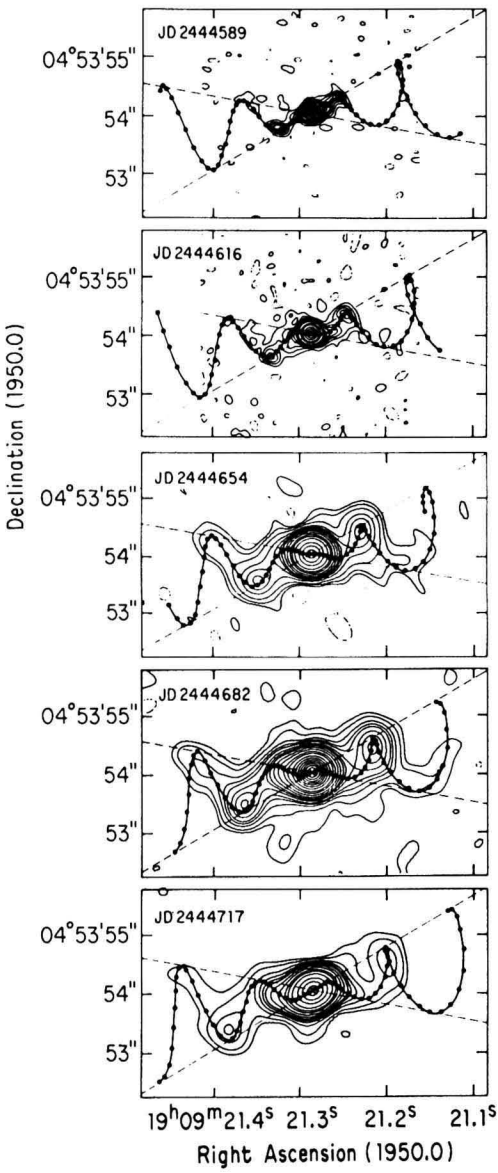

Figure 2: A sequence of five SS433 VLA at roughly monthly intervals (Hjellming and Johnston 1986).

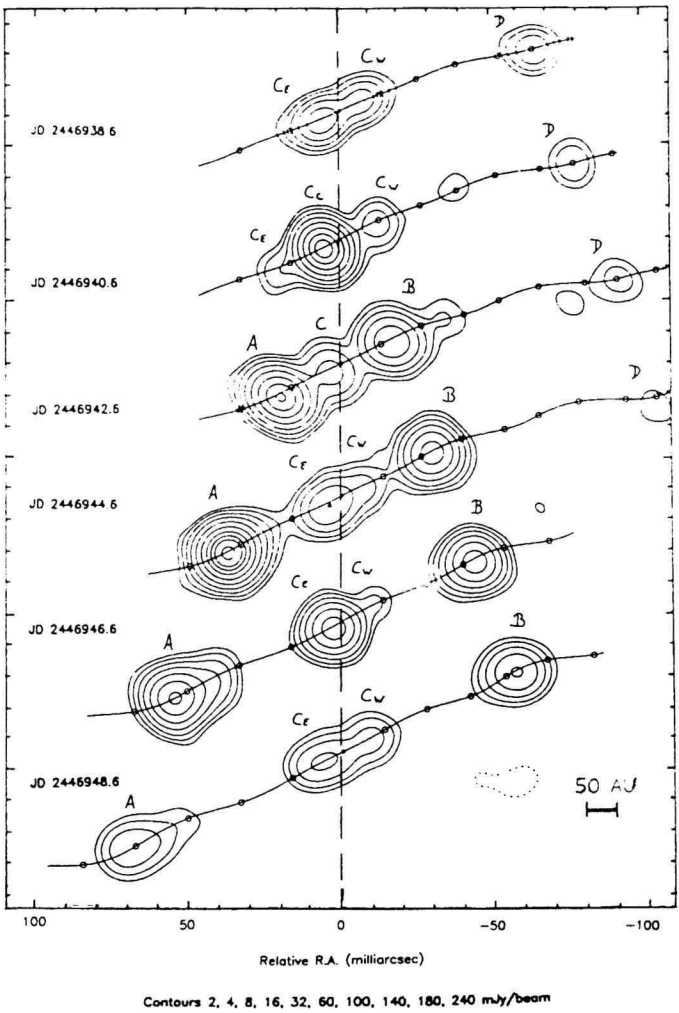

Figure 3: High resolution sequence of SS433 at VLB resolution (Vermeulen 1989)

that move outward from the stellar system with a proper motion of 3.0″ per year (Hjellming and Johnston 1985, 1988). Figure 2 shows a sequence of VLA radio images of SS433 taken at roughly monthly intervals in 1980-81 using 15 GHz for the first two images and 5 GHz for the last three images (Hjellming and Johnston 1985). The proper motion, and the E-W asymmetry in angular extent, can be directly measured from the sequence of images in Figure 2. The optical and X-ray Doppler shifts, and radio jet proper motions, have a period of 162.5 days which is believed to be the precession period of a thick accretion disk surrounding the compact object in the SS433 binary system. The E-W asymmetry is due to the relativistic effect of the time delay of the emission from the more distant (Western) component relative to the near (Eastern) component; the proper motions and E-W asymmetry seen in sequences of radio images, which now have been obtained over a time base of ten years, determine the velocity of motion in the jets to be 0.26c and the distance of SS433 to be 5.5 kpc. The 'corkscrew' pattern of jet ejection reflect the same kinematics and jet geometry seen in the Doppler shifts of optical and X-ray emission.

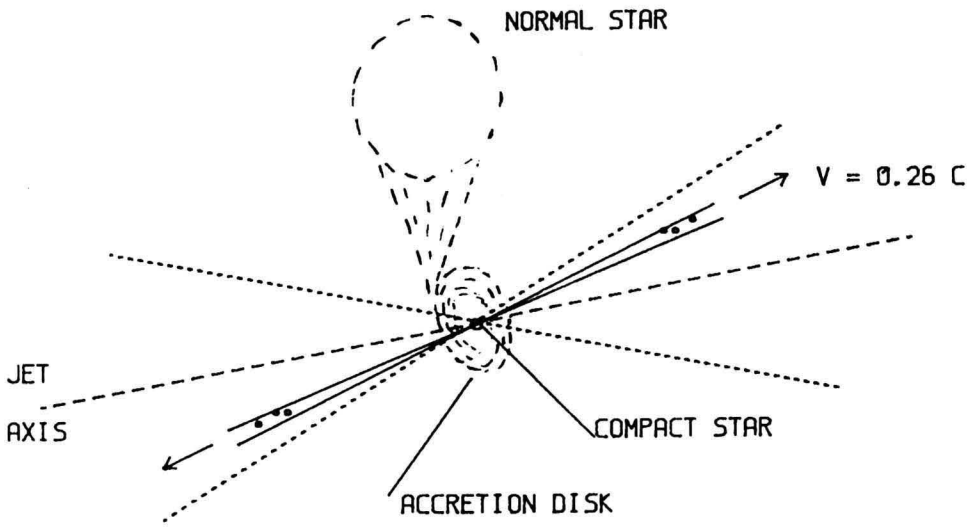

Figure 4: Schematic picture of SS433 (Hjellming and Johnston 1988)

The work of Vermeulen *et al.* (1987) and Vermeulen (1989) has shown that high resolution VLB observations of knots in the SS433 jet not only exhibit the same jet kinematics near the central object, but provide the first direct evidence of a phenomena theoretically inferred for many jet sources: in situ particle acceleration in the jets. Sequences of images made with the European VLBI Network show that the radio emission does not originate ab initio from a central region, but rather exhibits a brightening during motion very close to the center, followed by a peak preceding the steady decay that is the dominant factor in the evolution of the ejecta in the radio images on VLA resolution scales of 0.1″ (Figure 3).

Figure 4 is a schematic of the probable geometry of the SS433 binary system with mass transfer from one star to an accretion disk surrounding the compact neutron star or black hole. The X-ray 'jets' are an extension of the X-ray emitting accretion disk environment, the optically emitting knots are recombining 10^4 K gas further outside the jet flowing at 0.26c, and the radio emission begins to appear a few light days further out, at angular scales of a few milli-arcseconds, and continues out to size scales of several arcseconds.

Hjellming and Johnston (1988) have shown that a conical jet model of laterally expanding sheaths of relativistic plasma, that is initially decelerated by interaction with surrounding gas, has optically thin decay characteristics that matches the principal decay behavior of the SS433 radio jets. This model is based upon the idea that the driving force behind the production of relativistic particles is the lateral expansion of a hot, X-ray emitting gas jet with an initial internal sound speed of the order of 2000 km/sec, with a geometry of a conical shock sheath in which the particle acceleration occurs. This hydrodynamical acceleration mechanism may be one of the principal scenarios for the production of relativistic electrons in this and other X-ray binaries. However, even though models of this type have the correct behavior for SS433, it is possible that even with this object other scenarios involving non-emitting jets of relativistic particles being ejected on the axis of the accretion disk environment will produce the same result. Particle acceleration in a sheath surrounding laterally expanding shocks is consistent with the most

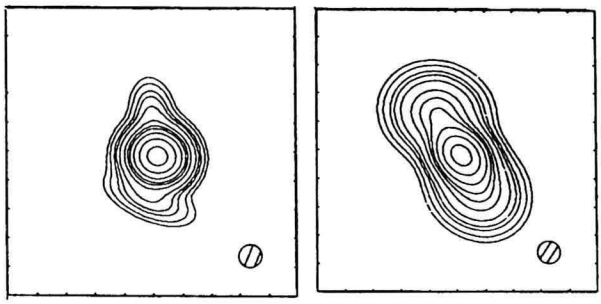

Figure 5: VLB images of Cyg X-3 on Oct. 10 and Oct. 15/16 1988 (Schalinski *et al.* 1990)

commonly discussed mechanisms for particle acceleration of cosmic rays and strong radio sources, but the observations of SS433, where more detailed data are available than for any other radio-emitting X-ray binary, do not yet rule out other models.

3.3 Cir X-1

Cir X-1 is an X-ray binary with a neutron star as compact object, which has exhibited periodic radio variations that match the 16.595 day period of the binary system. The mass donor is probably a low-mass star, see Stewart *et al.* (1991). Haynes *et al.* 1986 have imaged the region around Cir X-1 at 843 MHz, showing that there is a 3′ by 5′ synchrotron radiation nebulosity surrounding the X-ray binary with more compact structures near the center. The completion of the Australian Radio Telescope in the early 1990's is awaited eagerly so high resolution observations can be made to determine the lobe and jet characteristics of the regions close to the compact object.

3.4 Cyg X-3

We will shortly be discussing Cyg X-3 as the proto-type object for sudden bursts of production of large amounts of relativistic electron plasma, in very short periods of time, that exhibit the classic 'synchrotron' bubble events. On rare occasions following some strong flares of this type the Cyg X-3 radio emission is found to result in outward moving jets with proper motions of 0.17″ per year (Geldzahler *et al.* 1983, Johnston *et al.* 1986, and Spencer *et al.* 1986). High resolution VLB images of this type of resolved emission in Cyg X-3 (Schalinski *et al.* 1990) are shown in Figure 5. Unfortunately, the distance to Cyg X-3 is poorly known because dust obscuration makes it invisible at optical wavelengths; however, 21 cm absorption experiments indicate distances between 8 and 15 kpc. If the correct distance is 12 kpc, the 'jet' velocities of Cyg X-3 are consistent with the highly stable 0.26c velocities of SS433. Radio lobes have reported by Strom *et al.* (1988). Earlier observations failed to detect these lobes, which suggests that such lobes are a temporary phenomenon. The future of studying the Cyg X-3 jets is promising if high resolution VLB observations can be performed systematically following the 'right' large flares.

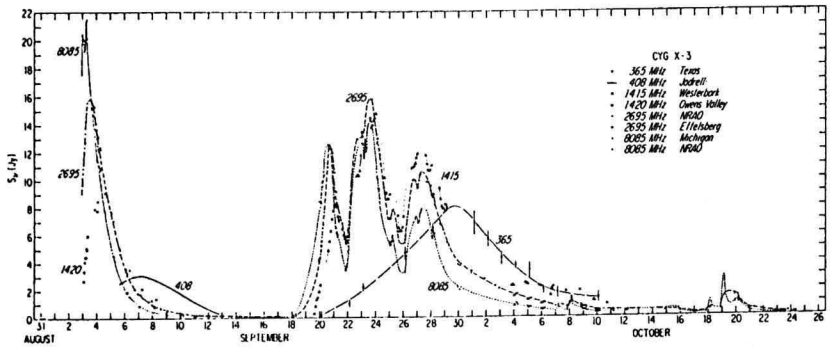

Figure 6: Large radio flares of Cyg X-3 in 1972

4 RADIO EVENTS IN COMPACT ACCRETING OBJECTS

4.1 Cyg X-3 flares

Figure 6 shows the sequence of multi-frequency radio observations in 1972 that showed that Cyg X-3 exhibits extremely strong radio flares (Gregory *et al.* 1972, and 20 papers following this article). These and subsequent observations have established that the major flares in Cyg X-3 behave like the synchrotron 'bubble' events first discussed by van der Laan (1966) and Kellermann (1966) to explain the months to years time scale radio flaring events in quasars. Irrespective of whether the relativistic plasma is suddenly created with a mixture of magnetic fields in shell, sphere, or conical sheath environments, the subsequent behavior has time variation characteristics of one (or multiple simultaneous) regions of relativistic plasma expanding at high speeds in three dimensions with adiabatic expansion dominating the energy losses of the relativistic electrons. Figures 7a, b, and c show the classic behavior of synchrotron 'bubble' events in the form of log S_ν vs log (t/t_0) for a several frequencies, S_ν vs t/t_0 for several frequencies, and log S_ν vs log ν at several times.

The 'typical' synchrotron 'bubble' event involves an optically thick rise of the radio flux, with weaker and later peaks as radio frequency decreases, followed by an optically thin power law decay proportional to $\nu^{-(\gamma-1)/2} \cdot t^{-2\gamma}$, where γ is the energy spectral index of a power law spectrum of relativistic electrons. If energy losses are dominated by adiabatic expansion, all event look like Figures 7. However, if other energy loss mechanisms become important, and the real geometry of expansion is not a homogeneous sphere, the optical thick rise, the peaks and initial pre-power law decays are often more complicated (Marscher and Brown 1975). The linear polarization characteristic of synchrotron radio emission is often seen and sometimes the presence of large quantities of co-existing thermal plasma is inferred from the changes in the Faraday rotation of linear polarization angle (Seaquist *et al.* 1974).

The appearance of radio events with the observational signatures of synchrotron 'bubbles' establish the sudden appearance of relativistic plasma mixed with magnetic fields. However, the signatures of the size scales, and properties of the acceleration regions and their geometry, are lost, except for the qualitative result that the scale of time variation of an event is proportional to the size scale of the region when it begins behaving like an adiabatically expanding relativistic plasmoid.

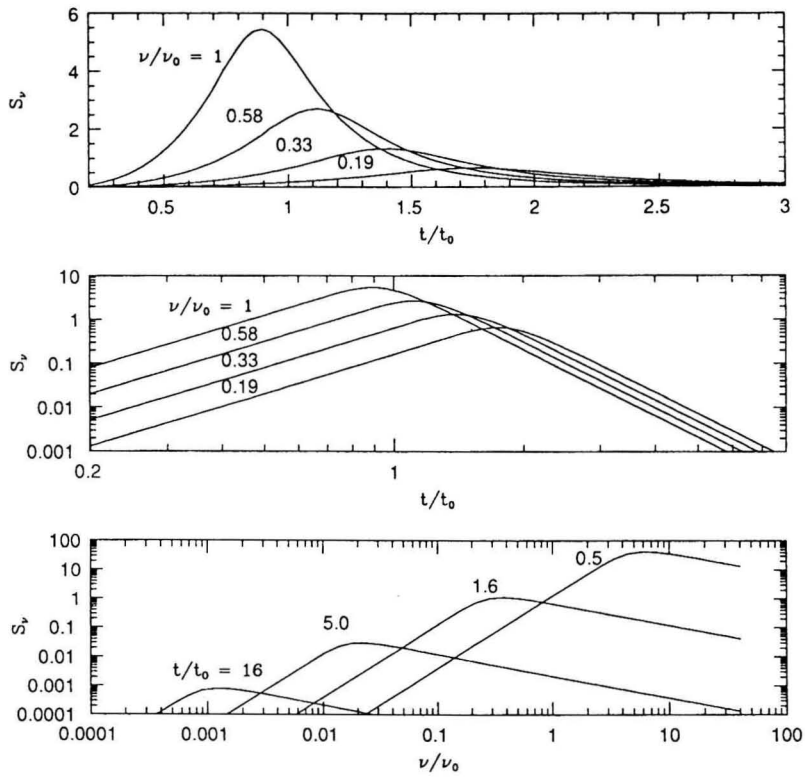

Figure 7: Three panel plot of S_ν vs t for four frequencies (a), log S_ν vs log t (b), and log S_ν vs log ν (c).

4.2 Transient XRB's

The transient X-ray binaries A0620-00, Cen X-4, GS2000+35 and Aql X-1 have each exhibited transient synchrotron bubble events at radio wavelengths following a change in each system that produced a transient X-ray source (probably the accretion rate reached the Eddington limit). Figure 8 shows the data and synchrotron bubble model fits for the events in the first three objects (adapted from Hjellming *et al.* 1988). These events indicate that one of the side effects of the sudden appearance of a transient accretion disk environment in these systems is a sudden, effectively single event production of a compact volume of mixed relativistic electrons and magnetic fields. The bubble subsequently expands adiabatically with all the observational signatures of synchrotron bubble events (Fig. 7). From the point of view of this conference, it indicates massive particle acceleration in a short period of time.

4.3 The coupling between radio emission and X-ray states in Z sources

Recent observations have shown that some low-mass X-ray binaries have state changes that are coupled in the sense that changes in behavior in one wavelength region are correlated with state changes in other wavelength regions. Based upon the results of extensive

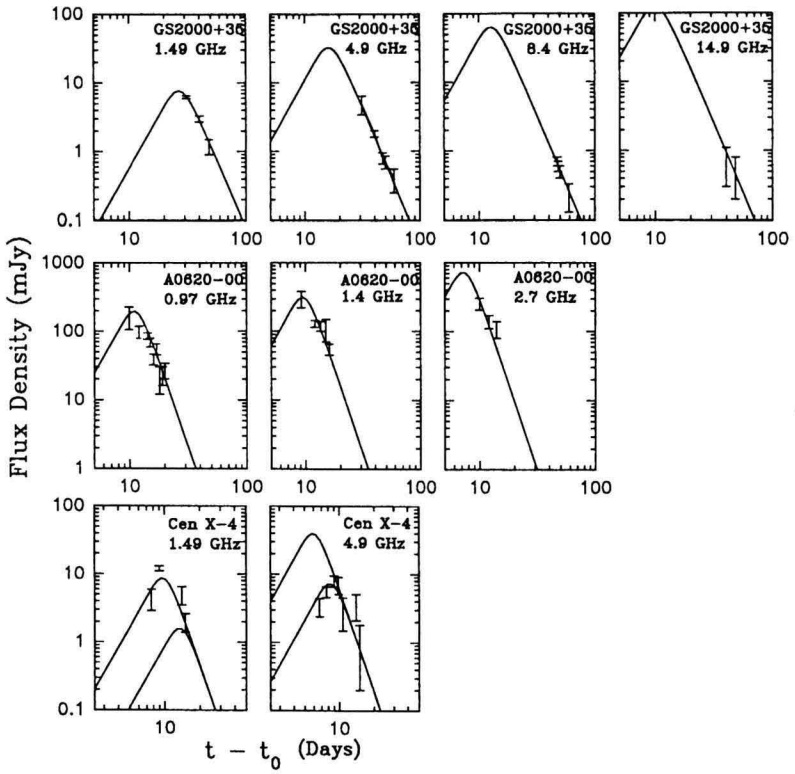

Figure 8: Data and models for synchroton bubble events in A0620-00, Cen X-4, and GS2000+35 (Hjellming *et al.* 1988).

multi-wavelength observing campaigns on Sco X-1, Priedhorsky *et al.* (1986) suggested that the X-ray, optical, and radio states of Sco X-1 were related in a predictable way. The nature of this relationship has been more definitively established in recent years through multi-wavelength campaigns involving ground-based observations at radio and optical wavelengths simultaneously with satellite observations in the ultra-violet (IUE) and the X-ray (Ginga). X-ray observations with sensitive measurements in four independent energy ranges and high timing resolution have provided the key classification system for X-ray states; the intensities in the four energy ranges allow one to define a 'hard' hardness (e.g. $H_1 = I(9-18\text{keV}) \ / \ I(6-9\text{keV})$) and a 'soft' hardness (e.g. $H_2 = I(4-6\text{keV}) \ / \ I(1-4\text{keV})$). For the X-ray binaries Sco X-1, Cyg X-2, GX17+2, GX5-1, GX349+2, and GX340+0 plots of H_1 vs H_2 indicate three branches (roughly Z-shaped), which are correlated with the high timing properties (QPO and noise), and are called 'horizontal', 'normal', and 'flaring' branches (Hasinger and van der Klis 1989). Figure 9 shows the so-called 'Z-diagram' of a six day observation of GX17+2, with the three branches indicated. The observing campaigns for GX17+2 (Penninx *et al.* 1988), Cyg X-2 (Hjellming *et al.* 1990a), and Sco X-1 (Hjellming *et al.* 1990b) show that for these Z-sources the radio emission is strongest on the horizontal branch, decreases as the source proceeds down the normal branch, and is weakest when the source is on the flaring branch. Figure 9a shows an X-ray colour-colour diagram of GX 17+2 during a six day simultaneous VLA-Ginga campaign; in Fig. 9b the radio brightness is plotted (size of symbols scales with the radio

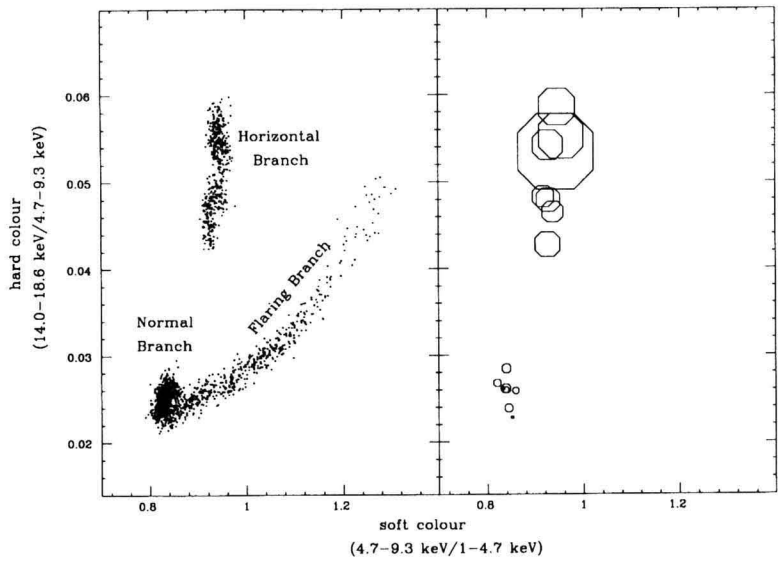

Figure 9: The X-ray colour-colour diagram of GX 17+2 showing the three X-ray spectral branches (left). The right figure shows the simultaneous radio data, whereby the radius of the symbol is linear with the 4.8 GHz brightness (Penninx *et al.* 1988).

brightness) in the same colour-colour diagram at the position where the X-ray source was at that moment. Simultaneous radio – X-ray observations of the Z source GX 5-1 (Tan *et al.* 1991) have not led to a similar correlation. During most of the time the X-ray source was on the horizontal branch and the radio emission was quiet ($\sim$ 0.6 mJy). When the X-ray source was on the normal branch (once) a radio flare occured ($\sim$ 3 mJy).

Penninx (1989) suggested that the average radio luminosity of the Z sources is approximately the same on the normal branch. The two Z sources that had not yet been detected at radio wavelengths at that time (GX 349+2 and GX 340+0), have now been detected with approximately the expected radio brightnesses (Cooke and Ponman 1991, Zwarthoed *et al.* 1991).

4.4 Other X-ray binaries radiating non-thermal radio emission

We have already mentioned that radio outbursts of the low-mass X-ray binary Cir X-1 occur with a period of 16.6 days, probably the binary orbit of the system. The radio flares occur near a transition in the X-ray brightness (either a high-low transition as often observed in the 70's, or a low-high transition at the end of the 80's), which has the same periodicity of 16.6 days (see e.g. Stewart *et al.* 1991 and ref.). The brightness and occurence of the radio flares and the IR brightness increase appear to be related with the type of X-ray transition (high-low versus low-high). It has been suggested that the orbit of the neutron star around the mass-donor star is eccentric, in which case the transition might

occur near periastron; still, how and what causes the transition is unclear.

Another system with periodic radio behavior is the radio, optical, X-ray, and (probably) γ-ray emitting Be binary LSI+61°303. Gregory and Taylor (1978) first determined the period of this system to be 26.5 days from the radio flaring data. Some observations indicate that between phase 0.25 and 0.5 the radio source is optically thick (when the radio flux is increasing), but becomes a flat spectrum or optically thin source at other phases (when the radio flux is decreasing). Recent five frequency spectrum variations sampled at four day intervals over two separate binary periods show spectrum variations in a highly broadened spectrum that can be fit with optically thick, conical jet models of the type discussed by Hjellming and Johnston (1988).

The radio counterpart of the high-mass X-ray binary Cyg X-1 shows mostly a relatively stable radio source of $\sim$ 15 mJy with a very flat radio spectrum. The radio component was first identified with the optical and X-ray object because of an X-ray state change that result in an increase from an unobservable to stable radio source between March 22 and March 31, 1972 (Tananbaum *et al.* 1972; Hjellming 1973). Except for a radio flaring event at the time of an X-ray flare in 1975, Cyg X-1 has since maintained a radio flux level near 15 mJy. This type of stability is inherently difficult to maintain in relativistic plasma regions which are essentially impossible to confine, hence at the very least adiabatic losses should cause source decay. Optically thick, conical jet models can produce stable radio sources due to continuous production of relativistic plasma at the base of the jets; however, an change in aspect angle due to motions in the system would cause a periodic modulation of the radio emission. Recent observations at two day intervals over the binary period by Hjellming and Han (1991) show that modulations in a broad spectrum match the binary period and can be fit by an optically thick conical jet model with variations in angle of inclination with respect to the observer over the binary period.

The distinction between synchrotron bubble events and conical jets models is that of three- vs two-dimensional expansions of small volumes of mixed relativistic electrons and fields. As discussed by Hjellming and Johnston (1988) a mixture of these types of behavior can be found if the geometry of particle acceleration occurs in twin-jet geometries à la SS433.

Variable radio emission has been observed from the atoll source GX 13+1 (Garcia *et al.* 1988). The origin of this non-thermal radio emission is unclear. Radio emission has been detected from the low-mass X-ray binaries (both probably atoll sources) in the globular clusters NGC7078 and NGC6712 (Machin *et al.* 1990).

4.5 Cataclysmic Variables

Some cataclysmic variables are radio sources; however only a very few are believed to exhibit the type of radio emission that indicates particle acceleration is occuring in the vicinity of the compact object in these binary systems. The radio emission from the novae HR Del 1967, FH Ser 1970, V1500 Cyg 1975, V1270 Aql 1982, PW Vul 1986, QU Vul 1986, V1819 Cyg 1986, and V827 Her 1987 is predominantly thermal emission from the ejected material associated with the nova outburst. Similarly the two recurrent novae that have been observed at radio wavelengths, the RS Oph event in 1985 and the 1990 event in V745 Sco exhibit thermal emission processes. However, for two of these objects, QU Vul 1986 (Taylor *et al.* 1987) and RS Oph (Padin, Davis and Bode 1985), in addition to the normal and expected thermal emission (Hjellming *et al.* 1986, Taylor *et al.* 1987) there were very high brightness temperature components, mainly seen early in the evolution of these objects. These are enough to indicate the possibility of particle acceleration, probably in strong shock environments produced when the ejecta interact with surrounding gas.

It has been argued that for two magnetic CVs, AM Her (Chanmugam and Dulk 1982)

and AE Aqr (Bookbinder and Lamb 1987), particle acceleration must be occuring in the vicinity of the magnetized white dwarfs in each of these systems. Both gyrosynchrotron and synchrotron emission are suspected in these two systems. Bastian, Dulk and Chanmugam (1988) have described the radio flares of AE Aqr as a low power of Cyg X-3 and suggested that they may be connected to the disruption of the accretion disk near the white dwarf. Bookbinder and Lamb (1987) argued that the magnetic field of the white dwarf is insufficient to produce the radio flares and suggested a possible coupling with the magnetic field of the mass donating K5 dwarf.

5 MODELS OF COMPACT RADIO EMISSION

5.1 Synchrotron Bubble Events - Single Events

The simplest type of radio event involving relativistic particles, which occurs frequently in Cyg X-3 and transient X-ray sources, is the synchrotron 'bubble event' (see section 4.1 and 4.2, and Figures 6, 7, and 8). The theory for these events as examples of expanding, spherical bubbles of relativistic plasma, treated as uniform layers with respect to the line of sight to an observer, was first discussed by van der Laan (1966) and Kellermann (1966). A recent discussion by Hjellming and Johnston (1988) adds a correction factor for spherical geometry, and provides a formulation that can be directly compared with the two-dimensional twin jet version with the same level of theory as the expanding relativistic plasmas that we will summarize in a coming section. In this formulation we assume that a spherical 'bubble' of relativistic plasma at time t has a radius r, an angular radius $\theta = r/d$ (where d is the distance), a uniform magnetic field (with a random distribution of orientations with respect to the observer) of strength H, and a power law spectrum of $N(E) = KE^{-\gamma}$. All variables scale with time, so one assumes that at a time t_0 the size is r_0 (or θ_0), the magnetic field is H_0, each particle has an energy E_0, and the fixed number of relativistic electrons is set by K_0; then each particle loses energy according to $E = E_0(r/r_0)^{-1}$, an effect which has its greatest impact on the upper and lower energy cut-offs (E_1 and E_2) assumed for the power law spectrum. Conservation of magnetic flux implies that $H = H_0(r/r_0)^2$, and conservation of particles between the evolving cut-off energies gives $K = K_0(r/r_0)^{-(\gamma+2)}$, a result which is independent of the values of cut-off energies. The optical depth for a radius $a \leq r$ is then (cf Equations 1 and 2)

$$\tau_\nu(a) = \tau'_\nu \left[1 - \left(\frac{a}{r}\right)^2\right]^{1/2} \tag{4}$$

where

$$\tau'_\nu = \tau_0 \left(\frac{r}{r_0}\right)^{-(2\gamma+3)} \left(\frac{\nu}{\nu_0}\right)^{-(\gamma+4)/2} \tag{5}$$

and $\tau_0 = 0.019 g(\gamma)(3.5 \cdot 10^9)^\gamma K_0 H_0^{(\gamma+2)/2} \cdot 2 \cdot r_0$, with ν_0 being a fixed reference frequency. Since the source is homogenous at any point in time the radio flux density equation can be integrated over the spherically symmetric volume of the source to give

$$S_\nu = S_0 \left(\frac{\nu}{\nu_0}\right)^{5/2} \left(\frac{r}{r_0}\right)^3 \left\{1 - exp\left[-\tau_0 \left(\frac{r}{r_0}\right)^{-(2\gamma+3)} \left(\frac{\nu}{\nu_0}\right)^{-(\gamma+4)/2}\right]\right\} \cdot \xi_{sph}(\tau). \tag{6}$$

The function $\xi_{sph}(x)$ can be approximated by the power law expansion $\xi_{sph}(x) \simeq 0.66584 + 0.09089\tau - 0.009989\tau^2 + 0.0005208\tau^3 - 0.00001268\tau^4 + 0.000000115\tau^5$ for $\tau < 40$ and $\xi_{sph}(x) = 1$ for $\tau > 40$.

If the spherical bubbles of relativistic plasma expand freely with constant velocity, one can assume the radius scales with time according to $t/t_0 = r/r_0$. However, if there is significant decelaration due to interaction with surrounding material, the mapping of spatial into time variations is different: $t/t_0 = (r/r_0)^{2.5}$ or $t/t_0 = (r/r_0)^4$ for the phases where energy or momentum, respectively, are conserved.

5.2 Non-varying or relatively unvarying synchrotron radio emission

Because relativistic plasmas are difficult, if not impossible, to confine in the natural environments of astronomical objects, synchrotron radiation sources in stellar environments will always tend to be variable in time. This means the most difficult behavior to explain is long term constancy of radio emission. Cyg X-1 is an extreme example where, except for the very rare flares and state changes, its radio emission is almost always very close to 15 mJy over a range of frequencies (the relative quiescent radio fluxes in Cyg X-3 and in the Z sources have also fairly flat spectra). Flat radio spectra can be produced by a source which is inhomogeneous, that is, has a range of optical depths and apparent surface brightness. These facts, and the fact that the radio emission has angular scales less than 0.1″, allow one to eliminate two of the three obvious possibilities, and conclude that it is likely that inhomogeneous jet structures are the sources of the relatively steady radio emission.

The larger the size scale of the synchrotron radio source, the longer the time scale of variation due to expansion effects. The extended SS433 jets have time scales for variations of several tens of days, and this is related to these jets being resolved and imageable. The lack of resolution of the Cyg X-1 radio source on these angular scales eliminates this reason for its relative flux stability. The next most obvious reason for this stability is indicated by the relatively flat radio spectra: continuous ejection of relativistic electron plasma, at the same rate with the same properties, will produce an radio emitting structure that can be constant in time. There are two obvious types of ejecta that will have these properties: a spherical 'wind' of relativistic plasma; and conical jets resulting from continuous ejection along opposite axes as is seen directly in the images of SS433. The decay of the ejecta limits the size scales over which the jets can be observed. There are three obvious scenarios that can achieve the desired effects: (a) sequential ejection of spherical bubbles of relativistic plasma along ejection axes, where each bubble segment behaves as discussed in the previous section, but the sum over a continuous history of ejected bubbles is a segmented structure with constant emission properties as a whole; (b) continuous ejection of plasma along twin axes with constant axial velocity and only lateral expansion perpindicular to these axes; and (c) a spherically symmetric, continuous 'wind' of relativistic plasma.

It is important to note that all scenarios involving non-spherically symmetric ejection, where the emitting regions range from optically thick to thin extremes from inner to outer regions, have the potential of showing periodic modulation of the strength of the observed radio emission. This is because changes in angle with respect to the observer change the apparent flux of a structures that would have no variation if there were no changes in this angle. SS433 is an example of twin-jet precessing with a 162.5 day period; however, the SS433 radio emission is always from optically thin regions, so this modulation effect has not been seen. The observable characteristics of optically thick, asymmetric structures changing with a periodicity based upon precession and/or orbital motion would be: broad/flat radio spectra; spectral variations as a function of the precessional and/or orbital period.

Recently Hjellming *et al.* 1991 have searched for these signatures of optically thick, periodically varying radio 'jets' in the relatively stable radio emission of Cyg X-1 and the known periodic emission of LSI+61°303. In both cases the expected broad, but variable spectra for inhomogeneous sources were found, and the observed emission could be fit by the simple conical jet models we will discuss in a moment; however, the other two asymmetric structure models may fit equally well.

5.3 Multiple Synchrotron bubble ejection (episodic/periodic)

If we assume that, at every Δt interval in time, two spherically symmetric plasmoids are ejected from an object, each plasmoid will expand with the optical depth evolution described by the equations for expanding spherical bubbles. However, the continual replacement of newer, younger bubbles results in a continuous structure that, in outline, would look like a twin cones. In the extreme where succesive bubbles do not interact one can sum over the radio properties of each bubble, and allow for multiple bubbles along individual lines of sight, and predict the total radio emission and a function of Δt and the angle with respect to the line of sight. Penninx (1990) made a crude calculation and summed the timedependent spectra of the spherical bubbles of van der Laan (1966) for γ = 2 and 3 respectively. Assuming that the bubbles expand freely, $t/t_0 = r/r_0$,the radio spectral index α ranges between 0.79–0.95 respectively. If there is significant deceleration, $t/t_0 = (r/r_0)^2$ or $t/t_0 = (r/r_0)^3$, the spectra indices α will range between 0.36–0.56 (γ=2–3) and –0.07–0.17 (γ=2–3) respectively. This suggests that a constant and fairly flat spectrum can be observed by a simple sum of van der Laan models, but only if the individual blobs are significantly slowed. Several obvious effects make the real situation much more complicated. If, after a finite time, successive bubbles 'collide' because of internal expansion, shock-like structures will occur requiring a much more complicated model. In addition, if the ejection paths precess, as seen for SS433, the angle with respect to the observer will vary over each segment ejected during a precession period. Finally, modulation of the relativistic electron content and magnetic field at fixed distances along the jet add a dimension of time variability that is very difficult to model.

However, there is one simple case of continous ejection where the theory of the behavior of the radio emission is almost as simple as the theory of isolated synchrotron bubbles: continuously ejected conical jets (Hjellming and Johnston 1988).

5.4 Continuous Ejection with Conical Jet Geometry

If we assume that there is no acceleration or decelaration of relativistic plasma ejected along twin-jet axes, the expansion effects that determine the simple properties of synchrtron bubbles are changed from three-dimensional to two-dimensional in character. Let z be the coordinate of the jet axis and r be a radius perpindicular to this axis. At any point z_2 the radius of the cross-section of the jet will be r_2. The result is the energy of each particle scales as $E = E_0(r_2/r_0)^{-2/3}$, the fields scale as $H = H_0(r_2/r_0)^{-1}$, and the relativistic electron concentration scales as $K = K_0(r_2/r_0)^{-2(\gamma+2)/3}$. As shown by Hjellming and Johnston (1988) the differential contribution to the observed flux density as a function of z along the twin jets is

$$\frac{dS_\nu}{dz} = \left(\frac{S_0}{r_0}\right)\left(\frac{\nu}{\nu_0}\right)^{5/2} sin(\Theta)\left(\frac{r_2}{r_0}\right)^{3/2}\left[1 - exp(-\tau'_\nu)\right]\xi_{con}(\tau'_\nu) \tag{7}$$

where

$$\tau'_\nu = \left[\frac{\tau_0}{sin(\Theta)}\right]\left(\frac{\nu}{\nu_0}\right)^{-(\gamma+4)/2}\left(\frac{r_2}{r_0}\right)^{-(7\gamma+8)/6} \tag{8}$$

and, analogous to the geometry correction for the spherical case, one has a geometry correction factor that can be approximated (for $\tau < 40$) by
$\xi_{con}(\tau) = 0.78517 + 0.06273\tau - 0.007242\tau^2 + 0.0003905\tau^3 - 0.00000973\tau^4 + 0.00000009\tau^5$, and unity otherwise.

The total flux density for twin-conical jets is obtained by numerically integrating Equation (7) along the jet. If Θ is constant, this is a simple calculation; however, if there if Θ varies with z because of precessional and/or orbital motion, the details of the variations of Θ with z must be included.

If the lateral expansion occurs with constant velocity, one can assume r_2 scales with z according to $r_2/r_0 = z_2/z_0$. However, if there is significant decelaration due to interaction with surrounding material, the mapping of z into r_2 is different: $r_2/r_0 = (z/z_0)^{1/2}$ or $r_2/r_0 = (z/z_0)^{1/2}$ for the phases where energy and momentum, respectively, are conserved.

5.5 Continuous Ejection with Spherical Geometry

The 'wind-like' ejection of relativistic plasma in a spherically symmetric manner is another way to obtain a broad spectrum, inhomogenous radio source. However, this model has not yet be developed in the context of X-ray binaries.

6 ORIGINS OF RELATIVISTIC ELECTRONS

The previous discussion of spherically symmetric and twin-jet models for synchrotron radio emission addresses the question of what determines the observed radio flux for these geometries if a specific geometric and energy distribution of relativistic electrons and fields is assumed. It did not, however, address the question of how the relativistic electrons are accelerated. There are two extremes that can be discussed for the environements we are considering: on one extreme gas dynamical expansions accelerate particles in shocks or trapping regions, and in this case the problem is a two-stage sequence of acceleration of gaseous flows from the binary systems followed by particle acceleration; and on the other extreme the particle acceleration occurs in magnetospheric phenomena tied to either an accretion disk or the compact object itself.

6.1 Gas Dynamical Acceleration

6.1.1 Explosions

The acceleration of relativistic electrons, with concomitant generation of magnetic fields, has long been considered to be a natural byproduct of the interaction environment whereby supernova explosions expand into the interstellar medium. This acceleration is a result of turbulent acceleration processes behind shocks (Dickel *et al.* 1989). Single synchrotron bubble events in X-ray binaries like Cyg X-3 and the X-ray transients could be explained by completely analogous processes resulting from sudden changes in the state of the X-ray binary involved. In this scenario a spherical shock expands from the central region, and there is a sudden phase of relativistic electron acceleration behind/in the spherical shock which then can either move with the shock, if the sound speed of the relativistic electrons is set by the thermal sound speed, or they can rapidly expand in front of the shock with sound speeds up to the $c/3^{1/2}$ characteristic of a pure relativistic plasma. The resulting radio emission behaves according to the synchrotron bubble models already discussed.

The analogous situation in a twin-jet geometry, as suggested by SS433 (Hjellming and Johnston 1988), is based upon the assumption that there is a hot, X-ray twin-jet of 10^7 K gas emitted perpindicular to an accretion disk, and the $\sim$ 2000 km/sec sound speed in these

jets cause lateral expansion that produces a shock geometry in a conical sheath around the expanding, moving gas jet. The same turbulent acceleration, or trapped particle acceleration, mechanisms invoked for spherical shocks in the supernova remnant environment produce the relativistic electrons. Once the relativistic plasma has been produced the properties of the radio emitting regions can be desribed with variants on the previously discussed conical jet model.

While the radio outbursts of X-ray transients (Hjellming *et al.* 1988) have been attributed to the super-Eddington accretion rate, as indicated by the maximum X-ray fluxes, super-Eddington accretion rate has been observed in Cir X-1 (assuming spherical accretion and X-ray emission) without a large radio outburst (Stewart *et al.* 1991). A small radio outburst could still have taken place.

6.2 Magnetosphere Acceleration

Pulsars, which are rapidly rotating neutron stars with very strong magnetic fields, are known to accelerate relativistic electrons in regions near the polar caps of the neutron star magnetosphere (Lyne and Graham-Smith 1990). The acceleration process is not well understood, but can be considered to be empirically well established. Less spectacular, but possibly also analogous, are the particle acceleration processes that occur in the Earth's magnetosphere and the interaction regions between the Earth's magnetic field and the solar wind. These phenomena, plus the fact that the neutron star known in many X-ray binaries could be magnetized, makes it reasonable to consider magnetospheric acceleration for the relativistic electrons in radio emitting X-ray binaries. In addition, the accretion disk itself is likely to have a magnetic field that threads the accretions disk. Thus we are discussing object where magnetospheres associated with either, or both, compact object and accretion disk may accelerate relativistic particles.

The main difference between pulsars and X-ray binaries which accelerate relativistic electrons is that the latter are 'cocooned' by denser gas environments because of either the wind from a high-mass companion or the mass transfer from a low-mass companion that has filled its Roche lobe. Thus initially coherent beams of particles will interact with the surrounding medium, either to absorb the energy from the beamed particles, or to randomize the motions in mixtures of relativistic plasma, thermal gas, and magnetic fields.

We do not have any developed models for the transmutation of coherent beams of particles being turned into moving relativistic plasmoids, nor do we know whether this is possible. However, there is one observational signature that one might expect: highly bursty and erratic time variations. It is therefore very interesting that the strongest and most erratic time variability of the Z-source X-ray binaries occurs when the X-ray environment is 'hardest' (horizontal branch) and the strongest radio flares occur. On this branch the accretion rate is probably somewhat smaller, resulting in a somewhat smaller gas pressure, which subsequently results in a somewhat larger neutron-star magnetosphere. It is unclear whether the hard X-ray emission on this branch is coming from the surface of the neutron star, or from comptonization by a hot electron cloud (see e.g. Schulz and Wijers 1989). The increase of timing variability, hardening of the X-ray spectrum and, on average, increase of radio emission may be a signature of a situation asymptotically approaching that of the coherent beamed emission of a magnetized neutron star, but where the radiating regions are relativistic plasmoids activated by 'pulsar-like' coherent beams.

So far, no 'radio pulsar' type of emission (very steep spectra) has been found in X-ray binaries; also not during periods of quiescence (no mass transfer). One might have expected a radio pulsar when a low-mass X-ray binary shows no indication of mass transfer and the characteristics of neutron star and it's environment are similar to those of the msec radio pulsars.

7 CONCLUSIONS

Radio emission from various high- and low-mass X-ray binaries which can be shown to be due to synchrotron emission processes because of time variation and/or linear polarization is the most direct evidence that relativistic electrons are accelerated in the environment of these systems. In addition, bulk motion of relativistic plasma, with velocities of the order of 0.26c is seen, or inferred in some X-ray binaries. Whether gas dynamical effects are primary, with acceleration of electrons to relativistic energies as a byproduct of shock and trapping environments, or whether magnetospheres associated with either (or both) accretion disk and compact object are the primary sources of particle acceleration, with the randomization to moving plasmoinds be a result, represent the major options. The evidence for SS433, a high-mass binary, argues for gas dynamical acceleration of particles because the radio emission does not appear until a finite distance has occured in the jet flows. However, the Z-source low-mass binaries have a correlation of strongest, most variable radio emission when the accretion environment is at its lowest levels, indicating that magnetospheric processes may be primary, and that increases in the accretion environment obscure the magnetospheric processes.

Considerable progress can be expected in our understanding of these processes through more multi-wavelength campaigns and use of sensitive VLBI observations on the size scales of milli-arcseconds or smaller.

References

Bastian, T.S., Dulk, G.A., and Chanmugam, G.: 1988, *Astrophys. J.* **324**, 431

Bookbinder, J.A., and Lamb, D.Q.: 1987, *Astrophys. J.* **323**, L131

Bradt, H.V., Braes, L. L.E., Forman, W., Hesser, J.E., Hiltner, W.A., Hjellming, R.M., Kellogg, E., Kunkel, W.E., Miley, G.K., Moore, G., Pel, J.W., Thomas, J., Vanden Bout, P., Wade, C., and Warner, B.: 1975, *Astrophys. J.* **197**, 433

Chanmugam, G., and Dulk, G.A. : 1982, *Astrophys. J.* **255**, L107

Cooke, B.A., and Ponman, T.J.: 1991, *Astron. Astrophys.*, in press

Dickel, J.R., Eilek, J.A., Jones, E.M., and Reynolds, S.P.: 1989, *Astrophys. J. Suppl. Ser.* **70**, 497

Fomalont, E.B., Geldzahler, B.J., Hjellming, R.M., and Wade, C.M.: 1983, *Astrophys. J.* **275**, 802

Garcia, M.R., Grindlay, J.E., Molnar, L.A., Stella, L., White, N.E., and Seaquist, E.R.: 1988, *Astrophys. J.* **328**, 552

Geldzahler, B.J., *et al.*: 1983, *Astrophys. J.* **273**, L65

Geldzahler, B.J. and Fomalont, E.B.: 1986, *Astrophys. J.* **311**, 805

Ginzburg, V.L., and Syrovatskii, S.L.: 1965, *Ann. Rev. Astron. Astrophys.* **3**, 297

Gregory, P.C., *et al.*: 1972, *Nature Phys. Sc.* **239**, 114

Gregory, P.C. and Taylor, A.R.: 1978, *Nature* **272**, 704

Hasinger, G. and van der Klis, M.: 1989, *Astron. Astrophys.*, **225**, 79

Haynes, R.F., Komesaroff, M.M., Little, A.G., Jauncey, D.L., Caswell, J.L., Milne, D.K., Kesteven, M.J., Wellington, K.J., and Preston, R.A.: 1986, *Nature* **324**, 299

Hjellming, R.M.: 1988, in Verschuur, G.L. and Kellermann, K.I., eds., *Galactic and Extra-Galactic Radio Astronomy*, page 381, Springer-Verlag, New York

Hjellming, R.M. and Han, X.-H.: 1991, in preparation

Hjellming, R.M. and Johnston, K.J.: 1985, in Hjellming, R.M. and Gibson, D.M., eds., *Radio Stars*, pages 309–323, Reidel, Dordrecht

Hjellming, R.M. and Johnston, K.J.: 1988, *Astrophys. J.* **600**, 328

Hjellming, R.M. : 1973, *Astrophys. J.* **182**, L29

Hjellming, R.M. *et al.*: 1986, *Astrophys. J.* **305**, L71
Hjellming, R.M. and Wade, C.M.: 1971, *Astrophys. J.* **164**, L1
Hjellming, R.M., Calovini, T., Han, X.-H., and Córdova, F.A.: 1988, *Astrophys. J.* **335**, L75
Hjellming, R.M., Han, X.-H., Córdova, F.C., and Hasinger, G.: 1989, *Astron. Astrophys.* **235**, 147
Hjellming, R.M. *et al.*: 1990, *Astrophys. J.*, **365**, 681
Johnston, K.J., *et al.*: 1986, *Astrophys. J.* **309**, 707
Kellermann, K.I.: *Radio Galaxies and Quasars*, pages 320–352 Springer-Verlag, New York, 1974
Kellermann, K.I., and Owen, F.N.: 1988, in Verschuur, G.L. and Kellermann, K.I., eds., *Galactic and Extra-Galactic Radio Astronomy*, page 563, Springer-Verlag, New York
Königl, A.: 1983, *Monthly Notices Roy. Astron. Soc.* **205**, 471
Lyne, A.G., and Graham-Smith, F.: 1990, *Pulsar Astronomy*, pages 184-210, Cambridge Univ. Press, Cambridge.
Margon, B.: 1984, *Ann. Rev. Astron. Astrophys.* **22**, 507
Marscher, A.P., and Brown, R.L.: 1975, *Astrophys. J.* **200**, 707
Machin, G., Lehto, H.J., McHardy, I.M., Callanan, P.J.: 1990, *Monthly Notices Roy. Astron. Soc.* **246**, 237
Padin, S., Davis, R.J., and Bode, M.T.: 1985, *Nature* **315**, 306
Penninx, W., Lewin, W. H.G., Zijlstra, A.A., Mitsuda, K., van Paradijs, J., and van der Klis, M.: 1988, *Nature* **336**, 146
Penninx, W.: 1989, in Hunt, J. and Battrick, B. eds. *23rd ESLAB Symp. on Two Topics in X-ray Astronomy, Bologna, Italy 13–20 September, 1989*, pages 185–196, ESA SP-296
Penninx, W.: *X-ray and radio studies of low-mass X-ray binaries*, PhD thesis, University of Amsterdam, Amsterdam, Netherlands, 1990
Priedhorsky, W., Hasinger, G., Lewin, W. H.G., Middleditch, J., Parmar, A., Stella, L., and White, N.E.: 1986, *Astrophys. J.* **306**, L91
Schalinskii, *et al.*: 1990, in press
Schulz, N.S., and Wijers, R.A.M.J.:1989, in Hunt, J. and Battrick, B. eds. *23rd ESLAB Symp. on Two Topics in X-ray Astronomy, Bologna, Italy 13–20 September, 1989*, pages 601–606, ESA SP-296
Seaquist, E.R., *et al.*: 1974, *Nature* **251**, 394
Spencer, R.E., Swinney, R.W., Johnston, K.J., and Hjellming, R.M.: 1986, *Astrophys. J.* **309**, 694
Stewart, R.T., Nelson, G.J., Penninx, W., Kitamoto, S., Miyamoto, S., and Nicolson, G.D.: 1991, *Monthly Notices Roy. Astron. Soc.*, submitted
Strom, R., van Paradijs, J., and van der Klis, M.: 1989, *Nature* **337**, 234
Tan, J., *et al.*: 1991, *Astrophys. J.*, submitted
Tananbaum, H., *et al.*: 1972, *Astrophys. J.* **177**, L5
Taylor, A.R., Seaquist, E.R., Hollis, J.M., and Hjellming, R.M.: 1987, *Astron Astrophys.* **187**, 38
van der Laan, H.: 1966, *Nature* **211**, 1131
Vermeulen, R.: *Multi-wavelength studies of SS433*, PhD thesis, Rijksuniversiteit Leiden, Leiden, Netherlands, 1989
Vermeulen, R.C., Schilizzi, R.T., Icke, V., Fejes, I., and Spencer, R.E.: 1987, *Nature* **328**, 309
Watson, M.G., Stewart, G.C., Brinkmann, W., and King, A.R.: 1986, *Monthly Notices Roy. Astron. Soc.* **222**, 261
Zwarthoed, G.A.A., *et al.*: 1991, *Astron. Astrophys.*, in preparation
Zheleznyakov, V.V.: 1970, *Radio Emission of the Sun and Planets*, Pergamon Press, Oxford

Participants

A. Achterberg
Sterrenkundig Instituut, Rijksuniversiteit Utrecht, Postbus 80000, 3508 TA Utrecht

P. Barthel
Kapteyn Laboratorium, Zernike Gebouw, Postbus 800, 9700 AV Groningen

D. Bhattacharya
Sterrenkundig Instituut 'Anton Pannekoek', Universiteit van Amsterdam, Kruislaan 403, 1098 SJ Amsterdam

R.D. Blandford
Theoretical Astrophysics, 130-33 Caltech, Pasadena, California 91125, USA

K. Chambers
Sterrewacht Leiden, Huygens Laboratorium, Niels Bohrweg 2, 2300 RA Leiden

B. Espey
Sterrewacht Leiden, Huygens Laboratorium, Niels Bohrweg 2, 2300 RA Leiden

A.C. Fabian
Institute of Astronomy, Madingly Road, Cambridge CB3 0HA, UK

G. Geertsema
Sterrenkundig Instituut, Rijksuniversiteit Utrecht, Princetonplein 5, Postbus 80000, 3508 TA Utrecht

J.P. Goedbloed
FOM Instituut voor Plasmafysica 'Rijnhuizen', Postbus 1207, 3430 BE Nieuwegein

T. Hanawa
Department of Astrophysics, University of Nagoya, Chikusa-ku, Nagoya 464, Japan

G. Hasinger
Max-Planck-Institut für extraterrestrische Physik, 8046 Garching, FRG

E.P.J. van den Heuvel
Sterrenkundig Instituut 'Anton Pannekoek', Universiteit van Amsterdam, Kruislaan 403, 1098 SJ Amsterdam

A.M. Hillas
Physics Department, University of Leeds, Leeds LS2 9JT, UK

R.M. Hjellming
National Radio Astronomy Observatory, PO Box O, Socorro, NM 87801-0387, USA

L. van den Horn
Centrum voor Hoge Energie Astrofysica, NIKHEF-H, Postbus 41882, 1009 DB Amsterdam

P. Hoyng
Laboratorium voor Ruimteonderzoek, Sorbonnelaan 2, 3584 CA Utrecht

V. Icke
Sterrewacht Leiden, Huygens Laboratorium, Niels Bohrweg 2, 2300 RA Leiden

O. de Jager
Department of Physics, Potchefstroom University, Potchefstroom, 2520 South Africa

J. Kaastra
Laboratorium voor Ruimteonderzoek, Huygens Laboratorium, Niels Bohrweg 2, 2300 RA Leiden

M. van Kerkwijk
Sterrenkundig Instituut 'Anton Pannekoek', Universiteit van Amsterdam, Kruislaan 403, 1098 SJ Amsterdam

M. van der Klis
Sterrenkundig Instituut 'Anton Pannekoek', University of Amsterdam, Kruislaan 403, 1098 SJ Amsterdam

J. Kuijpers
Sterrenkundig Instituut, Rijksuniversiteit Utrecht, Princetonplein 5, Postbus 80000, 3508 TA Utrecht

L. Kuiper
Laboratorium voor Ruimteonderzoek, Huygens Laboratorium, Niels Bohrweg 2, 2300 RA Leiden

M. Kuperus
Sterrenkundig Instituut, Rijksuniversiteit Utrecht, Princetonplein 5, Postbus 80000, 3508 TA Utrecht

F.K. Lamb
Physics Department, University of Illinois, 1110 W. Green Street, Urbana, IL 61801, USA

W.H.G. Lewin
M.I.T. 37-627, Cambridge, MA 02139, USA

G. Mellema
Sterrewacht Leiden, Huygens Laboratorium, Niels Bohrweg 2, 2300 RA Leiden

G. Miley
Sterrewacht Leiden, Huygens Laboratorium, Niels Bohrweg 2, 2300 RA Leiden

L. Molnar
Department of Physics and Astronomy, University of Iowa, Iowa City, IA 52242, USA

H. Oegelman
Max-Planck-Institut für Extraterrestrische Physik, D8046 Garching, BRD

J. van Paradijs
Sterrenkundig Instituut 'Anton Pannekoek', Universiteit van Amsterdam, Kruislaan 403, 1098 SJ Amsterdam

W. Penninx
Sterrenkundig Instituut 'Anton Pannekoek', Universiteit van Amsterdam, Kruislaan 403, 1098 SJ Amsterdam

S. Phinney
Theoretical Astrophysics, 130-33 Caltech, Pasadena, CA 91125, USA

A. Piters
Sterrenkundig Instituut, Rijksuniversiteit Utrecht, Princetonplein 5, Postbus 80000, 3508 TA Utrecht

H. Röttgerink
Sterrewacht Leiden, Huygens Laboratorium, Niels Bohrweg 2, 2300 RA Leiden

M. Ruderman
Department of Physics, Columbia University, Pupin Hall, New York, NY 10027, USA

G. Schramkowski
Sterrewacht Leiden, Huygens Laboratorium, Niels Bohrweg 2, 2300 RA Leiden

L. Stella
ESTEC, Postbus 299, 2200 AG Noordwijk

R.G. Strom
Radiosterrewacht Dwingeloo, Oude Hoogeveensedijk 4, Postbus 2, 7990 AA Dwingeloo

F. Verbunt
Sterrenkundig Instituut, Rijksuniversiteit Utrecht, Princetonplein 5, Postbus 80000, 3508 TA Utrecht

M. de Vries
Sterrewacht Leiden, Huygens Laboratorium, Niels Bohrweg 2, 2300 RA Leiden

R.A.M.J. Wijers
Sterrenkundig Instituut 'Anton Pannekoek', Universiteit van Amsterdam

R. Zwarthoed
Sterrenkundig Instituut 'Anton Pannekoek', Universiteit van Amsterdam, Kruislaan 403, 1098 SJ Amsterdam